



MINISTÉRIO DA CIÊNCIA, TECNOLOGIA, INOVAÇÕES E COMUNICAÇÕES
INSTITUTO NACIONAL DE PESQUISAS ESPACIAIS

sid.inpe.br/mtc-m16c/2019/10.21.13.12-TDI

CONTROLLING COLLECTIVE BEHAVIORS AND AUTONOMOUS MOBILE AGENTS

Vander Luís de Souza Freitas

Doctorate Thesis of the Graduate Course in Applied Computing, guided by Drs. Elbert Einstein Nehrer Macau, and Serhiy Yanchuk, approved in October 16, 2019.

URL of the original document:

<<http://urlib.net/8JMKD3MGPDW34P/3U9CUG2>>

INPE
São José dos Campos
2019

PUBLISHED BY:

Instituto Nacional de Pesquisas Espaciais - INPE
Gabinete do Diretor (GBDIR)
Serviço de Informação e Documentação (SESID)
CEP 12.227-010
São José dos Campos - SP - Brasil
Tel.:(012) 3208-6923/7348
E-mail: pubtc@inpe.br

**BOARD OF PUBLISHING AND PRESERVATION OF INPE
INTELLECTUAL PRODUCTION - CEPPII (PORTARIA Nº
176/2018/SEI-INPE):****Chairperson:**

Dra. Marley Cavalcante de Lima Moscati - Centro de Previsão de Tempo e Estudos
Climáticos (CGCPT)

Members:

Dra. Carina Barros Mello - Coordenação de Laboratórios Associados (COCTE)
Dr. Alisson Dal Lago - Coordenação-Geral de Ciências Espaciais e Atmosféricas
(CGCEA)
Dr. Evandro Albiach Branco - Centro de Ciência do Sistema Terrestre (COCST)
Dr. Evandro Marconi Rocco - Coordenação-Geral de Engenharia e Tecnologia
Espacial (CGETE)
Dr. Hermann Johann Heinrich Kux - Coordenação-Geral de Observação da Terra
(CGOBT)
Dra. Ieda Del Arco Sanches - Conselho de Pós-Graduação - (CPG)
Sílvia Castro Marcelino - Serviço de Informação e Documentação (SESID)

DIGITAL LIBRARY:

Dr. Gerald Jean Francis Banon
Clayton Martins Pereira - Serviço de Informação e Documentação (SESID)

DOCUMENT REVIEW:

Simone Angélica Del Ducca Barbedo - Serviço de Informação e Documentação
(SESID)
André Luis Dias Fernandes - Serviço de Informação e Documentação (SESID)

ELECTRONIC EDITING:

Ivone Martins - Serviço de Informação e Documentação (SESID)
Cauê Silva Fróes - Serviço de Informação e Documentação (SESID)



MINISTÉRIO DA CIÊNCIA, TECNOLOGIA, INOVAÇÕES E COMUNICAÇÕES
INSTITUTO NACIONAL DE PESQUISAS ESPACIAIS

sid.inpe.br/mtc-m16c/2019/10.21.13.12-TDI

CONTROLLING COLLECTIVE BEHAVIORS AND AUTONOMOUS MOBILE AGENTS

Vander Luís de Souza Freitas

Doctorate Thesis of the Graduate Course in Applied Computing, guided by Drs. Elbert Einstein Nehrer Macau, and Serhiy Yanchuk, approved in October 16, 2019.

URL of the original document:

<<http://urlib.net/8JMKD3MGPDW34P/3U9CUG2>>

INPE
São José dos Campos
2019

Cataloging in Publication Data

Freitas, Vander Luís de Souza.

F884c Controlling collective behaviors and autonomous mobile agents / Vander Luís de Souza Freitas. – São José dos Campos : INPE, 2019.

xxviii + 108 p. ; (sid.inpe.br/mtc-m16c/2019/10.21.13.12-TDI)

Thesis (Doctorate in Applied Computing) – Instituto Nacional de Pesquisas Espaciais, São José dos Campos, 2019.

Guiding : Drs. Elbert Einstein Nehrer Macau, and Serhiy Yanchuk.

1. Reactive models. 2. Nonlinear dynamics. 3. Collective motion. 4. Symmetric circular formation. 5. Kilobots. I.Title.

CDU 007.52:004.023



Esta obra foi licenciada sob uma Licença [Creative Commons Atribuição-NãoComercial 3.0 Não Adaptada](https://creativecommons.org/licenses/by-nc/3.0/).

This work is licensed under a [Creative Commons Attribution-NonCommercial 3.0 Unported License](https://creativecommons.org/licenses/by-nc/3.0/).

Aluno (a): **Vander Luís de Souza Freitas**

Título: "CONTROLLING COLLECTIVE BEHAVIORS AND AUTONOMOUS MOBILE AGENTS"

Aprovado (a) pela Banca Examinadora em cumprimento ao requisito exigido para obtenção do Título de **Doutor(a)** em **Computação Aplicada**

Dr. **Marcos Gonçalves Quiles**



Presidente / INPE / São José dos Campos - SP

Participação por Vídeo - Conferência

Aprovado Reprovado

Dr. **Elbert Einstein Nehrer Macau**



Orientador(a) / INPE / São José dos Campos - SP

Participação por Vídeo - Conferência

Aprovado Reprovado

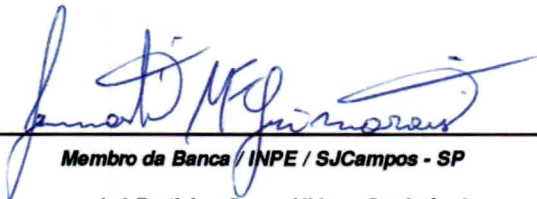
Dr. **Serhiy Yanchuk**

Orientador(a) / TU/Berlin / Berlin - GER

Participação por Vídeo - Conferência

Aprovado Reprovado

Dr. **Lamartine Nogueira Frutuoso Guimaraes**



Membro da Banca / INPE / SJC Campos - SP

Participação por Vídeo - Conferência

Aprovado Reprovado

Este trabalho foi aprovado por:

maioria simples

unanimidade

São José dos Campos, 16 de outubro de 2019

Aprovado (a) pela Banca Examinadora
em cumprimento ao requisito exigido para
obtenção do Título de **Doutor(a)** em
Computação Aplicada

Dr. Solon Venâncio de Carvalho



Membro da Banca / INPE / SJCampos - SP

() Participação por Video - Conferência

Aprovado () Reprovado

Dr. Patricia Romano Cirilo



Convidado(a) / UNIFESP / São José dos Campos - SP

() Participação por Video - Conferência

Aprovado () Reprovado

Dr. José Roberto Castilho Piqueira



Convidado(a) / USP / São Paulo - SP

() Participação por Video - Conferência

Aprovado () Reprovado

Este trabalho foi aprovado por:

() maioria simples

unanimidade

São José dos Campos, 16 de outubro de 2019

“In theory, there is no difference between theory and practice. In practice, there is”.

BENJAMIN BREWSTER, 1882

*To my parents **Sueli** and **Sergio**, my sisters **Tamires**
and **Laura** and my wife **Natália***

ACKNOWLEDGEMENTS

Firstly, thanks God and my family for all the support, especially my wife Natalia, whose companionship is priceless.

Special thanks to my supervisors Dr. Elbert Macau and Dr. Serhiy Yanchuk, whose support was vital for the completion of this thesis. To the institutions INPE, Humboldt, and TU-Berlin, my most sincere thanks for providing me healthy and fruitful environments.

I acknowledge my friends and colleagues from the aforementioned institutions for the pleasant time we spent working and discussing science and life.

Additionally, I cannot forget to mention the Libercanto choir, where I met interesting people and good music.

Lastly I would like to thank the Coordenação de Aperfeiçoamento de Pessoal de Nível Superior (CAPES) and Fundação de Amparo à Pesquisa do Estado de São Paulo (Fapesp), grants 2017/24224-6, 2017/04552-9 and 2015/50122-0 for allowing me to do science.

ABSTRACT

Collective behaviors emerge from interactions among living beings. Similarly, engineering applications with mobile robots might employ bio-inspired strategies to reach desired group configurations. This thesis proposes strategies that exploit communication among close agents to obtain the desired behavior. Firstly, a reactive model of agents that group into a certain neighborhood and follow a mobile reference is presented. The adopted parameters are achieved via heuristics that target specific formation topologies. Each agent has a sensory region around itself that allows perceiving neighbors that come close. Furthermore, the group follows the so-called virtual agent (VA), a non-real agent that dictates the trajectory to be chased. The second part of the thesis is devoted to a first-order model of particles with coupled oscillator dynamics, focusing on the specific case of particles moving in circular trajectories and reaching clusters of the same size that are symmetrically distributed along the trajectory. The study starts with an investigation of the control parameters space in order to find regions where particles reach desired formations regardless of initial conditions. After that, the effects of adding and removing particles from already stable ensembles are explored. Simulations show that some particles never join clusters when the number of new elements is smaller than a certain critical value. In a similar fashion, clusters start to break only after a critical number of removed elements. Additionally, a strategy is proposed to change from one cluster configuration to another. Finally, the so-called Switching System is proposed, allowing for symmetric circular formations with time-periodic and chaotic dynamics. The model for obtaining cluster configurations is implemented in a simulator of mobile robots as a proof of concept.

Keywords: Reactive models. Nonlinear dynamics. Collective motion. Symmetric circular formation. Kilobots.

CONTROLANDO COMPORTAMENTOS COLETIVOS E AGENTES MÓVEIS AUTÔNOMOS

RESUMO

Comportamentos coletivos complexos emergem de interações entre seres vivos. Da mesma forma, aplicações de engenharia com robôs móveis podem empregar estratégias bio-inspiradas para obtenção de configurações de grupo desejadas. Esta tese propõe estratégias que exploram comunicação entre agentes próximos para obter o comportamento almejado. Inicialmente, apresenta-se um modelo reativo de agentes que se agrupam em uma dada vizinhança e seguem uma referência móvel. Os parâmetros adotados são provenientes de heurísticas que objetivam topologias de formação específicas. Cada agente possui uma região sensorial que o permite se comunicar com agentes próximos. Ainda, o grupo segue o chamado agente virtual, um agente fictício que indica a trajetória a ser seguida. A segunda parte da tese se concentra em um modelo de primeira ordem de partículas com dinâmica de osciladores de fase acoplados. Trata-se do caso específico de partículas se movendo em trajetórias circulares e subdividindo-se em clusters de mesmo tamanho e distribuídos simetricamente pela trajetória. O estudo inicia-se com a investigação do espaço dos parâmetros de controle a fim de encontrar regiões onde as partículas atingem as formações desejadas, independentemente das condições iniciais. Em seguida, explora-se os efeitos da adição e remoção de partículas em arranjos já estáveis. Simulações mostram que algumas partículas nunca integram clusters quando o número de novos elementos é menor do que um valor crítico. Do mesmo modo, os clusters começam a se quebrar apenas a partir de um certo número crítico de partículas removidas do arranjo. Além disso, propõe-se uma estratégia para realizar transições entre uma formação de clusters para outra. Por fim, apresenta-se o chamado “Switching system”, que permite formações circulares simétricas com partículas que não se sobrepõem e trajetórias caóticas. O modelo para obtenção das configurações de clusters é implementado em um simulador de robôs móveis como uma prova de conceito.

Palavras-chave: Modelos reativos. Dinâmica não-linear. Movimento coletivo. Formações circulares simétricas. Kilobots.

LIST OF FIGURES

	<u>Page</u>
2.1 Interpolation $y_{n-T+1/2} = F(y(t_{n-T-1}), y(t_{n-T}), y(t_{n-T+1}), y(t_{n-T+2}))$ using the four closest points. The desired point has symbol ‘o’.	18
3.1 Initial conditions of a simulation scenario, with agents represented in red, their vision radii in gray, and the VA in blue. Agents are randomly placed inside the dotted area when the simulation begins, with random associated velocities.	24
3.2 Perception zones. Zone of Separation (ZS), Zone of Alignment (ZA) and Zone of Cohesion (ZC).	25
3.3 Virtual forces. The dotted circumferences represent the vision radius constituted of the three perception zones of one agent (in black). The gray region in subfigures (a), (b) and (c) contains the neighbors used to calculate the forces F_s , F_a and F_c , respectively. At (d) and (e) the blue agent is the VA. F_s is calculated considering only the neighbors inside the zone of separation (ZS), F_a with the individuals inside the zone of alignment (ZA), and F_c with those inside the zone of cohesion (ZC).	29
3.4 Simple circular dynamics of (3.14) for the case of a constant control $u_k = \omega_0 \neq 0$. The particle is moving around the center c_k given by Equation (3.16) and radius $ \omega_0 ^{-1}$	33
3.5 (a) Phases in a splay state as blue circles and its perturbed version as red symbols +; (b) m -th phase order parameters of the perturbed system as symbols x and the corresponding normalized version as stars.	36
3.6 Simulations of model (3.14) under the control for symmetric circular formations of Equation (3.28). Parameters: $N = 6$, $K_0 = 0.1$, $\omega_0 = 0.05$, $K_m = 0.18$ for $m < M$ and $K_M = -0.02$. Particles are the red circles and the center of mass is in blue.	38
3.7 Time series of the order parameters of model (3.14), with control (3.28) and parameters: $N = 6$, $M = 3$, $K_0 = 0.1$, $\omega_0 = 0.05$, $K_m = 0.18$ for $m < M$ and $K_M = -0.02$	38
4.1 Objective functions: a) Convergence time f_{time} when every agent is inside the FR and $ \theta_i - \theta_a < 5$ degrees; b) Angular uniformity $f_{ang} = \frac{1}{N} \sum_{i=1}^N e^{i\Theta_i} $ and; c) Radial uniformity $f_{rad} = \frac{1}{N} \sum_{i=1}^N d_i$, for $i = \{1, \dots, N\}$	45

4.2	Results of optimization problem (4.3): (a) Optimal f_{time} for different values of τ . (b) Optimal f_{time} , after 50 simulations of GEO_{var} with $\tau = 1.75$. Best result is the purple thick line and the average case is the dashed red line. The 50 simulations are represented by the thin gray lines.	47
4.3	Results of optimization problem (4.4): (a) Optimal f_{ang} for different values of τ . (b) Optimal f_{ang} measure after 50 simulations of GEO_{var} with $\tau = 1.5$. Best result is the purple thick line and the average case is the dashed red line. The 50 simulations are represented by the thin gray lines.	48
4.4	Results of optimization problem (4.5): (a) Optimal f_{rad} for different values of τ . (b) Optimal f_{rad} after 50 simulations of GEO_{var} with $\tau = 1.5$. Best result is the purple thick line and the average case is the dashed red line. The 50 simulations are represented by the thin gray lines.	49
4.5	Pareto Frontier obtained from M-GEO with $\tau = 1.50$. Colors represent f_{time} . The black arrow indicates the chosen solution for the simulations of Section 4.2, whose values for the objective functions are $f_{time} = 779$, $f_{ang} = 0.0582744$ and $f_{rad} = 4.71353$, and control coefficients $\alpha_a = 0.23622$, $\alpha_c = 0.212598$, $\alpha_{av} = 0.488189$ and $\alpha_{cv} = 0.976378$. The vertical dashed line highlights the $f_{ang} = 0$ to show how close the solutions approach to it.	50
4.6	Simulation results with the VA following a circular trajectory with dynamics of Equation (4.8). Parameters: $\alpha_a = 0.23622$, $\alpha_c = 0.212598$, $\alpha_{av} = 0.488189$ and $\alpha_{cv} = 0.976378$, $\omega = 1$ and maximum turning angle $\gamma = 10$ decimal degrees. We present three simulation snapshots, with the time units indicated near them.	52
4.7	Simulation results with the VA performing a random walk inside a bounded region with dynamics of Equations (4.10) and (4.11). Parameters: $\alpha_a = 0.23622$, $\alpha_c = 0.212598$, $\alpha_{av} = 0.488189$ and $\alpha_{cv} = 0.976378$, $\omega = 1$ and maximum turning angle $\gamma = 10$ decimal degrees. We present three simulation snapshots, with the time units indicated near them. . .	53
4.8	Simulation results with the VA performing a random walk inside a bounded region as in Figure 4.7, but the agents maintain their relative positions fixed, after a transient (notice that relative positions do not change from $t=1375$ to $t=3675$). Parameters: $\alpha_a = 0.23622$, $\alpha_c = 0.212598$, $\alpha_{av} = 0.488189$ and $\alpha_{cv} = 0.976378$, $\omega = 1$ and maximum turning angle $\gamma = 10$ decimal degrees. We present three simulation snapshots, with the time units indicated near them.	54

5.1	Parameter space $K_M \times K_1$. The black regions correspond to the parameter values, for which symmetric M -cluster formations emerge after the transient $t_f = 15000$. More specifically, for these parameters, the conditions $m p_{m\theta} < 10^{-3}$ for $m < M$ and $M p_{M\theta} > 1 - 10^{-3}$ are fulfilled. Other parameters: $N = 12$, $\omega_0 = 0.05$	58
5.2	Normalized order parameter $Mp_{M\theta}$ (left) and potential $U^{M,N}$ (right) for different number N_{add} of added elements to already formed clusters. The dashed gray line on the right plot corresponds to the potential minimum $U^{M,N} = (K_m N)/(2M^2)$. The system starts with $N = 12$ particles with the following number of clusters: (a) $M = 2$, (b) $M = 3$, (c) $M = 4$, (d) $M = 6$, and (e) $M = 12$. The chosen integration time is $t = 15000$	61
5.3	Positions of new added particles (green) and clusters (red) after transient $t_f = 15000$. Crosses denote randomly chosen initial positions of the added particles. Initial configuration: $N = 12$ particles, $M = 4$ clusters, $\omega_0 = 0.05$, $K_m = 0.18$ for $m < M$ and $K_M = -0.02$	62
5.4	Normalized order parameter $M p_{M\theta} $ (left) and potential $U^{M,N}$ (right) for different number N_{rem} of removed elements from already formed clusters. The dashed gray line on the right plot corresponds to the potential minimum $U^{M,N} = (K_m N)/(2M^2)$. The system starts with $N = 108$ particles with the following number of clusters: (a) $M = 2$, (b) $M = 3$, (c) $M = 4$, (d) $M = 6$, and (e) $M = 12$. The chosen integration time is $t = 15000$	63
5.5	Time series of the order parameters $m p_{m\theta} $ for system (3.14) with the control (3.28). The system starts with M_f symmetric clusters and its potential is switched from $U^{M_f,12}$ to $U^{M_t,12}$ at time $t = 0$. The order parameters indicate successful switching to the desired number of clusters M_t	65
5.6	Changing between formations with $M_f = 3$ and $M_t = 2$, for $N = 12$. Particles start at a symmetric circular formation with $M = 3$ and we added a small perturbation of amplitude ϵ and start the control (3.28) integration. We evaluated the potentials (3.25) at $t = 0$ and $t = 15000$ and observed that transitions start to occur when perturbations are high enough to make particles move from local minima.	66
5.7	Illustration of a successful control by the modified potential (5.4). Time series of the order parameters $m p_{m\theta} $ for different m using model (3.14), under conventional control (a) (3.28) and modified (b) (5.4), which is applied at time $t = 0$. The system stays initially in the symmetric M_f cluster state. Panel (b) shows successful switching between M_f to M_t symmetric cluster formation.	68

5.8	Transition times for a switching from M_f to M_t symmetric cluster formations in system (3.14) with control (5.4). The changing time is calculated whenever the order parameters achieve $M p_{M\theta} > 0.999$ and $ p_\theta < 0.001$. The almost white squares are of order 10000. Every bin is the average of 10 simulations.	68
5.9	Alternating M_A , M_B , with $T = 20s$	70
5.10	Largest Lyapunov Exponents for different M_A , M_B and T	72
5.11	Error between the map (5.6) and a copy with a perturbation $\epsilon = 10^{-3}$ (horizontal dashed line) as time evolves: (a) Stable solution $M_A = 3$, $M_B = 6$, $T = 100$, $\lambda \approx 0$: trajectories do not diverge with the small perturbation; (b) Chaotic solutions $M_A = 3$, $M_B = 6$, $T = 160$: trajectories diverge with small perturbations from time $n = 1/\lambda$ on. Recall from Figure 5.10 that (b) has $\lambda = 0.57$, therefore trajectories should diverge at $n \approx 2$ map iterations, as observed.	73
5.12	Time series of θ for the switched system with $N = 12$ particles, $\omega_0 = 0.05$ and control parameters from Section 5.1. From top to bottom: (a) $M_A = 2$, $M_B = 6$, $T = 40$; (b) $M_A = 2$, $M_B = 5$, $T = 40$ and; (c) $M_A = 2$, $M_B = 6$, $T = 175$	74
5.13	Delay τ over natural frequency ω_0 . Colors represent the resulting number of clusters, in which “zero” means disorder. We used the phase order parameters to characterize the clusters, with $m p_{m\theta} < 10^{-1}$ for $m < M$ and $M p_{M\theta} > 1 - 10^{-1}$	76
5.14	Pareto frontier of the multiobjective optimization problem (minimization), with objective functions $ p_\theta $ and f_{ncoll} , and design variables K and K_r	79
5.15	All-to-all: symmetric circular formation with control (3.36). Configuration: $N = 6$, $K = 0.00787402$, $K_r = 0.0866142$, $\omega_0 = 0.05$, $\rho = 20$ and $d = 5$. The red circles correspond to the agents, and the blue circle is their center of mass.	80
5.16	All-to-all (not optimal): symmetric circular formation with control (3.36). Configuration: $N = 6$, $K = 0.1$, $K_r = 0.1$, $\omega_0 = 0.05$, $\rho = 20$ and $d = 5$. The red circles correspond to the agents, and the blue circle is their center of mass.	80
5.17	Ring-like network topology: symmetric circular formation with control (3.37). Configuration: $N = 6$, $K = 0.00787402$, $K_r = 0.0866142$, $\omega_0 = 0.05$, $\rho = 20$ and $d = 5$. The red circles correspond to the agents, and the blue circle is their center of mass.	81

5.18	Ring-like network topology (not optimal): symmetric circular formation with control (3.37). Configuration: $N = 6$, $K = 0.1$, $K_r = 0.1$, $\omega_0 = 0.05$, $\rho = 20$ and $d = 5$. The red circles correspond to the agents, and the blue circle is their center of mass.	81
5.19	Dynamic networks: symmetric circular formation with control (3.37). Configuration: $N = 6$, $K = 0.00787402$, $K_r = 0.0866142$, $\omega_0 = 0.05$, $\rho = 20$ and $d = 5$. The red circles correspond to the agents, and the blue circle is their center of mass.	82
5.20	Dynamic networks (not optimal): symmetric circular formation with control (3.37). Configuration: $N = 6$, $K = 0.1$, $K_r = 0.1$, $\omega_0 = 0.05$, $\rho = 20$ and $d = 5$. The red circles correspond to the agents, and the blue circle is their center of mass.	83
6.1	ARK system.	86
6.2	Simulation of model (6.9) under the control for symmetric circular formations of Equation (3.28). Parameters: $N = 6$, $K_0 = 10$, $\omega_0 = 0.05$, $K_m = 0.18$ for $m < M$ and $K_M = -0.02$, $v = 0.01$. a) $M = 1$, b) $M = 2$, c) $M = 3$, d) $M = 6$	90
6.3	Varying σ_f . Configuration: $N = 6$, $K_0 = 10$, $\omega_0 = 0.025$, $K_m = 0.18$ for $m < M$ and $K_M = -0.02$, $v = 0.01$. (a) $M = 1$, (b) $M = 2$, (c) $M = 3$, (d) $M = 6$	91

LIST OF TABLES

	<u>Page</u>
4.1 Results of optimization problems (4.3), (4.4), and (4.5), using the algorithm GEO_{var}	48
5.1 The Switching System outcomes for period $T < T_1$	70

LIST OF ABBREVIATIONS

ARK	–	Augmented Reality for Kilobots
bl	–	body length
DDE	–	Delay Differential Equations
FR	–	Formation Region
GA	–	Genetic algorithm
GEO	–	Generalized Extremal Optimization
HL	–	Hierarchical Leadership
LLE	–	Largest Lyapunov exponent
M-GEO	–	Multiobjective Generalized Extremal Optimization
NFE	–	Number of object function evaluations
ODE	–	Ordinary Differential Equations
OHC	–	Overhead controller
PCOD	–	Particles with coupled-oscillator dynamics
PID	–	Proportional, Integral and Derivative
RK4	–	Runge Kutta of 4th order
SS	–	Switching System
tu	–	time unit
UAV	–	Unmanned aerial vehicle
VA	–	Virtual Agent
ZA	–	Zone of Alignment
ZC	–	Zone of Cohesion
ZS	–	Zone of separation

LIST OF SYMBOLS

A	–	Adjacency Matrix
α	–	Control parameters of the Reactive model
c	–	Rotation center
e	–	Error
F	–	Force
f_{time}	–	Convergence time
f_{ang}	–	Angular uniformity
f_{rad}	–	Radial uniformity
Γ	–	Coupling function
γ	–	Angular speed
h	–	Integration time step
I	–	Identity matrix
k	–	Index / intermediary steps of RK4 / rank of evolutionary algorithms' solutions
K	–	Coupling strength, gain
κ	–	Coupling strength
L	–	Graph Laplacian / Length of a solution in evolutionary algorithms
λ	–	Lyapunov exponent
M	–	Number of clusters
N	–	Number of particles
ν	–	Number of times a population restarts on the evolutionary algorithms
N	–	Set of neighbors
ω	–	Natural frequency
P	–	Projection Matrix
p_θ	–	Kuramoto order parameter
$p_{m\theta}$	–	m -th order parameter
r	–	Particle's coordinates
rep	–	Repulsion control
ρ	–	Circular trajectory radius
RND	–	Uniformly distributed random variable
S	–	Common center potential
s	–	Speed
T	–	Period
τ	–	Time delay / Parameter of the GEO algorithm
θ	–	Phase
Θ	–	Phase
u	–	Control
U	–	Potential function
v	–	Speed
V	–	Lyapunov function
W	–	Potential

CONTENTS

	<u>Page</u>
1 INTRODUCTION	1
1.1 Main research questions	3
1.2 Contents and main findings	4
1.3 Thesis organization	6
2 DYNAMICAL SYSTEMS, SYNCHRONIZATION AND EVOLUTIONARY OPTIMIZATION	7
2.1 Gradient systems	8
2.2 Phase-coupled oscillators	9
2.2.1 Two coupled oscillators	10
2.2.2 N phase-coupled oscillators	11
2.3 Delayed phase oscillators	13
2.4 Chaotic systems and Lyapunov exponents	14
2.5 Numerical integration	15
2.6 Evolutionary optimization	17
2.6.1 Generalized Extremal Optimization	18
2.6.2 Multiobjective Generalized Extremal Optimization	20
2.7 Conclusions	21
3 COLLECTIVE MOTION SYSTEMS	23
3.1 Unicycle models	23
3.2 Reactive model for autonomous vehicles formation following a mobile reference	23
3.3 Particles with phase-coupled oscillator dynamics (PCOD)	32
3.3.1 Circular formations	33
3.3.2 Symmetric circular formations	34
3.3.3 Limited communication	39
3.3.4 Collision avoidance	40
3.4 Conclusions	41
4 REACTIVE MODEL FOR AUTONOMOUS VEHICLES FORMATION FOLLOWING A MOBILE REFERENCE: SIMULATIONS AND NUMERICAL RESULTS	43

4.1	Evolutionary Optimization	43
4.1.1	Objective functions	44
4.1.1.1	Results	45
4.1.2	Mono-objective problem	47
4.1.3	Multi-objective problem	49
4.2	Path planning simulation	51
4.3	Conclusions	55
5	PARTICLES WITH PHASE-COUPLED OSCILLATOR DY-	
	NAMICS: SIMULATIONS AND NUMERICAL RESULTS	57
5.1	Effect of control parameters on cluster emergence	57
5.2	Adding and removing particles	59
5.3	Changing between formations	64
5.4	The Switching System	69
5.4.1	Non-overlapping particles	70
5.4.2	Chaotic trajectories	71
5.5	Delayed communication	74
5.6	Collision avoidance	77
5.7	Conclusions	83
6	MOBILE ROBOT SIMULATIONS	85
6.1	PCOD model	89
6.1.1	Effect of Noise	90
6.2	Conclusions	92
7	CONCLUSIONS AND FUTURE WORK	93
	REFERENCES	99

1 INTRODUCTION

Living beings such as bacteria, insects, fish schools and flocks of birds exhibit collective behaviors (VICSEK; ZAFEIRIS, 2012) that emerge when they are escaping from a predator, seeking for food, building a shelter, etc.

The word “flock” is the collective noun for a group of birds, but also used by the research community as synonym of the coordinated ordered motion of a group of individuals. On the other hand, when the motion is disordered the collective noun of insects takes place: swarm (ALGAR et al., 2019).

Czirók et al. (1996) studied the simpler beings that behave collectively: the bacteria. They observed spiral formations and cluster migration, which inspired a model of self-propelled particles.

Sumpter (2006) points out that in an ants colony, the sum of individual contributions is less than the teamwork capacity. The short explanation is that when an ant finds a food source, it creates a pheromone trail that is used by the others to recover the path to the food. Also, the trail is reinforced every time an ant passes over. Without this communication mechanism, each ant would have to find food alone and the total amount of collected resources would probably be smaller.

Some studies with fish evidence that a natural control parameter for them is the shoal density (BECCO et al., 2006; MAKRIS et al., 2009). Herbert-Read et al. (2011) and Katz et al. (2011) analyzed shoals trajectories and observed attraction and repulsion rules in their interactions, and speed adjustments based on neighbors distance.

Interestingly, Potts (1984) and Ballerini et al. (2008) found the emergency of leadership behaviors and communication limitations in some bird species. More specifically, Ballerini et al. (2008) realized that *Starling* birds normally interact with their 6 or 7 closest conspecifics and not with all nearby neighbors.

The aforementioned results serve as inspiration for the development of autonomous mobile agents strategies for formation emergence (REYNOLDS, 1987; VICSEK et al., 1995; COUZIN et al., 2002; CUCKER; SMALE, 2007; FREITAS; MACAU, 2017b; FREITAS et al., 2018; BALAZS; VÁSÁRHELYI, 2018; VÁSÁRHELYI et al., 2018). The aim here is not to reproduce the animal world behaviors, but to learn from them and design strategies to obtain desired formations. These strategies can be thought in terms of alignment, attraction and repulsion rules, for example.

A common problem of those models is that the rules are usually employed simultaneously and one should design coefficients to weight their contributions in order to properly lead the agents to desired formations. When only the alignment rule is considered, the agents are able to reach consensus, moving to the same direction. However, this is not enough to prevent them to collide or to keep a tight formation. Rules should be combined, and the task to find proper weights that balance their contributions towards the desired formation is of great importance (FREITAS; MACAU, 2017b; FREITAS et al., 2018).

Chapter 4 displays some results on this matter with a model of agents that follow a mobile reference. An optimization problem is formulated to find proper coefficients to ponder interaction rules that drive the agents to desired formations (FREITAS et al., 2018).

Another approach is to create artificial network-based controls that abstracts the interaction rules. Some examples can be seen in Dierks et al. (2013), that defined a model with a leader-follower scheme; Li et al. (2014) worked with quadruped robots; Habibi et al. (2015) focused on the problem of moving an object with the cooperative work of multiple robots and; Duarte et al. (2016) developed controls for aquatic robots from neural networks generated with the Neuroevolution of Augmenting Topologies (NEAT) algorithm (STANLEY; MIIKKULAINEN, 2002).

We also explored this approach to design a model of agents following a mobile reference (FREITAS et al., 2017b) with the NEAT algorithm for network generation as in Duarte et al. (2016). The network inputs are the robots' sensors measurements like distance until the nearest neighbor in each quadrant and the coordinates of the mobile reference. The output is the angular velocity and speed.

Other design strategy for mobile agents in formation is the framework of phase-coupled oscillators, whereupon each vehicle dynamics is described by an oscillator. Their coupling is mediated by the information exchange between neighboring agents. One of the most famous models for synchronization of phase oscillators is the Kuramoto model (KURAMOTO, 1984; ACEBRÓN et al., 2005), in which the coupling is a sinusoidal function. This model opened possibilities for the study of synchronization in myriad areas (ACEBRÓN et al., 2005; VLASOV et al., 2014; VLASOV et al., 2015; FREITAS et al., 2015a; FREITAS et al., 2015b; PETER et al., 2019). Many collective motion models (SEPULCHRE et al., 2007; SEPULCHRE et al., 2008; LEONARD et al., 2007; JAIN; GHOSE, 2018; FREITAS; MACAU, 2018; FREITAS et al., 2019, Submitted) derive from the Kuramoto's and the physical meaning of the phase might be the

heading direction of the agent. In this sense, synchronized agents move in parallel and consensus is directly connected with the concept of synchronization.

The coupling among oscillators (interaction) can be mediated via fixed or dynamic topology networks. Fixed topologies mean that every oscillator communicates with the same neighbors. Oppositely, dynamic networks are usually employed when the vehicles have sensory limitations or preferences, exchanging information only with the neighbors inside their sensory region. This results in a network whose connections continuously modify as the agents get in touch to each other or move away.

Stradner et al. (2013) distinguish among different levels of coupling: weak, medium and strong. Weak is usually observed in systems whose information exchange between a pair of agents does not happen during a long time, such as particles diffusion, in which two particles occasionally meet and then separate. Medium level refers to systems where neighbor agents communicate for a long time frame, as in a flocking. Lastly, strong couple relates to agents that have a static and constant communication framework, like crystals, solid bodies, cells of an organism. This thesis explores medium and strong couplings in Chapters 4 and 5, respectively.

1.1 Main research questions

Following are the main research questions we address with a phenomenological model of reactive agents that follow a mobile reference:

- How do we model the interactions among close neighbors in order to build a formation that follows a given trajectory?
- What are the proper parameters to weight the interaction rules' contributions?

Secondly, we study a model of symmetric circular formations, for which we ask the following questions:

- What are the conditions for the emergence of symmetric circular formations?
- What is the effect of adding and removing agents to/from already stable formations?
- Is it possible to simply tune the parameters to exchange from one formation to another?

- How could clusters with non-overlapping particles be formed?
- Is it possible to generate chaotic circular-like trajectories?
- Do time delayed interactions play any role?

1.2 Contents and main findings

The terms *particles*, *mobile agents* and *agents* are used interchangeably in this document, referring to elements that move and interact to each other.

The main findings we present start with a phenomenological reactive model of particles following a mobile reference (FREITAS et al., 2018). We employ the sensory regions defined in Couzin et al. (2002), whose subdivisions have inspiration in schools of fish. It accounts for agents' interaction rules depending on the distances between close neighbors. Too close neighbors avoid collisions, medium range interactions lead to alignment, and attraction rises in long range neighborhoods.

Besides, we introduce a speed regulation to allow distant agents to catch up the group so that the formation emerges around the mobile reference. This is an interesting feature since most models consider unitary speed and an interaction area in the 2D plane with periodic boundary conditions. This means that agents that reach a border, appear at the diametrically opposite border. In real-world scenarios, the agents might reach very far places and eventually go to infinity.

We model the system without the aforementioned constraint and use the mobile reference as a meeting point for the group. This along with the speed regulation guarantee the group not to disperse to infinity and uniformly distribute around the reference so to better occupy the so-called *Formation Region* (FR), centered at the reference.

One important result is the definition of optimal weights for the interaction rules through heuristics that drive the system towards the minimum of some objective functions. Formations must happen as fast as possible with agents uniformly distributed inside the FR.

The second part of the thesis is devoted to the study of a model of particles with phase-coupled oscillator dynamics (SEPULCHRE et al., 2007; PALEY, 2007) that move with unitary speed in the plane. Their heading angles are abstracted as oscillators' phases that synchronize or distribute into groups of same size. Their dynamics is

driven by potentials whose minima correspond to concentric circular trajectories of particles that converge to a chosen number of groups, that we call *clusters*. Each cluster has the same number of participants and is symmetrically positioned along the trajectory.

Driven by potential applications with mobile robots we conducted several tests to assess the model response to realistic problems (FREITAS et al., 2019, Submitted), such as failure and addition of new robots, in which a phase transition is observed. Some particles join clusters only if the number of new members being added is higher than a certain critical value, that depends on the total number of agents already in the formation. The inverse situation also happens when removing particles from already stable formations.

Another issue of the Sepulchre et al. (2007) model is to exchange from one cluster configuration to another. Some configurations are local minimum of others and the transition may never happen. We then include a new term into the potentials to suppress the previous formation.

Furthermore, we introduce the so-called Switching System, that allows for the emergence of clusters with non-overlapping particles and the generation of chaotic circular-like formations.

Some tests with time delay in the inter-agents communication are conducted. We observe that delay plays the role of a control parameter as well and solutions reappear with increasing delay.

Finally, we present some results with an implementation of the model in a mobile robot simulator, the ARGoS (PINCIROLI et al., 2012). We use an emulator (PINCIROLI et al., 2018) for both the Kilobot platform (RUBENSTEIN et al., 2014) and the tracking system *Augmented Reality for Kilobots* (ARK) (REINA et al., 2017).

The investigated strategies must account for real-world aspects like noise from sensors and communication delay. The latter may occur due to large distances between agents and hardware limitations, like in satellites in formation fly (SCHETTER et al., 2003; NATIONAL AERONAUTICS AND SPACE ADMINISTRATION - NASA, 2017; CHUNG et al., 2016; BAKER, J. et al., 2019; YAO et al., 2019)

Some systems, like the Robot Soccer (KITANO et al., 1997; ROBOCUP FEDERATION, 2016), use a centralized control strategy that distributes tasks among the robots. This works well for a small number of agents, but this has impact in the system

scalability due to processing and communication limitations. The control strategies presented in this thesis are designed for autonomous agents that are able to perceive the environment and change direction by themselves.

We aim to present and discuss control strategies for autonomous mobile agents based on interaction rules and phase-coupled oscillators synchronization. The problem of delayed communication is also addressed for the latter. The main applications are data collection systems, surveillance and monitoring (LEONARD et al., 2007; DUARTE et al., 2016), tasks that demand autonomous vehicles to interact and maintain their formations.

The motivation behind the study of systems with circular motions are formations with vehicles such as satellites, drones and others that perform data collection and patrol with the desired spatial and temporal separation.

The subsequent publications were issued as part of the development of this thesis: Freitas and Macau (2017a), Freitas et al. (2017b), Freitas et al. (2018), Freitas and Macau (2018), Noetel et al. (2018a), Noetel et al. (2018b), Freitas et al. (2019, Submitted).

Other publications from this period, but not directly related to the thesis content are: Freitas et al. (2017), Freitas et al. (2019).

1.3 Thesis organization

The thesis is organized as follows: Chapter 2 introduces some theoretical definitions about dynamical systems, oscillators, synchronization, numerical integration and evolutionary optimization. Some introductory material is presented in Chapter 3 about collective motion systems, in which we introduce and discuss aspects of the phenomenological reactive model and the model of particles with coupled-oscillator dynamics. In the first case, particles follow bio-inspired interaction rules and non-unitary speed. The second model is focused on the specific case of particles moving in circular trajectories and grouping in symmetric clusters. After this theoretical-based chapters, we present in Chapter 4 the first part of our results: a reactive model for autonomous vehicles formation following a mobile reference with corresponding simulations and control strategies. Chapter 5 is devoted to the study of the model of particles with coupled-oscillator dynamics. Finally, robot simulations are shown in Chapter 6 with the model of symmetric circular formations, followed by the Conclusions in Chapter 7.

2 DYNAMICAL SYSTEMS, SYNCHRONIZATION AND EVOLUTIONARY OPTIMIZATION

This Chapter aims to present and discuss some aspects of the theory of dynamical systems, phase-coupled oscillators, and synchronization, which are the grounding for the thesis understanding. Furthermore, we present Evolutionary optimization techniques that are used in due course.

Systems composed of phase-coupled oscillators are nonlinear and with a high number of variables. This class of problem was considered a great challenge in the last two decades (STROGATZ, 1994) and is a trend nowadays (FREITAS et al., 2015b; O'KEEFFE et al., 2017; PETER; PIKOVSKY, 2018; JAIN; GHOSE, 2018; PETER et al., 2019)

Before diving into coupled oscillators, let us start with some dynamical system definitions. Consider the system of ordinary differential equations (ODE):

$$\dot{x} = f(x) \tag{2.1}$$

with $f : \Omega \subseteq \mathbb{R}^m \rightarrow \mathbb{R}^m$, Ω open, $f \in C^1(\Omega)$.

Theorem 1. (*Lyapunov Stability*) *Let x^* be an equilibrium point for (2.1). Let $V : \mathcal{O} \rightarrow \mathbb{R}$ be a differentiable function defined on an open set \mathcal{O} containing x^* . Suppose further that*

a) $V(x^*) = 0$ and $V(x) > 0$ if $x \neq x^*$;

b) $\dot{V} \leq 0$ in $\mathcal{O} - x^*$.

Then x^ is stable. Furthermore, if V also satisfies:*

c) $\dot{V} < 0$ in $\mathcal{O} - x^*$,

then x^ is asymptotically stable.*

A function V satisfying (a) and (b) is called a Lyapunov function for x^* . If (c) also holds, we call V a *strict* Lyapunov function (HIRSCH et al., 2004).

There is no technique for Lyapunov function generation for a given system, but some kinds of functions are natural candidates, like potentials. The model of particles with coupled-oscillator dynamics of Section 3.3 is built from potential functions and its stability is guaranteed from their analysis.

2.1 Gradient systems

This section briefly presents the Theory of Gradient Systems that is used in the rest of this chapter¹. Gradient systems are differential equations that have the form

$$\dot{x} = \frac{dx}{dt} = -\frac{\partial V(x)}{\partial x} \quad (2.2)$$

with $V : \mathbb{R}^n \rightarrow \mathbb{R}$ a C^∞ function, and

$$\frac{\partial V}{\partial x} = \left(\frac{\partial V}{\partial x_1}, \dots, \frac{\partial V}{\partial x_n} \right). \quad (2.3)$$

Let the system with $x(0) = x_0$ have solution $x(t)$ and $\dot{V} : \mathbb{R}^n \rightarrow \mathbb{R}$ be the derivative of V along $x(t)$, so that

$$\dot{V}(x) = \frac{d}{dt} V(x(t)). \quad (2.4)$$

Proposition: The function V is a Lyapunov function for the system $\dot{x} = -\partial V/\partial x$. Moreover, $\dot{V} = 0$ if and only if x is an equilibrium point.

Proof:

$$\dot{V}(x) = \frac{dV(x)}{dt} = \frac{\partial V(x)}{\partial x} \left(-\frac{dx}{dt} \right) = - \left| \frac{\partial V}{\partial x} \right|^2 \leq 0. \quad (2.5)$$

In particular, $\dot{V}(x) = 0$ if and only if $V(x) = 0$. □

Thus, V decreases towards zero and converges to the equilibrium point at $\dot{x} = 0$.

In summary, if one can build a Lyapunov function to a system, it is possible to lead it to equilibrium through the Theory of Gradient Systems. The next section presents the so-called Phase-coupled oscillators and we show that certain models have a Gradient structure.

¹For a more detailed description, please refer to [Hirsch et al. \(2004, p. 203\)](#) and [Strogatz \(1994, p. 30\)](#)

2.2 Phase-coupled oscillators

Christiaan Huygens, physicist and inventor of the pendulum clock, observed the synchronization phenomena involving two suspended clocks on the wall, in the 17th century. After some transient, they showed the same motion that remained stable even under small perturbations. Huygens then started to perform a series of experiments that resulted in the beginning of the *Theory of coupled oscillators* (STROGATZ; STEWART, 1993).

In southeast Asia, one can find male fireflies flashing on and off in unison in an attempt to attract females (STROGATZ, 1994). Other examples are the synchronization of menstrual cycles due to some interpersonal physiological process, hand clapping in a crowd and neurons of a Parkinsonian patient.

From the engineering perspective, a well-known case is the swaying of the Millennium bridge during its opening due to the large number of pedestrians that somehow synchronized their gaits (STROGATZ et al., 2005). In Neuroscience, scientists are working on strategies to control the onset and breakage of synchronization in specific brain regions to deal with epileptic seizures, Parkinson disease and to improve some cognition processes (JIRUSKA et al., 2013; PROTACHEVICZ et al., 2019).

In the late sixties, Winfree started to work with the theory of nonlinear oscillators in biology (WINFREE, 1967). In the eighties, Kuramoto (1984) formalized the theory of coupled-oscillators that is nowadays used as a paradigm of coupled dynamical systems, with the famous Kuramoto model.

The interplay among oscillators has a parallel with the spring-mass system. When the spring is not at its resting position, the (deformation) force F_d drives the spring towards a stretched or contracted form. When the spring is released from this point, it right away moves to the opposite direction, under a restoring force F , toward the equilibrium.

Intuitively, one can tell that the further away a spring is stretched (or squeezed) the higher is the associated energy. This is the so-called potential energy $U(x)$, that can be associated with the deformation distance x , with $U(0) = 0$ and $U(x) > 0$ for $|x| > 0$.

If the $U(x)$ is known then

$$F_x = -\frac{dU}{dx}$$

is the force associated with each x . The minus sign represents the spring attempt to return to its resting position, i.e., the force pushes the object back to lower potential.

The coupled oscillators tend to the equilibrium when proper coupling function and strength are chosen so that it lowers the associated potential function. It is worth mentioning that this thesis deals with systems whose vector field is on a circle $\dot{\theta} = f(\theta)$, which is a special case of a vector field on the line. The notation $\theta \in S^1$ means that $\theta = \theta + 2\pi n$ for $n \in \mathbb{Z}$.

2.2.1 Two coupled oscillators

Before starting the discussion about many phase-coupled oscillators, let us first discuss a simple case of two coupled oscillators:

$$\dot{\theta}_1 = \omega_1 + K_1 \sin(\theta_2 - \theta_1) \tag{2.6a}$$

$$\dot{\theta}_2 = \omega_2 + K_2 \sin(\theta_1 - \theta_2) \tag{2.6b}$$

with θ_1 and θ_2 the respective phases, ω_1 and ω_2 their natural oscillating frequencies and K_1 and K_2 the coupling strength. The phase space is the Torus $S^1 \times S^1$.

Initially, let's consider the uncoupled case with $K_1 = K_2 = 0$, so that

$$\begin{aligned} \dot{\theta}_1 &= \omega_1 \\ \dot{\theta}_2 &= \omega_2 \end{aligned} \tag{2.7}$$

Two possibilities may occur:

- a) $\frac{\omega_1}{\omega_2} = \frac{p}{q} \in \mathbb{N}$: all trajectories are closed, so that θ_1 makes q full rotations and θ_2 makes p full rotations to close the orbit.
- b) $\frac{\omega_1}{\omega_2}$ is irrational: trajectories never intersect nor close, which means that they are dense on torus.

When the system is coupled as in Equation (2.6), one might observe: i) $\dot{\theta}_1 = \dot{\theta}_2$ (phase-locking) i.e. the relative distance between phases is fixed; ii) out of sync solutions. When the frequencies are the same, the phases may synchronize and exhibit the very same value after some transient of interactions, characterizing the so-called full synchronization.

2.2.2 N phase-coupled oscillators

The interactions in a system of coupled oscillators are characterized by coupling, delay and topology (MALLADA; TANG, 2013). Equation (2.8) presents an example

$$\dot{\theta}_i(t) = f(\theta_i(t)) + \kappa \sum_{j=1}^N A_{ij} \Gamma(\theta_j(t) - \theta_i(t)) \quad (2.8)$$

where $i = 1, \dots, N$, $\kappa > 0$ is the coupling strength, and A is the adjacency matrix, such that $A_{ij} = 1$ if there is a connection between i and j , or $A_{ij} = 0$ otherwise. The function $f(\theta_i(t))$ describes the internal dynamics of each oscillator and Γ is the coupling function.

The oscillators eventually synchronize when under certain conditions. We understand synchronization as “an adjustment of rhythms of oscillating objects due to their weak interaction” (PIKOVSKY et al., 2001). For instance, when the coupling strength is high enough, the oscillators achieve synchronized states (STROGATZ, 2000).

Many works on this field mention that the coupling (interaction) is “weak”. This comes from the fact that the coupling strength should not be so big that the individual behavior of the oscillators is totally suppressed. Otherwise, one could argue that it is about a unique system, instead of many coupled parts. Still, it means that one expects the internal dynamics $f(\theta_i(t))$ not to be irrelevant in view of the coupling term.

When two oscillators are identical, there are only two kinds of phase synchronization: *in-phase* and *anti-phase* (STROGATZ; STEWART, 1993). The term *in-phase* refers to complete synchronization, when phases converge to the same value. Two oscillators establish an *anti-phase* synchronization if their derivatives have the same modulus but different sign: $\dot{\theta}_1 = a$ e $\dot{\theta}_2 = -a$. Thus, their motion are similar but opposite, similar to two pendulums moving in opposite directions.

A third possibility is the *phase-locking*, which happens when oscillators are not identical. Phases oscillate together at the same pace $\dot{\theta}_i$ but do not converge to the same state. They keep fixed relative states.

The Kuramoto model (KURAMOTO, 1984) is described by

$$\dot{\theta}_i = \omega_i + \frac{K}{N} \sum_{j=1}^N A_{ij} \sin(\theta_j - \theta_i). \quad (2.9)$$

which resembles the form of Equation (2.8).

This system presents various behaviors that depend on the coupling strength K , synchronizing when $K > K_c$, for a given critical K_c and an all-to-all type adjacency matrix (STROGATZ, 2000).

When the coupling function Γ_{ij} of Equation (2.8) is symmetric and odd, the effect of oscillator j on i has the same magnitude but opposite sign in contrast to oscillator i on j . It means that $\Gamma_{ij}(\theta_k - \theta_i) = \Gamma_{ji}(\theta_k - \theta_i) = -\Gamma_{ij}(\theta_i - \theta_k)$ (MALLADA; TANG, 2013). Two coupled phases move towards each other with same magnitude but different direction. Besides, one foresees that the influence on an oscillator upon itself is null: $\Gamma_{ij}(\theta_k - \theta_k) = 0$. The sine function holds all the discussed characteristics and is therefore a natural candidate for a coupling function of phase oscillators.

One special synchronization measure is the Kuramoto order parameter

$$p_\theta = |p_\theta| e^{i\psi} = \frac{1}{N} \sum_{i=1}^N e^{i\theta} \quad (2.10)$$

where $|p_\theta| \in [0, 1]$ with $|p_\theta| = 1$ when the phases are synchronized and $p_\theta = 0$ when they are balanced.

The Kuramoto model has a so-called gradient structure. One may define a potential from the order parameter so that it is minimum when phases are balanced, and positive otherwise. Consider the special case in which the frequencies are zero $\omega_1 = \dots = \omega_N = 0$:

$$V(\boldsymbol{\theta}) = \frac{1}{2} |p_\theta|^2. \quad (2.11)$$

This is a Lyapunov function and the next step is to calculate its gradient

$$\dot{\boldsymbol{\theta}} = -\nabla V(\boldsymbol{\theta}). \quad (2.12)$$

The contribution of every single oscillator in the system can be computed with the corresponding partial derivatives:

$$\dot{\theta}_j = -\frac{\partial V(\boldsymbol{\theta})}{\partial \theta_j} = \frac{1}{N} \sum_l^N \sin(\theta_l - \theta_j), \quad j = 1, \dots, N. \quad (2.13)$$

The phase space of the Kuramoto system can be considered as $S^1 \times S^1 \times \dots \times S^1 = \mathbb{T}^N$, the N -th torus, with solutions $\theta(t)$ moving towards the minimum of V , that means $\theta_1 = \theta_2 = \dots = \theta_N$.

Now, if we consider nonzero frequencies, the system becomes:

$$V(\boldsymbol{\theta}) = \frac{1}{2} |p_{\boldsymbol{\theta}}|^2 - \boldsymbol{\omega} \boldsymbol{\theta}, \quad (2.14)$$

with $\boldsymbol{\theta} = (\theta_1, \dots, \theta_N)$, $\boldsymbol{\omega} = (\omega_1, \dots, \omega_N)$,

with derivatives

$$\dot{\theta}_j = \omega_j + \frac{1}{N} \sum_l^N \sin(\theta_l - \theta_j), \quad j = 1, \dots, N. \quad (2.15)$$

Remark that it has no longer a gradient structure on \mathbb{T}^N , but on \mathbb{R}^N due to the $\boldsymbol{\omega} \boldsymbol{\theta}$ term.

2.3 Delayed phase oscillators

This section deals with the problem of delayed communication between neighboring oscillators. An example is the problem faced by soccer fans in a stadium. When they try to clap hands in unison, they do so from a local point of view, although the sound reaches far places with a certain time lag. This happens due to the finite sound speed and the fan has locally a sensation of global synchrony. Other examples are electronic, mechanic, biological and chemical systems. The delay corresponds to transport time (earth shock waves, fluids in a chemical process, space electromag-

netic radiation, etc) (HALE; LUNEL, 1993; YEUNG; STROGATZ, 1999; ERNEUX, 2009; ERNEUX et al., 2017; YANCHUK; GIACOMELLI, 2017).

This problem may be modeled as Delay Differential Equations (DDE) as follows

$$\dot{x} = F(t, x(t), x(t - \tau)) \quad (2.16)$$

in which $x(t) = \phi(t)$ is the initial condition, with $-\tau \leq t \leq 0$. Notice that, differently from the ODE, the DDE has a function as the initial condition and not a point. This function corresponds to a system history, given that it is necessary to possess the solution at time $t - \tau$ to integrate the system at time t .

A system of phase-coupled oscillators with delay τ is

$$\dot{x}_i = f(x_i(t)) + \kappa \sum_{j=1}^N A_{ij} \Gamma(x_j(t - \tau) - x_i(t)). \quad (2.17)$$

Yeung and Strogatz (1999) studied a noisy and delayed Kuramoto model and realized that when the delay is “small” the stability of the system is not affected. They considered both delay and coupling strength as control parameters. From a quantitative point of view, it is hard to establish what is a big or small delay, because it depends on the studied system (YANCHUK; GIACOMELLI, 2017). Furthermore, big delays may even help synchronization (MALLADA; TANG, 2013).

We will show later in Section 5.5 some results with isochronous synchronization, that is when the oscillators reach synchronization under delayed communication (GRZYBOWSKI et al., 2012).

2.4 Chaotic systems and Lyapunov exponents

“Chaos is aperiodic long-term behavior in a deterministic system that exhibits sensitive dependence on initial conditions” (STROGATZ, 1994). This means the trajectories are not attracted to fixed points, periodic or quasiperiodic orbits. Moreover, very close neighboring trajectories separate exponentially in average from each other and have different futures. One way to check whether the system has a chaotic signature is to compute its Lyapunov exponent, which measures the sensitivity of initial conditions.

Given some initial condition x_0 of a one-dimensional map and a nearby point $x_0 + \delta_0$, with small δ_0 , consider that after n iterations, the separation between the points is δ_n . We estimate that $|\delta_n| \approx |\delta_0|e^{n\lambda}$ and call λ the Lyapunov exponent. When the neighboring points converge after some transient of integration, it means that the system is stable and has negative λ . Nonetheless, positive λ is a signature of chaos (STROGATZ, 1994).

Firstly, lets compute $\delta_n = f^n(x_0 + \delta_0) - f^n(x_0)$. In this sense,

$$\lambda \approx \frac{1}{n} \ln \left| \frac{\delta_n}{\delta_0} \right| = \frac{1}{n} \ln \left| \frac{f^n(x_0 + \delta_0) - f^n(x_0)}{\delta_0} \right|. \quad (2.18)$$

Considering that $\delta_0 \rightarrow 0$, we have

$$\lambda \approx \frac{1}{n} \ln |(f^n)'(x_0)|. \quad (2.19)$$

From the chain rule,

$$(f^n)'(x_0) = \prod_{i=0}^{n-1} f'(x_i)$$

which leads to

$$\lambda \approx \frac{1}{n} \ln \left| \prod_{i=0}^{n-1} f'(x_i) \right| = \frac{1}{n} \sum_{i=0}^{n-1} \ln |f'(x_i)|$$

In the limit of $n \rightarrow \infty$, a trajectory with infinite length, the Lyapunov exponent is given by:

$$\lambda = \lim_{n \rightarrow \infty} \left\{ \frac{1}{n} \sum_{i=0}^{n-1} \ln |f'(x_i)| \right\}. \quad (2.20)$$

2.5 Numerical integration

This section presents the 4th order Runge-Kutta (RK4), a method for numerical integration of systems of ODEs (ZIEGEL et al., 2007):

$$\dot{y} = f(t, y), \quad y(t_0) = y_0. \quad (2.21)$$

We first discretize the integration time in steps of size h , so that $y_n = y(t_0 + nh)$.

The simplest way to integrate it is by using the so-called Euler method, that adds the derivative at the beginning of the interval to the current state:

$$y_{n+1} = y_n + hf(t_n, y_n), \quad (2.22)$$

being a first-order approximation for the problem. Other methods explore more sub-intervals within the step size h , like the Runge Kutta of 4th order:

$$y_{n+1} = y_n + \frac{1}{6}(k_1 + 2K_2 + 2k_3 + k_4), \quad (2.23a)$$

$$t_{n+1} = t_n + h \quad (2.23b)$$

$n = 0, 1, 2, \dots$, where

$$k_1 = hf(t_n, y_n), \quad (2.24a)$$

$$k_2 = hf\left(t_n + \frac{h}{2}, y_n + \frac{k_1}{2}\right), \quad (2.24b)$$

$$k_3 = hf\left(t_n + \frac{h}{2}, y_n + \frac{k_2}{2}\right), \quad (2.24c)$$

$$k_4 = hf(t_n + h, y_n + k_3). \quad (2.24d)$$

The y_{n+1} is the approximation of $y(t_{n+1})$, which depends on the present value y_n and the weighted average of four increments. The k_1 term corresponds to the Euler method, k_2 is an approximation of the midpoint between $t_n + \frac{h}{2}$ with k_1 representing the y component, k_3 is an approximation of the same point with k_2 as y and lastly k_4 is an approximation of the end of the interval $t_n + h$, using k_3 as y .

The error is of order $O(h^5)$, which means that the Euler method for a step size $h = 0.1$ presents errors of order 0.1 and the Runge Kutta of 10^{-5} . Although it

demands four times the calculation of function approximations, the gain is way bigger in regard to the error.

For the numerical integration of DDEs, we use the same method, however with some implementation differences. Assuming that the delay τ is known, one must store past calculated values of y from time $t - \tau$ to t . In this thesis, we use a queue of size $T = \tau/h$, that always discard the oldest element y_{n-T} whenever receiving a new y_{n+1} . Then, every time one needs to compute the DDE (2.16), the corresponding $y(t - \tau)$ is available.

From here on we use the time notation with a subscript of the form $t - \tau = t_{n-T}$. Rewriting (2.24) for the DDE integration, gives:

$$k_1 = hf(t_{n-T}, y_{n-T}), \quad (2.25a)$$

$$k_2 = hf\left(t_{n-T+\frac{1}{2}}, y_{n-T} + \frac{k_1}{2}\right), \quad (2.25b)$$

$$k_3 = hf\left(t_{n-T+\frac{1}{2}}, y_{n-T} + \frac{k_2}{2}\right), \quad (2.25c)$$

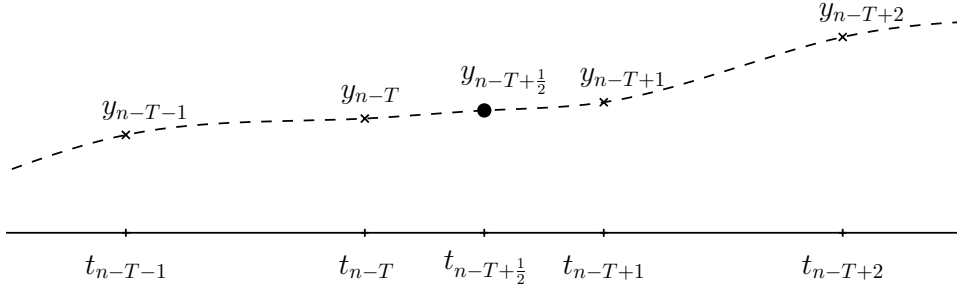
$$k_4 = hf(t_{n-T+1}, y_{n-T} + k_3). \quad (2.25d)$$

As mentioned before, $f(t_{n-T}, y_{n-T})$ is known (stored in the queue), so we always have k_1 . The same happens for k_4 , since we have the state at t_{n-T+1} . The problems arise when we compute k_2 and k_3 , because only time instants that are multiples of h are stored and here we would need also $t_{n-T+\frac{1}{2}}$. We overcome this problem with a polynomial interpolation F (ZIEGEL et al., 2007) that depends on four states, so that $y_{n-T+\frac{1}{2}} = F(y(t_{n-T-1}), y(t_{n-T}), y(t_{n-T+1}), y(t_{n-T+2}))$. The desired state seats exactly at the middle point of the considered time frame, as shown in Figure 2.1.

2.6 Evolutionary optimization

The basic structure of Evolutionary algorithms consists of selecting an initial population, applying random modifications (also referred to as mutation) and evolutionary operations into the individuals, evaluation according to a fitness criterion (objective function) and selection of the next generation (FOGEL, 2006). In this section, the word “population” refers to individuals of evolutionary algorithms and not the agents of our model. As a matter of fact, the most well known evolutionary algorithm is the Genetic Algorithm (GA) (GOTMARE et al., 2017).

Figure 2.1 - Interpolation $y_{n-T+1/2} = F(y(t_{n-T-1}), y(t_{n-T}), y(t_{n-T+1}), y(t_{n-T+2}))$ using the four closest points. The desired point has symbol ‘o’.



SOURCE: Produced by the author.

A member of the population is composed of the variables used for the calculation of the objective function, the “design variables”. Their values change over time according to evolutionary operations such as mutation and crossover. These operations alter the characteristics of an individual or combine pairs of individuals to generate new ones. The aim is to seek the most adapted solutions for the problem, taking into account the direction of maximization or minimization of the chosen objective function.

The two optimization algorithms we use are the *Generalized Extremal Optimization* (GEO) (DE SOUSA et al., 2003) for mono objective purpose, and the *Multiobjective Generalized Extremal Optimization* (M-GEO) (CUCO et al., 2011), for multiple functions. DE SOUSA et al. (2003) showed that GEO is competitive with GA and its main advantage over other algorithms is the need of adjusting only a few parameters.

2.6.1 Generalized Extremal Optimization

This section describes the Generalized Extremal Optimization (GEO), a global search metaheuristic used for complex optimization problems. DE SOUSA et al. (2003) introduce the canonical GEO and a variation, the GEO_{var} . In the former, only one evolutionary operation is carried out in the design variables per iteration. The latter, on the other hand, executes one operation per variable, which results in bigger jumps in the search space than in the canonical GEO. When the problem has a highly constrained design space, GEO seems to perform better than GEO_{var} , since the solutions tend not to leave the feasible area of the design space during the search. However, for problems with only lateral constraints the solutions remain

in the feasible area during all the time. Under those conditions, GEO_{var} converges faster than the canonical GEO (DE SOUSA et al., 2003).

Every solution is constituted of a sequence of bits in which each element is called an individual of the population. Yet, the binary representation of these variables must meet a precision requirement that is application dependent. The minimum number of bits m necessary to obtain a desired precision p is given by

$$2^m \geq \lceil (x_j'' - x_j')/p + 1 \rceil, \quad (2.26)$$

for x_j' and x_j'' are the lower and upper bounds, respectively of variable j , with $j \in \{1, 2, \dots, M\}$.

The conversion from the binary representation to the correspondent decimal number is

$$x = x_j' + (x_j'' - x_j') \cdot \frac{\sum_{i=1}^m b_i \cdot 2^{i-1}}{(2^m - 1)} \quad (2.27)$$

in which x is the decimal number and b_i is the bit value in the i -th position of the string, from right to left.

One solution is the concatenation of the sequences of bits that correspond to each design variable. It has L bits of length from M variables of L/M bits each, all randomly chosen at the beginning.

The GEO_{var} algorithm works as follows (CUCO et al., 2011):

1. For each bit, flip its value, calculate the objective function V_i , and compute the gain or loss $\Delta V_i = (V_i - V_{ref})$, when compared to the best value V_{ref} achieved so far. After each calculation, return the bit to the original value.
2. For each variable, rank the bits from the most adapted ($k = L/M$) to the least ($k = 1$), considering the obtained ΔV_i . If two or more bits have the same fitness, rank them randomly. Remark that the canonical GEO ranks the bits for the entire sequence and not per variable.
3. The mutation operation is proportional to the following power-law probability

distribution:

$$P_i(k) = k^{-\tau} \quad (2.28)$$

for $\tau > 0$ the only free parameter. The more adapted a bit is the less likely it is to flip. For each variable, one chooses a candidate bit i with uniform distribution, then generates a random number $\text{RND} \in [0, 1]$. If $P_i(k) \geq \text{RND}$, the bit is flipped. Otherwise, one chooses another bit and generates RND again. The process repeats until one bit is flipped in each variable. The reason why it is possible to flip bits that correspond to well-adapted solutions resides on the necessity of avoiding local minima. Sometimes the solutions must degrade a little to glimpse the global optimum.

4. Save the best results and perform the steps 1 to 3 until meeting stop criteria, that can be: the maximum number of objective function evaluations (NFE), iterations of the GEO_{var} , or a desired value of the objective function.

2.6.2 Multiobjective Generalized Extremal Optimization

As an extension of the GEO algorithm, the Multiobjective Generalized Extremal Optimization (M-GEO) (CUCO et al., 2011) is concerned with the problem of optimizing multiple objective problems at a time. In this instance, there can exist more than one optimum, and these values constitute the so-called *Pareto Frontier*, whose number of dimensions corresponds to the number of objective functions.

One objective function is randomly chosen at every algorithm iteration and evolutionary operations are performed alike in GEO. In contrast to mono-objective problems, the M-GEO must keep a set of trade-off solutions known as Pareto Frontier. They may all be considered optimal because every single solution is better than the others in at least some specific objective function.

Another characteristic of M-GEO is the possibility of restarting the population during the search. In addition to the parameter τ , one sets the number of times η the population will restart during the simulation and the maximum number of objective functions' evaluations NFE . This is important to build a more robust Pareto set, with a variety of solutions, and results in NFE/η evaluations in total for each new population.

2.7 Conclusions

This Chapter presented selected elements from the theory of Dynamical Systems, gradient systems, phase-coupled oscillators, synchronization, time delay, numerical integration, and evolutionary optimization. Moreover, we showed that the classic Kuramoto model of coupled oscillators has a gradient structure, the principle behind the system of particles with phase-coupled oscillators dynamics that we study hereafter.

3 COLLECTIVE MOTION SYSTEMS

This Chapter presents systems of mobile agents that work together towards a common task. We first introduce the unicycle model, common in mobile robotics and particle systems, which is used hereafter. Following, we present a Reactive model with bio-inspired weighted interaction rules, whose coefficients are chosen with a heuristics algorithm. Finally, we discuss a model of particles with phase-coupled oscillator dynamics.

3.1 Unicycle models

A unicycle-type model is characterized by agents having some forward speed but zero instantaneous lateral motion, a non-holonomic system. The unicycle robot can only turn right or left and cannot perform the lateral motion. Instead, a holonomic agent can navigate from any state to any other.

The unicycle model can be described as:

$$\begin{aligned}\dot{x} &= v \cos(\theta(t)) \\ \dot{y} &= v \sin(\theta(t)) \\ \dot{\theta} &= \omega\end{aligned}\tag{3.1}$$

so that $[x, y]^T \in \mathbb{R}^2$ are the coordinates, v is the forward speed, θ is the heading angle and ω is the angular velocity. When ω is constant, the particle moves in circles.

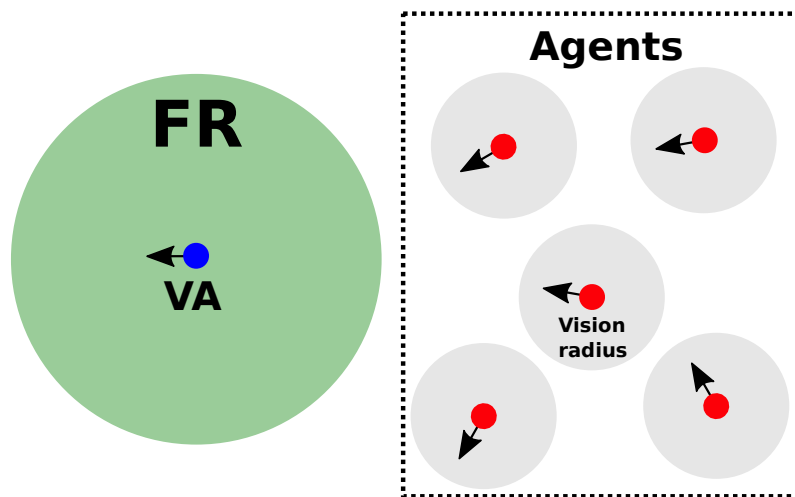
3.2 Reactive model for autonomous vehicles formation following a mobile reference

This Section presents a model of mobile agents that group into a certain neighborhood and follow a mobile reference (FREITAS, 2016; FREITAS; MACAU, 2017b; FREITAS et al., 2018). The elements are considered reactive because they respond to the stimuli from nearby agents in the form of heading angle adjustments. It is inspired by the alignment, attraction and repulsion rules of Reynolds' *boids* (REYNOLDS, 1987).

Each agent has a vision radius around itself within which the neighbors are perceived. Besides the interactions, the agent also follows the so-called virtual agent (VA), a non-real agent that dictates the trajectory to be chased, as shown in Figure 3.1. The

VA can be thought of as a changing in time GPS signal that shows the trajectory to be followed by all the agents. The model groups the agents around the VA, while it moves to predefined directions. In a real-world scenario, this model can be used before turning to other models that require the agents to be close to each other. Also, it is important in applications that require the agents to move in specific paths, for example surveillance, area monitoring, chasing a specific target, imaging from multiple points, etc.

Figure 3.1 - Initial conditions of a simulation scenario, with agents represented in red, their vision radii in gray, and the VA in blue. Agents are randomly placed inside the dotted area when the simulation begins, with random associated velocities.



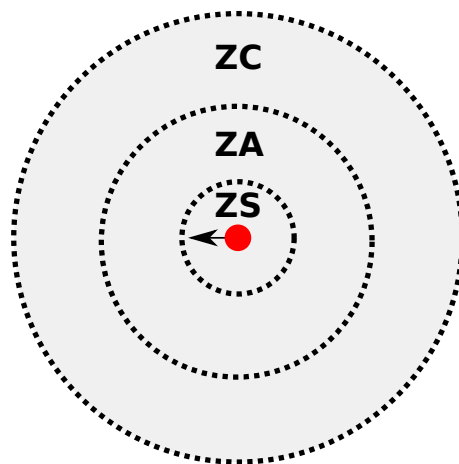
SOURCE: Produced by the author.

The interaction rules take place according to the neighbors' positions concerning the agent. The vision radius is divided into layers of specific radii, called *perception zones* as Figure 3.2 presents. Such zones first appeared in Couzin et al. (2002) as an attempt to capture the behaviors observed in groups of fish (HERBERT-READ et al., 2011), to keep the group cohesion.

The agents also have different speeds depending on whether they are close to the VA or not. The seminal work of Reynolds (REYNOLDS, 1987) considers unitary speed, which does not agree with agents closely following a mobile reference as in our case. One agent must accelerate to reach the group and be close enough to the VA.

The dynamics of the model is dictated by a linear combination of five interaction

Figure 3.2 - Perception zones. Zone of Separation (ZS), Zone of Alignment (ZA) and Zone of Cohesion (ZC).



SOURCE: Produced by the author.

rules that influences the direction changes on the agent's heading angle, exclusively. Besides, speed adjustments depend on its position concerning the VA.

This model is called reactive because it follows the architecture of reactive multi-agent systems, in which the agents do not keep memory from previous interactions (RUSSEL; NORVIG, 2010). They basically react to the current environment state at a discrete time.

The aim is to make the agents flock together in parallel following a moving reference, the so-called VA, maintaining their position in a certain range around it, wherever it goes. For this purpose, the agents interact with each other according to specific rules that impose group alignment, cohesion, collision avoidance, and VA tracking. We call them “virtual forces” or only “forces” because they represent the effect over each agent caused by its neighbors and VA states. An individual changes its heading angle based on what it perceives so the external stimuli applies some kind of “virtual force” on it.

This model first appeared in Freitas (2016) and Freitas and Macau (2017b), in which we defined strategies for the usage of the virtual forces. The main drawback is that we considered a limited set of forces' combinations and analyzed the possible model behaviors based on a few combinations of parameters. Those problems are addressed here with a more general model definition and a further introduction in Chapter 4 of quantifiers that characterize some desired configurations.

To elucidate the role of VA, we introduce a discussion about leadership. Shen (2007) describes a system with Hierarchical Leadership (HL), whose members can be ordered in such a way that lower-rank agents are led and only led by agents of higher rank. This hierarchy can emerge in two manners: passively or actively.

The former is built when an event occurs and the agent's reaction propagates to its neighbors, eventually reaching others in a wave-like form. In this case, the leader with higher rank will be the one who first reacts, and the other ranks are assigned according to the time response to this event. It means that the last agents to react will be led by the others. On the other hand, in an active HL, each agent has its role previously stated, as in military environments. It means the same agents always lead their subordinates.

One assumption of HL models is that the agents have the same dynamics but their state changes depend on their leaders with higher rank. In a specific case in which we have one agent with privileged information, and it is the only leader, one can assume the system as having an HL with two levels.

Albi et al. (2014) presents a model with two kinds of agents, the leaders, and the followers. The leaders' behavior is influenced by both the desire to achieve a prescribed opinion consensus and the mean opinion of the followers. Their model also includes the case of leaders that do not interact with the followers' population. In the absence of diffusion, each agent of the leaders' population reaches the target opinion and at the same time the followers may comply with them under suitable assumptions on the interaction function.

Our VA may be thought of as a leader, although it does not fit the aforementioned scenarios. Its dynamics is not related to the ordinary agents and it is not influenced by them. Besides, it is not an actual agent, but a trajectory for the agents to follow. For example: consider one wants to take several photos of an area, using a few UAVs (unmanned aerial vehicles) which have to follow a trajectory that covers the area. In this particular case, this trajectory must be time-integrated and its position is passed to the UAVs. Here, the UAVs are the agents and the trajectory is the VA.

The VA could be considered a real agent in the framework of an HL of two levels as the only leader. One application is a suspect over persecution (leader), represented by the VA being followed by other agents like cars, UAV's, drones, etc. Therefore, it should be included in the calculation of the collision avoidance routine.

The model dynamics is described in Equation (3.2):

$$\begin{aligned}\dot{x}_i &= s_i(t) \cos(\theta_i(t)) \\ \dot{y}_i &= s_i(t) \sin(\theta_i(t)) \\ \dot{\theta}_i &= F^i(t)\end{aligned}\tag{3.2}$$

where $[x_i, y_i]^T \in \mathbb{R}^2$ is the i -th agent's position, $s_i(t)$ is its speed, $\theta_i(t)$ is its heading angle and $F^i(t)$ represents the action of the virtual forces. This last term is a linear combination of five interaction rules, that will be conveniently shown later.

Figure 3.1 sketches N agents randomly positioned inside a certain area and the VA aside, like the initial conditions for the simulations of Chapter 4. The region around the VA is the *Formation Region* (FR), where agents are attracted after some transient and remain. Yet, it delimits where the group must be in order to end up with a tight formation following the VA closely. The *body length* (bl) of an agent is the diameter of the red circle, which is the same for all of them. This unit is later used to describe its speed.

The VA moves at constant speed s_{va} , and the i -th agent regulates its speed $s_i \in [s_{va}, s_{out}]$ depending on whether it is inside or outside the FR, in which s_{out} is the maximum speed the agent is able to reach, i.e., it is a physical aspect that depends on the hardware. When the agent is outside the FR its maximum speed is $s_{out} > s_{va}$, because it needs to reach the VA. On the other hand, when it is inside, its speed converges to s_{va} .

When entering the FR, the agent decreases its speed from its current value $s_i(t)$ to s_{va} as described in Equation (3.3):

$$s_i^d(t) = s_{va} - \frac{(s_{ini} - s_{va})(t - t_i^f)}{\Delta t_i},\tag{3.3}$$

with s_{ini} the agent speed at the moment it starts entering the VA.

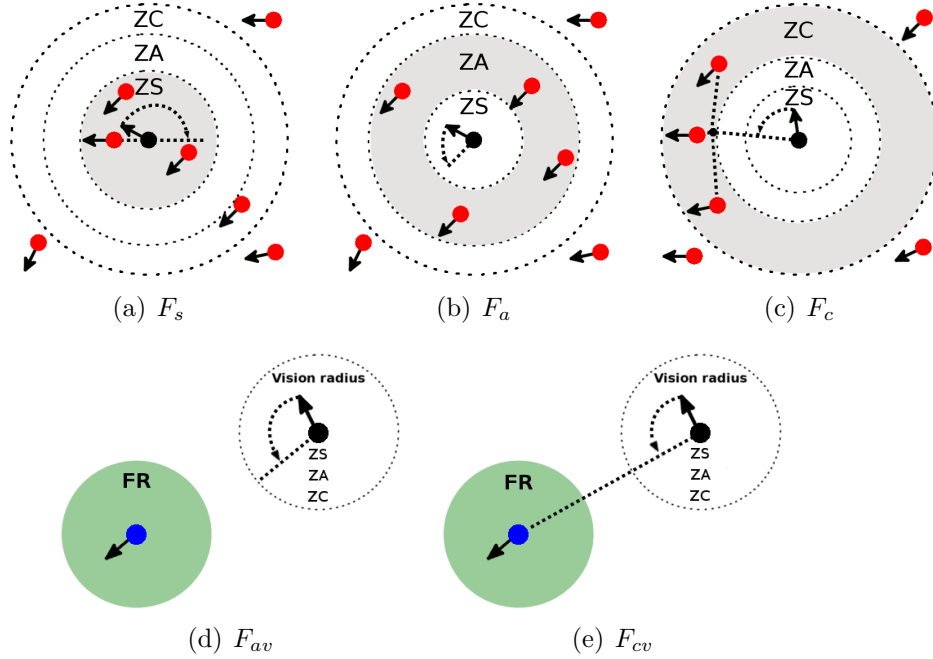
At each time unit of the deceleration process, the agent's speed is given by $s_i(t) = s_i^d(t)$. Still, when the agent leaves the FR, it accelerates from $s_i(t)$ to s_{out} according to $s_i(t) = s_i^a(t)$:

$$s_i^a(t) = s_{out} + \frac{(s_{out} - s_{ini})(t - t_i^f)}{\Delta t_i}. \quad (3.4)$$

In both situations, the speed change is not instantaneous but takes a random time $\Delta t_i \sim U(0, 2\bar{t})$ to happen. It follows a uniform distribution that gives the total time the agent i takes to adjust its speed. The \bar{t} is an empirical approximation of the time that the agent takes to reach the VA at constant speed $s_i = s_{out}$, departing from the FR fringe. That is, the time it takes from the border of the FR until reaching the VA. The intention is to uniformly distribute the agents inside the region. Each agent has its own Δt_i , although it does not depend on i . It possesses this index because, once generated, it is kept unchanged until the deceleration (or acceleration) finishes or the agent crosses the FR borders again. The term s_{ini} is the i -th agent speed at the time t_{ini} it crosses the FR border, and the time $t_i^f = t_{ini} + \Delta t_i$ is the time unit the speed regulation finishes. When $\Delta t_i = 0$ the speed changes instantaneously.

The virtual force $F^i(t)$ of Equation (3.2) is composed of five others that impose the agents some angle adjustments, i.e., angular velocity, resulting in changes of direction. The forces are: separation (F_s), alignment (F_a), cohesion (F_c), alignment with the VA (F_{av}) and cohesion with the VA (F_{ac}), depicted in Figure 3.3.

Figure 3.3 - Virtual forces. The dotted circumferences represent the vision radius constituted of the three perception zones of one agent (in black). The gray region in subfigures (a), (b) and (c) contains the neighbors used to calculate the forces F_s , F_a and F_c , respectively. At (d) and (e) the blue agent is the VA. F_s is calculated considering only the neighbors inside the zone of separation (ZS), F_a with the individuals inside the zone of alignment (ZA), and F_c with those inside the zone of cohesion (ZC).



SOURCE: Produced by the author. Appears in Freitas et al. (2018).

They are inspired by observations of groups of animals like birds and fish. Some species of fish increase their speed when a neighbor is far ahead (cohesion), decreases when it is too close (separation) and align with them for medium distances (KATZ et al., 2011). Following this principle, the calculation of each force depends not only on the heading angle differences but also on the relative positions between the agent and its neighbors, according to the perception zones of Figure 3.2. These zones are rings, i.e., they do not overlap, similar to the work of Couzin et al. (2002).

When a neighbor is present in the i -th agent's Zone of Separation (ZS), it computes the *separation* force F_s^i to adjust its heading angle to the opposite direction in relation to the neighbor. This angle adjustment is performed gradually each iteration until ZS is empty, as follows:

$$F_s^i(t) = f_{adj}(\theta_i, \theta_s + \pi) \quad (3.5)$$

with $\theta_s = \arctan(\Delta y / \Delta x)$, for $\Delta x = x_s - x_i$ and $\Delta y = y_s - y_i$. Coordinates $[x_i, y_i]^T \in \mathbb{R}^2$ are the i -th agent's position and $[x_s, y_s]^T \in \mathbb{R}^2$ are the neighbor's. The term f_{adj} corresponds to the step of the angle adjustment for one time unit. This formula leads a reference angle θ_{ref} until a target angle θ_{tgt} via Equation (3.6):

$$f_{adj}(\theta_{ref}, \theta_{tgt}) = \text{sign}(\Delta\theta_{ref,tgt} - \pi) \min(\gamma, |\Delta\theta_{ref,tgt} - \pi|) \quad (3.6)$$

in which $f_{adj} \in [-\gamma, \gamma]$, so that γ is the angular velocity that says how fast the agent is able to turn, i.e., hardware dependent. It is the maximum step that θ_{ref} is able to adjust to reach θ_{tgt} . A quantity is subtracted or added to θ_{ref} at each time unit. The signal of this operation is given by $\text{sign}(\Delta\theta_{ref,tgt} - \pi)$, and its intensity comes from $\min(\gamma, |\Delta\theta_{ref,tgt} - \pi|)$, whose maximum is γ . The term $\Delta\theta_{ref,tgt} \in [0, 2\pi)$ corresponds to the difference between the angles θ_{ref} and θ_{tgt} , according to Equation (3.7):

$$\Delta\theta_{ref,tgt} = (\theta_{tgt} - \theta_{ref} + \pi) \pmod{2\pi}. \quad (3.7)$$

As an example, the calculation of the separation force comprises $\theta_{ref} = \theta_i$ and $\theta_{tgt} = \theta_s + \pi$ and aims to decrease to zero the difference between θ_{ref} and θ_{tgt} . Yet it is important to highlight that both θ_i and θ_s change over time and there are moments in which there is no neighbor inside the ZS, resulting in $F_s^i(t) = 0$. The same happens to the $F_a^i(t)$ and $F_c^i(t)$, when there are not neighbors inside the Zone of Alignment (ZA) and Zone of Cohesion (ZC).

The alignment force F_a^i has the goal of aligning the heading angle of agent i with the average heading angles θ_{avg} of its neighbors inside the ZA (set \mathcal{N}_{ZA}), as follows:

$$F_a^i(t) = f_{adj}(\theta_i, \theta_{avg}), \quad \text{with} \quad \theta_{avg} = \frac{1}{|\mathcal{N}_{ZA}|} \sum_{j \in \mathcal{N}_{ZA}} \theta_j. \quad (3.8)$$

There is also a force F_{av} of alignment with the VA, that seeks to align the agent i with the VA's heading angle θ_a :

$$F_{av}^i(t) = f_{adj}(\theta_i, \theta_a). \quad (3.9)$$

The cohesion force F_c seeks to drive the agent i towards the center of mass of its neighbors \mathcal{N}_{ZC} from ZC, according to Equation 3.10:

$$F_c^i(t) = f_{adj}(\theta_i, \theta_{cm}), \quad (3.10)$$

in which $\theta_{cm} = \arctan(\Delta y / \Delta x)$, for $\Delta x = x_{avg} - x_i$ and $\Delta y = y_{avg} - y_i$. In this case, $[x_{avg}, y_{avg}]^T \in \mathbb{R}^2$ is the center of mass coordinates of the agent's neighbors, so that $x_{avg} = \frac{1}{|\mathcal{N}_{ZC}|} \sum_{j \in \mathcal{N}_{ZC}} x_j$, and $y_{avg} = \frac{1}{|\mathcal{N}_{ZC}|} \sum_{j \in \mathcal{N}_{ZC}} y_j$.

Similarly, the force F_{cv} of cohesion with the VA, given by Equation (3.11), leads the agent to move towards the VA's position according to

$$F_{cv}^i(t) = f_{adj}(\theta_i, \theta_{ca}), \quad (3.11)$$

where $\theta_{ca} = \arctan(\Delta y / \Delta x)$, for $\Delta x = x_a - x_i$ and $\Delta y = y_a - y_i$. The i -th agent's position is $[x_i, y_i]^T \in \mathbb{R}^2$ and $[x_a, y_a]^T \in \mathbb{R}^2$ are the VA's coordinates.

In summary, the force $F^i(t)$ is the weighted combination of the aforementioned virtual forces

$$F^i(t) = \alpha_s F_s^i(t) + (1 - \alpha_s) \frac{\alpha_a F_a^i(t) + \alpha_c F_c^i(t) + \alpha_{av} F_{av}^i(t) + \alpha_{cv} F_{cv}^i(t)}{\alpha_a + \alpha_c + \alpha_{av} + \alpha_{cv}}, \quad (3.12)$$

under the condition that

$$\alpha_s = \begin{cases} 0, & \text{if ZS is empty} \\ 1, & \text{otherwise,} \end{cases} \quad (3.13)$$

that is, $\alpha_s = 0$ when the particle is not about to collide, and $\alpha_s = 1$ when there is at least one individual inside the ZS, whereupon F_s overwrites the other forces.

The control coefficients α_s , α_a , α_c , α_{av} and α_{cv} are related to their respective forces,

and set the contribution of each force in $F^i(t)$. They also dictate if and how fast the group will converge to the parallel formation around the VA. The challenge is to find the correct α 's that lead the group to desired configurations.

The five forces are very important for the purpose of establishing formations of agents. Although the forces F_{av} , F_{cv} and F_s seem enough to achieve a formation, the optimization results of Section 2.6 show that F_a and F_c contribute when considering different formation objectives.

3.3 Particles with phase-coupled oscillator dynamics (PCOD)

This section is devoted to a first-order model of particles with phase-coupled oscillator dynamics, which is composed of N particles with unitary speed (SEPULCHRE et al., 2007; JUSTH; KRISHNAPRASAD, 2004; PALEY, 2007) that follow the dynamics

$$\dot{r}_k = e^{i\theta_k}, \quad (3.14a)$$

$$\dot{\theta}_k = u_k(\mathbf{r}, \boldsymbol{\theta}), \quad k = 1, \dots, N. \quad (3.14b)$$

The k -th particle position is described by the complex coordinate $r_k = x_k + iy_k$ and the phase/heading angle $\theta_k \in S^1$; $e^{i\theta_k}$ is the direction of the velocity vector; $\mathbf{r} = (r_1, \dots, r_N)^T \in \mathbb{C}^N$ is the vector of particles positions; $\boldsymbol{\theta} = (\theta_1, \dots, \theta_N)^T \in \mathbb{T}^N$ is the phases vector, and $u_k(\mathbf{r}, \boldsymbol{\theta})$ is the feedback control, which is a forcing in the direction normal to velocity.

For simplicity, we first study the trivial configuration of a unicycle model, with $u_k = \omega_0$, for $\omega_0 \neq 0$. This setup corresponds to particles moving in circles, without communication exchange, with $\dot{r}_k(t) = e^{i\omega_0 t}$. The integration of $\dot{r}_k(t)$ results in

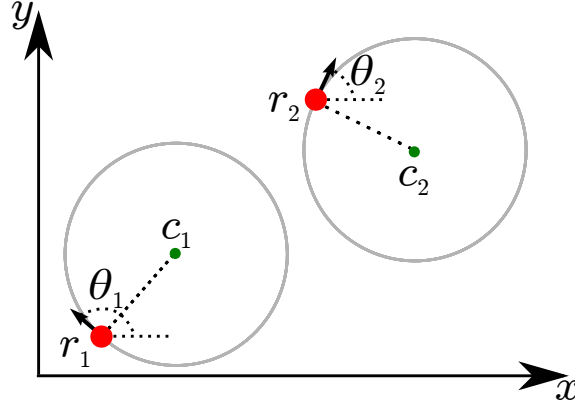
$$r_k(t) = r_k(0) + \frac{i}{\omega_0} - \frac{i}{\omega_0} e^{i\omega_0 t}, \quad (3.15)$$

which is a circular motion centered at

$$c_k(t) = r_k(t) + \frac{i}{\omega_0} e^{i\theta_k(t)}, \quad (3.16)$$

see Figure 3.4.

Figure 3.4 - Simple circular dynamics of (3.14) for the case of a constant control $u_k = \omega_0 \neq 0$. The particle is moving around the center c_k given by Equation (3.16) and radius $|\omega_0|^{-1}$.



SOURCE: Produced by the author.

Further on we present controls for circular formations, that are characterized by particles moving in circular trajectories with the same centroid. After the formation is reached, particles' phases are updated according to a constant force $u_k(\mathbf{r}, \boldsymbol{\theta}) = \omega_0$. It means that, during a certain transient, the system updates with $u_k(\mathbf{r}, \boldsymbol{\theta}) = \omega_0 + a$, for some $|a| > 0$ that correspond to the contribution of the coupling between particles. As soon as they are perfectly positioned within the formation, they simply rotate according to the mentioned constant force.

3.3.1 Circular formations

This Section aims to present how to achieve particles sharing the same rotation center $c_1 = c_2 = \dots = c_N$. Firstly, consider the following potential (SEFULCHRE et al., 2007):

$$S(\mathbf{r}, \boldsymbol{\theta}) = \frac{1}{2} \|P\mathbf{c}(\mathbf{r}, \boldsymbol{\theta})\|^2, \quad (3.17)$$

where

$$\mathbf{c}(\mathbf{r}, \boldsymbol{\theta}) = \mathbf{r} + \frac{i}{\omega_0} e^{i\boldsymbol{\theta}}, \quad P = I_N - \frac{1}{N} \mathbf{1}\mathbf{1}^T = L/N,$$

I_N is the $N \times N$ identity matrix, and $\mathbf{1} = (1, \dots, 1)$. The P matrix also corresponds to the graph Laplacian over N . In short, the centers are identical if and only if $P\mathbf{c} = 0$

and the potential S achieves its minimum. The time derivative of the potential (3.17) along the solutions of the particle model is given by

$$\dot{S} = \frac{\partial S}{\partial \boldsymbol{\theta}} \frac{d\boldsymbol{\theta}}{dt} = \frac{1}{\omega_0} \sum_{k=1}^N (\omega_0 - u_k) \langle e^{i\theta_k}, P_k \mathbf{c}(\mathbf{r}, \boldsymbol{\theta}) \rangle, \quad (3.18)$$

where $\langle z_1, z_2 \rangle = \text{Re}\{z_1^* z_2\}$ for $z_1, z_2 \in \mathbb{C}$, z_1^* is the complex conjugate of z_1 , and P_k is the k -th row of the matrix P .

Choosing the control u_k as follows

$$u_k(\mathbf{r}, \boldsymbol{\theta}) = \omega_0 (1 + K_0 \langle e^{i\theta_k}, P_k \mathbf{c}(\mathbf{r}, \boldsymbol{\theta}) \rangle) = \omega_0 - K_0 \omega_0^2 \frac{\partial S}{\partial \theta_k}, \quad (3.19)$$

equation (3.18) yields

$$\dot{S} = -K_0 \sum_{j=1}^N \langle e^{i\theta_j}, P_j \mathbf{c}(\mathbf{r}, \boldsymbol{\theta}) \rangle^2 \leq 0. \quad (3.20)$$

Therefore solutions of system (3.14) with the control (3.19) converge asymptotically to the same centers $c_1 = \dots = c_N$, which implies immediately that $u_k = \omega_0$ and the particle solutions are of the form (3.16), i.e. the particles move around the same centers with the same frequency ω_0 and radius $|\omega_0|^{-1}$.

The idea is to decrease the difference between pairs of centers so that the control gives

$$u_k(\mathbf{r}, \boldsymbol{\theta}) = \omega_0 + \omega_0 K_0 \cos(\theta_k) \sum_{j=1}^N \left(\frac{c_k}{N} - \frac{c_j}{N} \right),$$

which shows that the differences $(c_k/N - c_j/N)$ decrease and the control receives a contribution that is opposite to its counterpart $(c_j/N - c_k/N)$ due to the cosine function, making the centers of the particles to go toward each other.

3.3.2 Symmetric circular formations

This section introduces a phase control that aims to organize the particles into symmetric groups. So far, we only have control (3.19), whose role is to lead particles to concentric circular trajectories.

Let us define the so-called (M, N) pattern as a symmetric arrangement of N phases distributed in M clusters uniformly spaced around the unit circle, each with N/M synchronized phases (SEPULCHRE et al., 2007). The coveted symmetric circular for-

mations are made of (M, N) patterns orbiting a common center. Formally, the (M, N) pattern is characterized as

$$\begin{aligned}\theta_{j,k}(t) &= \omega_0 t + 2\pi k/M, \\ r_{j,k}(t) &= c - \frac{i}{\omega_0} e^{i\omega_0 t + i2\pi k/M},\end{aligned}\tag{3.21}$$

where the index $k = 1, \dots, M$ counts the clusters, $j = 1, \dots, N/M$ are the oscillators within each cluster, and c is the common center. In the following, we describe the choice of $u_k(\mathbf{r}, \boldsymbol{\theta})$ that guarantees the formation of symmetric circular clusters.

First note that the center of mass of the particles

$$R = \frac{1}{N} \sum_{j=1}^N r_j\tag{3.22}$$

moves with the velocity

$$\dot{R} = \frac{1}{N} \sum_{j=1}^N e^{i\theta_k} =: p_\theta = |p_\theta| e^{i\Psi},\tag{3.23}$$

which equals to the Kuramoto order parameter (KURAMOTO, 1984). Since $0 \leq |p_\theta| \leq 1$, the case $|p_\theta| = 1$ corresponds to the synchronized phase arrangement with particles heading to the same direction $\theta_1 = \dots = \theta_N$. Oppositely, $p_\theta = 0$ stands for balanced heading angles, so that the center of mass remains in a steady position. This is possible, in particular, when the particles are moving radially from their center of mass. Plus, this measure is important to characterize synchronized and balanced states of particles.

We further introduce the m -th moment of the Kuramoto order parameter (SEPULCHRE et al., 2007):

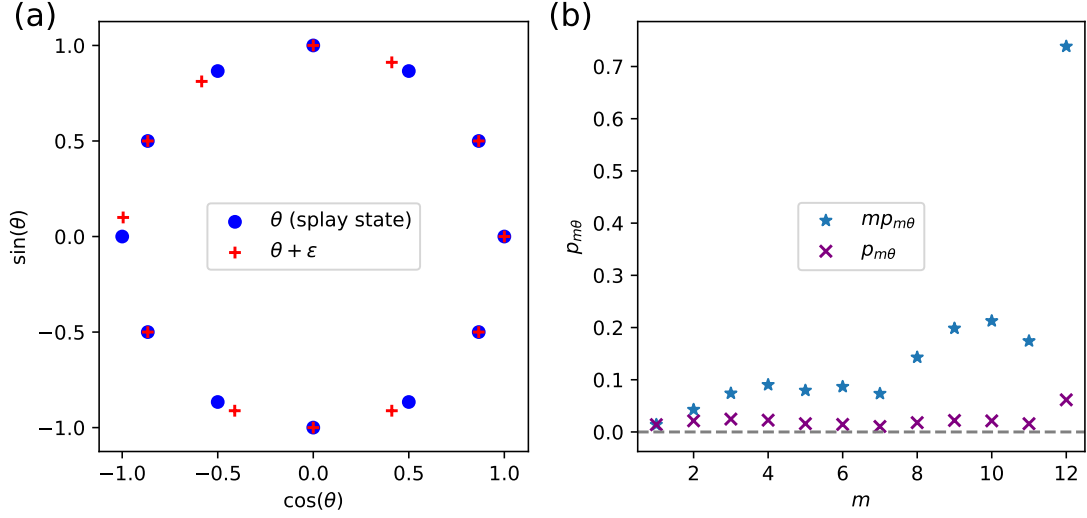
$$p_{m\theta} = \frac{1}{mN} \sum_{j=1}^N e^{im\theta_j}, \quad m = 1, 2, 3, \dots\tag{3.24}$$

with $0 \leq |p_{m\theta}| \leq 1/m$. Whenever the phases form uniformly distributed M -clusters, the (M, N) pattern, $|p_{m\theta}|$ achieves its minimum $|p_{m\theta}| = 0$ for $m < M$ and its maximum $|p_{M\theta}| = 1/M$ for $m = M$.

The division by m in the right hand side of Equation (3.24) acts as a normalization factor to guarantee that the scale of the deviations of $p_{m\theta}$ is the same for every m . In other words, since the derivative of $p_{m\theta}$ matters for the dynamics, the factor $1/m$ balances different m cases. Figure 3.5 (a) presents a splay state as blue circles

and its perturbed version as symbol ‘+’, in which we add a small perturbation ϵ . Figure 3.5 (b) shows the m -th order parameter $|p_{m\theta}|$ of the perturbed system and the normalized order parameter $m|p_{m\theta}|$. Notice that the $|p_{m\theta}|$ presents small differences for varying m , whilst its normalized version is less smooth.

Figure 3.5 - (a) Phases in a splay state as blue circles and its perturbed version as red symbols +; (b) m -th phase order parameters of the perturbed system as symbols x and the corresponding normalized version as stars.



SOURCE: Produced by the author

With the aim of minimizing $|p_{m\theta}|$ when $m < M$ and maximizing $|p_{M\theta}|$, the following potential is considered:

$$U^{M,N}(\boldsymbol{\theta}) = \sum_{m=1}^M K_m U_m(\boldsymbol{\theta}), \quad U_m(\boldsymbol{\theta}) = \frac{N}{2} |p_{m\theta}|^2, \quad (3.25)$$

where $K_m > 0$ for $m = \{1, \dots, M-1\}$ and $K_M < 0$. The (M, N) patterns correspond to the minimum of the potential $U^{M,N}(\boldsymbol{\theta}) = (K_M N)/(2M^2)$, as follows

$$U^{M,N}(\boldsymbol{\theta}) = \sum_{m=1}^M K_m \frac{N}{2} \left| \frac{1}{mN} \sum_{j=1}^N e^{im\theta_j} \right|^2.$$

When the particles assume a symmetric formation, $U_m = 0$ for $m < M$, and the

only nonzero potential is $U_M(\boldsymbol{\theta})$, that gives

$$\min\{U^{M,N}(\boldsymbol{\theta})\} = K_m \frac{N}{2} \frac{1}{M^2} = \frac{K_M N}{2M^2}. \quad (3.26)$$

The gradient of (3.25) is given by

$$\begin{aligned} \frac{\partial U_m}{\partial \theta_k} &= \frac{N}{2} \left(\frac{\partial p_{m\theta}}{\partial \theta_k} p_{m\theta}^* + p_{m\theta} \frac{\partial p_{m\theta}^*}{\partial \theta_k} \right) = \frac{1}{2m} \left(i m e^{im\theta_k} p_{m\theta}^* - p_{m\theta} i m e^{-im\theta_k} \right) \\ &= \frac{1}{2m} \left(i m e^{im\theta_k} \frac{1}{mN} \sum_{j=1}^N e^{-im\theta_j} - \frac{1}{mN} \sum_{j=1}^N e^{im\theta_j} i m e^{-im\theta_k} \right) \\ &= \frac{i}{2mN} \left(\sum_{j=1}^N e^{i(m(\theta_k - \theta_j))} - \sum_{j=1}^N e^{i(m(\theta_j - \theta_k))} \right) \\ &= \frac{1}{2mN} \sum_{j=1}^N i \cos(m(\theta_k - \theta_j)) - \sin(m(\theta_k - \theta_j)) - i \cos(m(\theta_j - \theta_k)) + \sin(m(\theta_j - \theta_k)), \end{aligned}$$

that results in:

$$- \frac{\partial U^{M,N}}{\partial \theta_k} = \frac{1}{N} \sum_{m=1}^M \sum_{j=1}^N \frac{K_m}{m} \sin(m(\theta_k - \theta_j)). \quad (3.27)$$

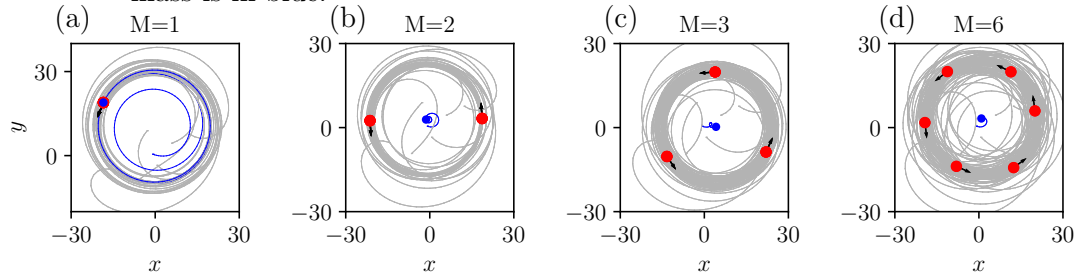
Gathering the control (3.19) for obtaining circular formations and the gradient of the phase potential (3.27) for symmetric phase arrangements, gives

$$\begin{aligned} u_k(\mathbf{r}, \boldsymbol{\theta}) &= \omega_0 - K_0 \omega_0^2 \frac{\partial S}{\partial \theta_k} - \frac{\partial U^{M,N}}{\partial \theta_k} = \\ &= \omega_0 (1 + K_0 \langle e^{i\theta_k}, P_k \mathbf{c}(\mathbf{r}, \boldsymbol{\theta}) \rangle) + \frac{1}{N} \sum_{m=1}^M \sum_{j=1}^N \frac{K_m}{m} \sin(m(\theta_k - \theta_j)). \end{aligned} \quad (3.28)$$

Figure 3.6 presents simulation results of model (3.14) under the control of Equation (3.28) for symmetric circular formations with $N = 6$ particles and $M = \{1, 2, 3, 6\}$ clusters. Trajectories are plotted in gray, the particles are the red circles with direc-

tion arrows and the center of mass is the smaller circle in blue.

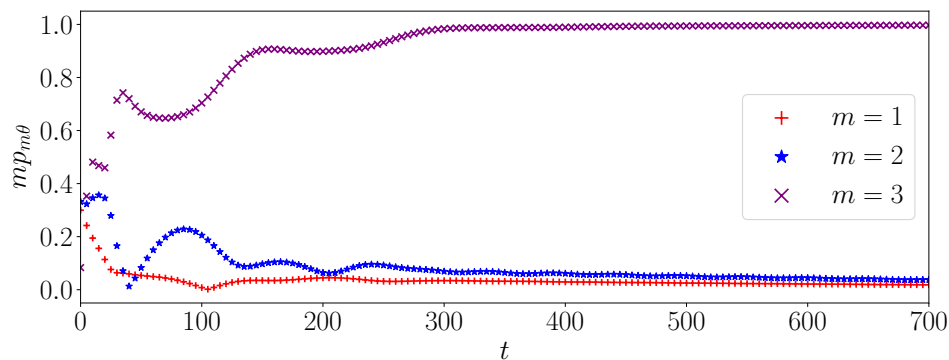
Figure 3.6 - Simulations of model (3.14) under the control for symmetric circular formations of Equation (3.28). Parameters: $N = 6$, $K_0 = 0.1$, $\omega_0 = 0.05$, $K_m = 0.18$ for $m < M$ and $K_M = -0.02$. Particles are the red circles and the center of mass is in blue.



SOURCE: Produced by the author

A nice hint of what are the order parameters measurements during the time integration of the system can be seen in Figure 3.7 with the example of $M = 3$. At the beginning, for small t , they exhibit a wiggling like form and after that, the $|p_\theta|$ and $|p_{2\theta}|$ decrease as expected, while $|p_{3\theta}|$ grows.

Figure 3.7 - Time series of the order parameters of model (3.14), with control (3.28) and parameters: $N = 6$, $M = 3$, $K_0 = 0.1$, $\omega_0 = 0.05$, $K_m = 0.18$ for $m < M$ and $K_M = -0.02$



SOURCE: Produced by the author

3.3.3 Limited communication

Here we present the generalization of the PCOD model for a limited communication scenario, where particles exchange information with neighbors according to a fixed network topology (SEPULCHRE et al., 2008).

We define the following phase potential

$$U(\boldsymbol{\theta}) = \frac{N}{2} \langle p_\theta, p_\theta \rangle = \frac{1}{2N} \langle \mathbf{1}^T e^{i\boldsymbol{\theta}}, \mathbf{1}^T e^{i\boldsymbol{\theta}} \rangle = \frac{1}{2} \left\langle e^{i\boldsymbol{\theta}}, \frac{1}{2} \mathbf{1} \mathbf{1}^T e^{i\boldsymbol{\theta}} \right\rangle \quad (3.29)$$

which, substituting the $(\mathbf{1} \mathbf{1}^T)/N = \text{diag}\{\mathbf{1}\} - P$ by L , gives

$$W_L(\boldsymbol{\theta}) = \frac{1}{2} \left\langle e^{i\boldsymbol{\theta}}, L e^{i\boldsymbol{\theta}} \right\rangle. \quad (3.30)$$

with $L = [l_{ij}] \in \mathbb{R}^2$ and

$$l_{ij} = \begin{cases} |\mathcal{N}_i^{\text{net}}| & \text{if } i = j \\ -1 & \text{if } j \in \mathcal{N}_i^{\text{net}} \\ 0 & \text{otherwise} \end{cases}$$

The potential for symmetric circular formations is as follows:

$$W_L^{M,N}(\boldsymbol{\theta}) = - \sum_{m=1}^M \frac{K_m}{m^2} W_L(m\boldsymbol{\theta}) = - \frac{1}{2} \sum_{m=1}^M \frac{K_m}{m^2} \left\langle e^{im\boldsymbol{\theta}}, L e^{im\boldsymbol{\theta}} \right\rangle \quad (3.31)$$

with $K_m > 0$ for $m = 1, \dots, M-1$, and $K_M < -\sum_{m=1}^{M-1} K_m$. The corresponding derivative with respect to θ_k is

$$\frac{W_L^{M,N}}{\partial \theta_k} = - \sum_{m=1}^M \frac{K_m}{m} \left\langle i e^{im\theta_k}, L_k e^{im\boldsymbol{\theta}} \right\rangle. \quad (3.32)$$

The corresponding control to undirected and incomplete interconnection networks is the following:

$$u_k = \omega_0 (1 + K \langle e^{i\theta_k}, L_k \mathbf{e} \rangle) - \frac{\partial W_L^{M,N}}{\partial \theta_k}, K > 0. \quad (3.33)$$

The potential of Equation (3.30) always decreases when the communication network is circulant (SEPULCHRE et al., 2008; JAIN; GHOSE, 2018). A circulant network is completely defined by its first row and each subsequent row is the previous row shifted one position to the right. Its first entry is equal to the last entry of the previous row.

3.3.4 Collision avoidance

Considering the Kuramoto model of Equation (2.9), when $K > 0$ the phases distribute around the unitary circle, leading the zero order parameter. Motivated by this behavior, we propose the introduction of a repulsion term *rep* in Equations (3.28) and (3.33), so that the phases of close range particles are adjusted to avoid collision, by moving apart.

The repulsion term comes from the potential of Equation (3.30), also called Laplacian phase potential (LEONARD et al., 2007). Its gradient is given by

$$\frac{\partial W_L}{\partial \theta_k} = \frac{1}{N} \langle i e^{i\theta_k}, L_k e^{i\theta} \rangle \quad (3.34)$$

which corresponds to

$$\frac{\partial W_L}{\partial \theta_k} = \frac{1}{|\mathcal{N}(r_k)|} \sum_{j \in \mathcal{N}(r_k)} \sin(\theta_k - \theta_j)$$

for $\mathcal{N}(r_k) = \{j \in \mathbb{N} \mid \|r_k - r_j\| < d\}$ is the set of neighbors of agent k and $|\mathcal{N}(r_k)|$ is the number of neighbors in $\mathcal{N}(r_k)$. An agent belongs to $\mathcal{N}(r_k)$ if it is within a predefined radius d , centered at r_k . This gradient leads the solutions to the stationary points when the Laplacian matrix is circulant. We employ the gradient of the Laplacian phase potential as a repulsion term:

$$\text{rep} = \frac{K_r}{|\mathcal{N}(r_k)|} \sum_{j \in \mathcal{N}(r_k)} \sin(\theta_k - \theta_j) \quad (3.35)$$

with $K_r > 0$ being the repulsion strength.

The idea behind the Equation (3.35) is that the agent k tries to balance its heading angle with its closest neighbors $\mathcal{N}(r_k)$. This results in an adjustment of agent's k

heading angle to the opposite direction concerning $\mathcal{N}(r_k)$.

One drawback of this approach is that it is not possible to guarantee that the matrix is circulant since L is time-varying. However, the neighbors indeed repel the agent as desired.

The new controls for symmetric circular formation with the *rep* term are shown in Equations (3.36) and (3.37) for all-to-all and limited coupling networks, respectively:

$$u_k = \omega_0(1 + K \langle e^{i\theta_k}, P_k \mathbf{c} \rangle) - \frac{\partial U^{M,N}}{\partial \theta_k} + \text{rep} \quad (3.36)$$

$$u_k = \omega_0(1 + K \langle e^{i\theta_k}, L_k \mathbf{c} \rangle) - \frac{\partial W_L^{M,N}}{\partial \theta_k} + \text{rep} \quad (3.37)$$

with $K > 0$.

3.4 Conclusions

This Chapter introduced the Unicycle model and two models we study throughout the thesis, namely the phenomenological reactive model of agents following a mobile reference and the particles with coupled-oscillator dynamics. We end the chapter with a collision avoidance strategy. The interaction rules are presented in detail and the synchronization-based strategies alike. Here we finish the presentation of all the necessary theoretical background for the understanding of the next Chapters.

4 REACTIVE MODEL FOR AUTONOMOUS VEHICLES FORMATION FOLLOWING A MOBILE REFERENCE: SIMULATIONS AND NUMERICAL RESULTS

This Chapter presents simulations and numerical results for the reactive model introduced in Section 3.2. We first solve the inverse problems of finding proper parameters that lead the group to specific behaviors with heuristics. The problems are initially solved considering single-objective functions and later we combine such functions in a multi-objective approach. Lastly, we present three simulation scenarios that mimic real-world applications.

The results we present are dependent on the model parameters and not on initial conditions. We simulate small numbers of agents and do not use boundary conditions on the 2D plane of the simulation scenario so that we can depict real-world aspects of systems with autonomous vehicles.

At the beginning, we employ a search in the control parameter space, to seek for “optimal” parameters that lead the agents to specific formation topologies. The chosen heuristics is based on evolutionary optimization, that start with random parameters and evolve them towards the minimization of certain objective functions. We propose three such functions that take into account how tight the formation is and how fast it converges.

In addition, we present three examples of path planning scenarios, in which the agents follow the VA considering fixed or dynamic relative positions. It means that the agents can follow the VA closely maintaining or not their relative distances. Fixed relative positions are important when the agents are satellites in formation fly, in which the formation must be rigid. Oppositely, dynamic positions are interesting in surveillance systems due to the desired agents’ unpredictability.

4.1 Evolutionary Optimization

In our reactive model, the control coefficients α ’s are the design variables of an optimization problem. However, there are four coefficients to be adjusted, and finding the optimal set is a hard task that is not feasible to be performed empirically, i.e., by only using the intuition to knob the values or through brute force, testing all the possibilities. The problem is then to find the sets of parameters that makes our system to converge as fast as possible, but keeping a cohesive group.

4.1.1 Objective functions

Find below the three objective functions that we use in the optimization procedures, also sketched in Figure 4.1:

- a) f_{time} (Convergence time): it corresponds to the time units (tu) from the beginning of the simulation until the first time the agents achieve a desired formation: all agents moving in an almost parallel formation inside the FR with the same speed of the VA. We consider that they are in the coveted almost parallel formation if their heading angle differences are up to 5 degrees.
- b) f_{ang} (Angular uniformity): This function characterizes the agents' distribution around the VA. The relative angles Θ_j between the position of each agent and the VA are calculated and used to evaluate the Order parameter p_Θ of Equation (4.1) (STROGATZ, 2000):

$$p_\Theta = \frac{1}{N} \sum_{j=1}^N e^{i\Theta_j} \quad (4.1)$$

with $e^{i\Theta_k} = \cos \Theta_j + i \sin \Theta_j$, such that $\Theta_j = \arctan(\Delta y / \Delta x)$, for $\Delta x = x_a - x_i$ and $\Delta y = y_a - y_i$, for $[x_i, y_i]^T \in \mathbb{R}^2$ is the i -th agent's position, and $[x_a, y_a]^T \in \mathbb{R}^2$ are the VA's coordinates.

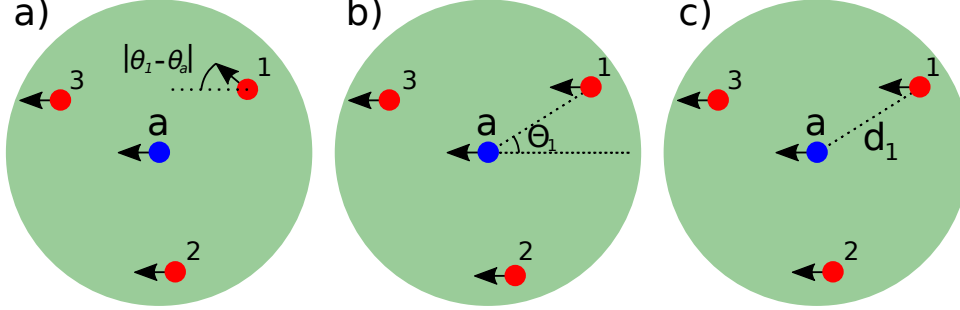
In this case, $f_{ang} = |p_\Theta|$. When $f_{ang} = 0$ the agents are uniformly distributed around the VA. On the other hand, if $f_{ang} = 1$ then the agents are at the same position, beside the VA.

- c) f_{rad} (Radial uniformity): The mean of the distances between each agent and the VA:

$$f_{rad} = \frac{1}{N} \sum_{j=1}^N d_j \quad (4.2)$$

in which d_j is the distance between the j -th agent and the VA.

Figure 4.1 - Objective functions: a) Convergence time f_{time} when every agent is inside the FR and $|\theta_i - \theta_a| < 5$ degrees; b) Angular uniformity $f_{ang} = |\frac{1}{N} \sum_{i=1}^N e^{i\theta_i}|$ and; c) Radial uniformity $f_{rad} = \frac{1}{N} \sum_{i=1}^N d_i$, for $i = \{1, \dots, N\}$.



SOURCE: Produced by the author.

The minimization of such functions lead the system to tight formations of agents distributed around the VA.

4.1.1.1 Results

Both GEO and M-GEO algorithms, described in Section 2.6, are employed. Besides, one solution corresponds to the four design variables α_a , α_c , α_{av} and α_{cv} , encoded as sequences of bits. We bound the $M = 4$ design variables to the interval $\alpha_a, \alpha_c, \alpha_{av}, \alpha_{cv} \in [0, 1]$ and define a precision of $p = 0.01$ for their representation, which gives $m = 7$ bits for each variable, as follows from Equation (2.26), $2^7 \geq (1 - 0)/0.01 + 1 \rightarrow 128 \geq 101$.

One solution is the concatenation of the four sequences of bits that correspond to the four design variables, regardless of initial conditions. This solution has $L = 28$ bits of length from $M = 4$ variables of $L/M = 7$ bits each, all randomly chosen at the beginning.

The three inverse problems to be solved are described by Equations (4.3), (4.4) and (4.5), whose goals are to minimize the time to reach the the desired formation, the angular uniformity and radial uniformity, respectively:

$$\begin{aligned} & \min \{f_{time}\} \\ & \text{subjected to design variables: } \alpha_a, \alpha_c, \alpha_{av}, \alpha_{cv} \in [0, 1], \end{aligned} \tag{4.3}$$

$$\begin{aligned} & \min \{f_{ang}\} \\ & \text{subjected to design variables: } \alpha_a, \alpha_c, \alpha_{av}, \alpha_{cv} \in [0, 1], \end{aligned} \quad (4.4)$$

$$\begin{aligned} & \min \{f_{rad}\} \\ & \text{subjected to design variables: } \alpha_a, \alpha_c, \alpha_{av}, \alpha_{cv} \in [0, 1]. \end{aligned} \quad (4.5)$$

The radii of the zones of perception are not included as design variables. Couzin et al. (2002) realized that $ZA+ZS \geq 2.5$ guarantees that the group reaches a polarized configuration, i.e., they reach consensus and move in parallel. They used $ZA=1$ so that the width of the zone of attraction is $ZA-ZS=1.5$. We employed slightly higher values so that the control parameters α 's could have room to properly regulate the contribution of each force.

The objective functions' calculation depends on model simulations using the design variables as parameters. The simulations are limited to 5000 time units (tu) because it is computationally expensive to run them longer, beyond the fact that waiting too long for the formation to emerge is not coveted. We empirically figured that for some hand-tuned parameters the agents take about 1500 tu to converge to desired formations. The extra 3500 tu is a margin to let the optimization algorithm evolve its population.

The τ parameter is investigated in the first place, to make sure that the optimization has the better setup possible. We run the model for varying $\tau \in [0.5, 2.5]$ in steps of $\Delta\tau = 0.25$ and NFE= 10000 evaluations of the objective function each run. This interval corresponds to the experiments of DE SOUSA et al. (2003) with various functions.

As soon as a suitable τ is found, we execute the optimization 50 times with NFE= 100000.

Find below the initial conditions and parameters for the reactive model:

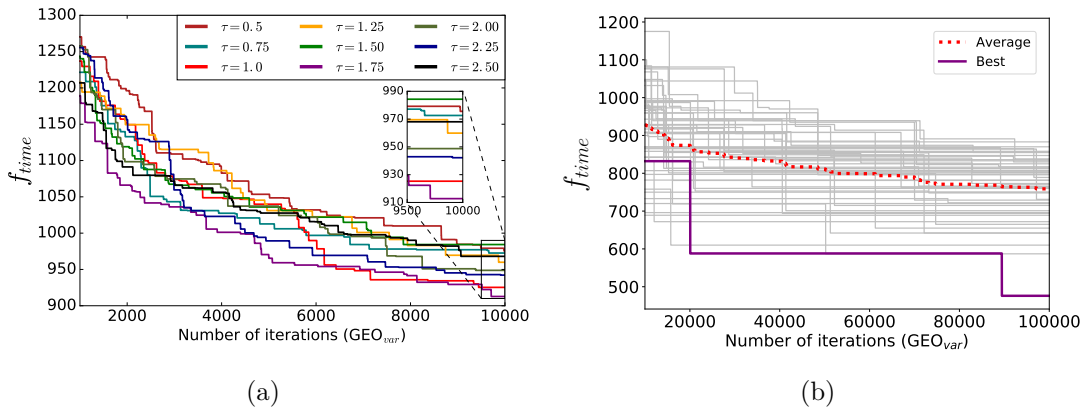
- $N = 12$ agents randomly positioned inside a rectangle of dimensions 36×76 bl alike in Figure 3.1.
- Perception zones: $ZS = 2.5bl$, $ZA = 4.0bl$ and $ZC = 5.5bl$.
- Maximum turning angle: $\gamma = 1$ decimal degree.
- Maximum F_s : 2γ .

- Maximum $F_a = F_c = F_{av} = F_{cv}$: γ .
- Initial heading angles θ : Random.
- $s_{va} = 1 \text{ bl/tu}$, $s_{out} = 1.4 \text{ bl/tu}$. This notation of speed stands for body-length per time unit. An agent moving at 1 bl/tu travel the distance of its length at every time unit.
- FR radius: 25 bl .
- VA heading angle: 180 decimal degrees, i.e., the VA is constantly moving in a straight line.
- $\bar{t} = 87.5tu$.
- Control coefficients: $\alpha_a, \alpha_c, \alpha_{av}, \alpha_{cv} \in [0, 1]$ and $\alpha_s = 1$.

4.1.2 Mono-objective problem

This Section starts with the results of optimization problem (4.3), in which Figure 4.2(a) is the investigation with varying τ and Figure 4.2(b) exhibits the optimization using the best $\tau = 1.75$. The abscissa gives the number of iterations of GEO_{var} and the ordinate shows the progress of the convergence time optimization in number of iterations of the reactive model. We present 50 runs in gray, the best highlighted in purple and the average case in red. The average of the 50 runs is $f_{time} = 758.76 \text{ tu}$. Table 4.1 shows the best results.

Figure 4.2 - Results of optimization problem (4.3): (a) Optimal f_{time} for different values of τ . (b) Optimal f_{time} , after 50 simulations of GEO_{var} with $\tau = 1.75$. Best result is the purple thick line and the average case is the dashed red line. The 50 simulations are represented by the thin gray lines.



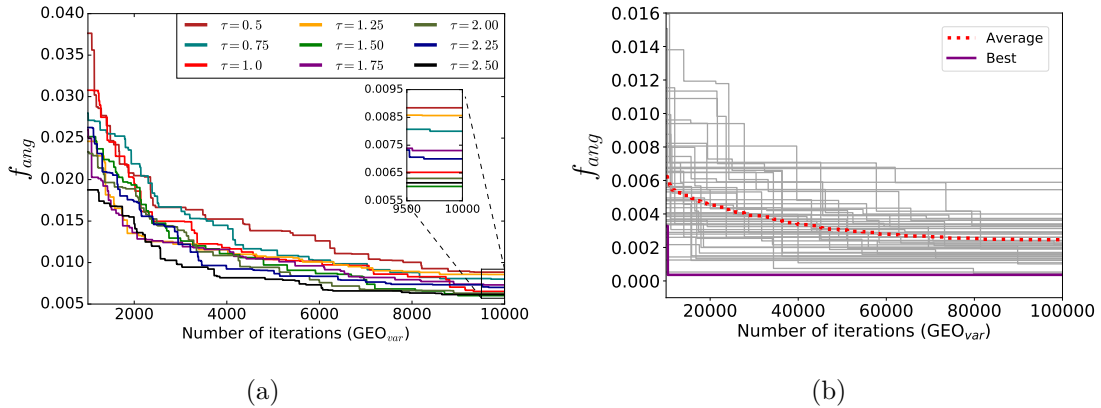
SOURCE: Produced by the author. Appears in Freitas et al. (2018).

Table 4.1 - Results of optimization problems (4.3), (4.4), and (4.5), using the algorithm GEO_{var} .

		α_a	α_c	α_{av}	α_{cv}	f
f_{time}	$\tau = 1.75$	0.417323	0.125984	0.19685	0.464567	476 <i>tu</i>
f_{ang}	$\tau = 1.50$	0.811024	0.598425	0.244094	0.456693	3.6398×10^{-4}
f_{rad}	$\tau = 1.50$	0.228346	0.80315	0.488189	0.669291	3.39412 <i>bl</i>

The optimization for the Angular uniformity f_{ang} is presented in Figure 4.3, for which $\tau = 1.5$ performed better. The near zero f_{ang} indicates that the agents are almost uniformly distributed around the VA. The best case is also presented in Table 4.1, and the average is $f_{ang} = 0.00246136174$.

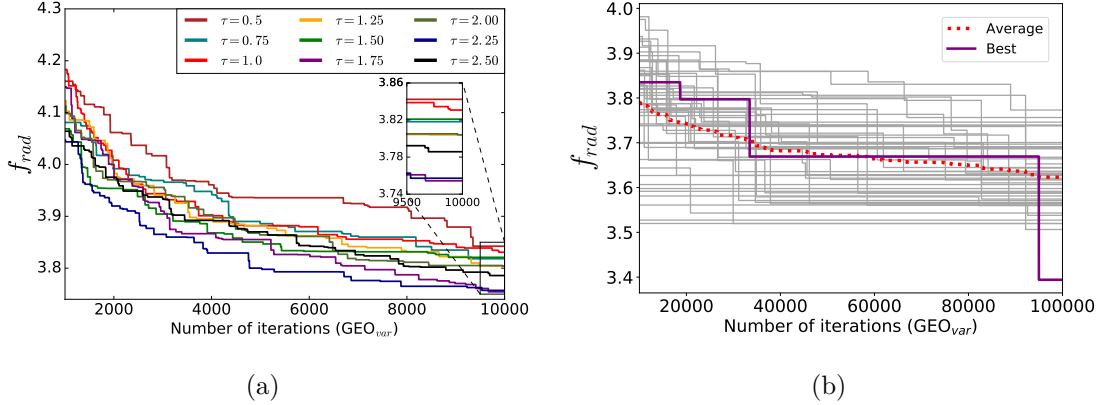
Figure 4.3 - Results of optimization problem (4.4): (a) Optimal f_{ang} for different values of τ . (b) Optimal f_{ang} measure after 50 simulations of GEO_{var} with $\tau = 1.5$. Best result is the purple thick line and the average case is the dashed red line. The 50 simulations are represented by the thin gray lines.



SOURCE: Produced by the author. Appears in Freitas et al. (2018).

The results for Radial uniformity are depicted in Figure 4.4, showing that $\tau = 1.5$ outperformed the others. In our setup, the FR radius equals $25bl$, then the higher possible Radial uniformity is $25bl$ and only happens if all agents sit on the FR boundaries. In contrast, the minimum value corresponds to how close the agents can be of VA without colliding with each other. The best result is depicted in Table 4.1, and the average of the 50 runs is $f_{rad} = 3.6232264$.

Figure 4.4 - Results of optimization problem (4.5): (a) Optimal f_{rad} for different values of τ . (b) Optimal f_{rad} after 50 simulations of GEO_{var} with $\tau = 1.5$. Best result is the purple thick line and the average case is the dashed red line. The 50 simulations are represented by the thin gray lines.



SOURCE: Produced by the author. Appears in Freitas et al. (2018).

The forces F_{av} , F_{cv} and F_s alone may lead the agents to formations around the VA, with the collision avoidance mechanism. They are responsible to attract the agents towards the VA, making them align with it without crashing events. One could now question the need of F_a and F_c , since at a first glance they look useless.

Yet, in the three aforementioned optimization cases, the contributions of F_a and F_c are indeed important. For the optimization of f_{time} , α_a is the second higher control coefficient, and it implies that aligning with neighbors is crucial to achieving small convergence time. Along with F_c , the force F_a plays an important role for the emergence of small angular uniformities, having the two higher coefficients. Lastly, the optimization of f_{rad} is highly influenced by F_c as well.

4.1.3 Multi-objective problem

The motivation behind this section is the possibility of achieving formations of agents close to each other, uniformly spread around the VA and with small convergence time. These three characteristics are explored individually in the previous section with the GEO_{var} . Here they are all taken into account at the same time.

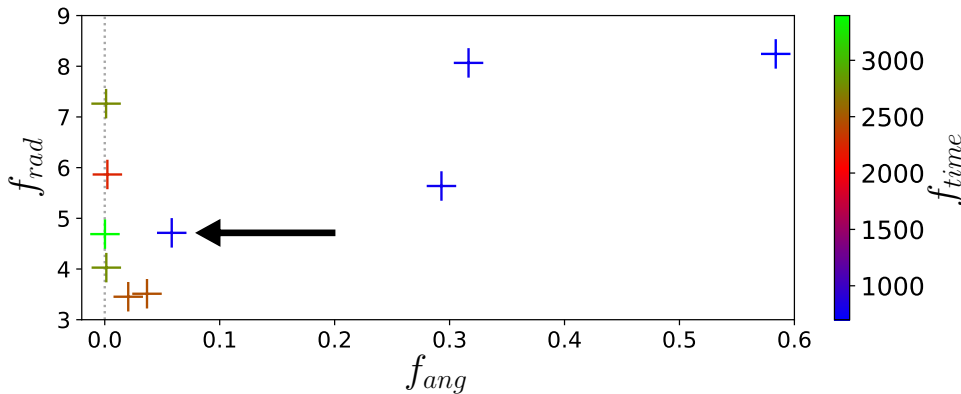
The multiobjective problem we are dealing with is:

$$\min \{f_i\}, \quad i = \{time, ang, rad\} \quad (4.6)$$

subjected to design variables: $\alpha_a, \alpha_c, \alpha_{av}, \alpha_{cv} \in [0, 1]$,

the simultaneous minimization of three functions: $f_{time}, f_{ang}, f_{rad}$. Figure 4.5 presents our results using the same configurations of Section 2.6.1 simulations, with $\tau = 1.50$, $\eta = 100$ and $NFE = 2000000$. The axes represent f_{ang} and f_{rad} and colors are the convergence time f_{time} , the latter given in time units (tu).

Figure 4.5 - Pareto Frontier obtained from M-GEO with $\tau = 1.50$. Colors represent f_{time} . The black arrow indicates the chosen solution for the simulations of Section 4.2, whose values for the objective functions are $f_{time} = 779$, $f_{ang} = 0.0582744$ and $f_{rad} = 4.71353$, and control coefficients $\alpha_a = 0.23622$, $\alpha_c = 0.212598$, $\alpha_{av} = 0.488189$ and $\alpha_{cv} = 0.976378$. The vertical dashed line highlights the $f_{ang} = 0$ to show how close the solutions approach to it.



SOURCE: Produced by the author. Appears in Freitas et al. (2018).

Remark that the choice of the “best” solution is not trivial. Notwithstanding, one good option is the one closer to the utopian solution, near the functions’ optimal values. In the present setup, the task is the minimization of non-negative functions so the utopian solution is the origin $(0, 0, 0)$. Considering the candidate solutions near the origin and also that convergence time is of great importance, we decided to pick the one with the time depicted in blue tonality with the smaller f_{ang} and f_{rad} , indicated by the black arrow in Figure 4.5 that corresponds to $f_{time} = 779$, $f_{ang} = 0.0582744$ and $f_{rad} = 4.71353$, with $\alpha_a = 0.23622$, $\alpha_c = 0.212598$, $\alpha_{av} = 0.488189$ and $\alpha_{cv} = 0.976378$.

4.2 Path planning simulation

This section aims to present realistic scenarios that could be handled by the reactive model. Since the role of the VA is to guide the formation, we model its motion according to three mission requirements with the parameters from the last paragraph of previous Section.

The three missions consist of:

1. Having the formation moving in a circular trajectory with a predefined radius.
2. Having the formation randomly moving inside a bounded area.
3. Having the formation randomly moving inside a bounded area with relative positions among agents preserved.

Remark that the performed optimization takes into account that the VA moves in a straight line, and here we use the obtained parameters for other motions. Better results may be obtained if the one optimizes the system depending on the desired motion of the VA. Our results are a simplification due to the complexity of considering all possibilities for the VA.

The dynamics of VA's position $[x_a, y_a]^T \in \mathbb{R}^2$ is calculated as follows:

$$\begin{aligned}\dot{x}_a &= s_a \cos(\theta_a) \\ \dot{y}_a &= s_a \sin(\theta_a)\end{aligned}\tag{4.7}$$

for s_a is its speed and θ_a the heading angle.

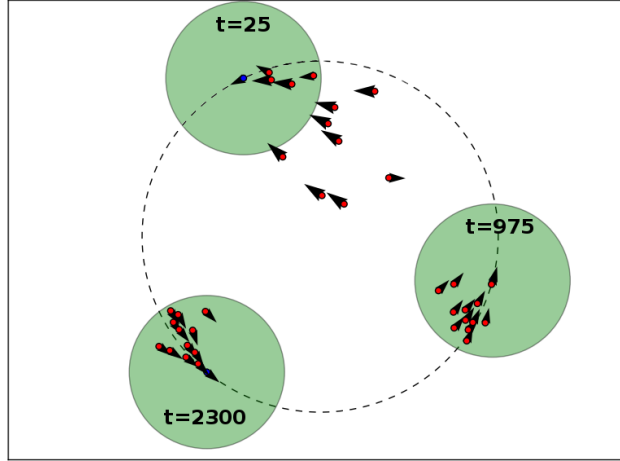
The dynamics of θ_a is mission dependent and we start with the first: the circular trajectory, in which it suffices for the VA's θ_a to evolve constantly

$$\dot{\theta}_a = \omega\tag{4.8}$$

for ω is the frequency of rotation. When ω is positive, VA moves clockwise, or counter-clockwise if negative. Here we consider that $v_a = 1 \text{ bl/tu}$, then the radius of such circular trajectory is $\rho = |\omega_a|^{-1}$. The simulations can be seen in Figure 4.6.

Figures 4.6, 4.7 and 4.8 all show simulation results using the optimized parameters of Section 4.1.3: $\alpha_a = 0.23622$, $\alpha_c = 0.212598$, $\alpha_{av} = 0.488189$, $\alpha_{cv} = 0.976378$, with $\omega = 1.0$ decimal degree, and maximum turning angle of $\gamma = 10$ decimal degrees. The pictures show the evolution of the crowd, with the individuals changing their direction with more freedom than in the optimization setup. This parameter γ dictates the angular velocity, which depends on the vehicle's hardware. The faster a vehicle can change its heading angle the higher is the γ value.

Figure 4.6 - Simulation results with the VA following a circular trajectory with dynamics of Equation (4.8). Parameters: $\alpha_a = 0.23622$, $\alpha_c = 0.212598$, $\alpha_{av} = 0.488189$ and $\alpha_{cv} = 0.976378$, $\omega = 1$ and maximum turning angle $\gamma = 10$ decimal degrees. We present three simulation snapshots, with the time units indicated near them.



SOURCE: Produced by the author. Appears in Freitas et al. (2018).

Regarding the second and third missions, we define a rectangular area in the 2D plan with vertices' coordinates $\{(x_{min}, y_{min}), (x_{max}, y_{min}), (x_{min}, y_{max}), (x_{max}, y_{max})\}$. The VA moves randomly within these boundaries. In order to maintain the motion bounded, at each time unit we compute the closest point $[x_c, y_c]^T \in \mathbb{R}^2$ the VA is from the region border

$$\begin{aligned} x_c &= \max(x_{min}, \min(x_{max}, x)) \\ y_c &= \max(y_{min}, \min(y_{max}, y)) \end{aligned} \quad (4.9)$$

Let $d = \sqrt{(x_a - x_c)^2 + (y_a - y_c)^2}$ be the distance from the VA's position to the boundary closest point, and d_{min} the VA's safe distance to the rectangle limit, a parameter. When $d > d_{min}$, the VA moves randomly, according to:

$$\dot{\theta}_a = \pm\gamma \quad (4.10)$$

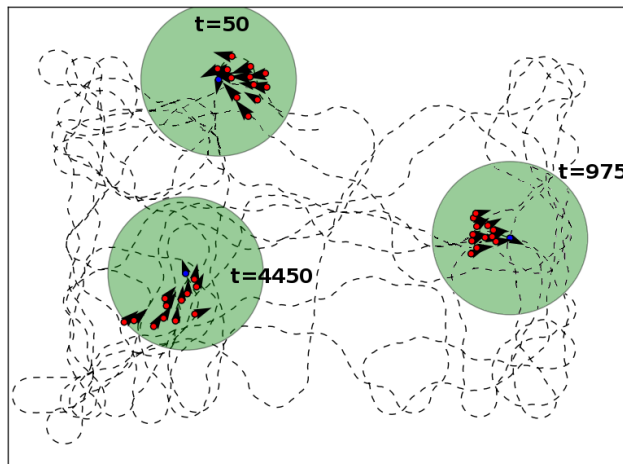
in which the assignment of the two possible values of $\dot{\theta}_a$ follows a discrete uniform distribution, such that $p(\dot{\theta}_a = \gamma) = p(\dot{\theta}_a = -\gamma) = 0.5$.

Contrarily, for $d < d_{min}$ the control θ_a is a bit different to avoid the VA from leaving the coveted area. One calculates the angle ϕ between the VA's position $[x_a, y_a]$ and the closest boundary point $[x_c, y_c]$: $\phi = \arctan(\Delta y/\Delta x)$ for $\Delta x = x_c - x_a$ and $\Delta y = y_c - y_a$. Its heading angle is adjusted to the opposite direction of ϕ , similar to the separation force, as shown in Equation (4.11), with $f_{adj} \in [-\gamma, \gamma]$:

$$\dot{\theta}_a = f_{adj}(\theta_a, \phi + \pi). \quad (4.11)$$

Simulation snapshots are exhibited in Figure 4.7.

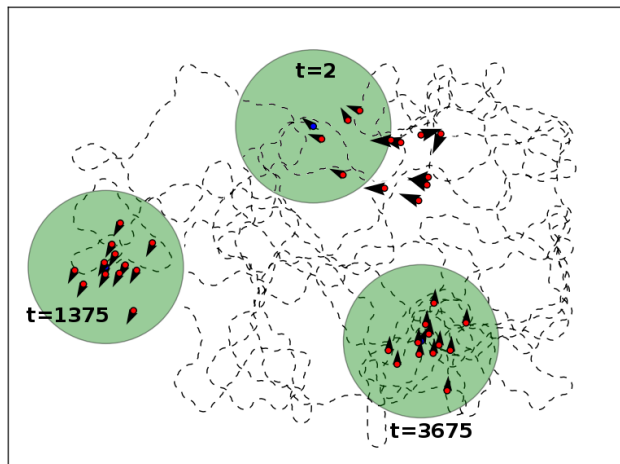
Figure 4.7 - Simulation results with the VA performing a random walk inside a bounded region with dynamics of Equations (4.10) and (4.11). Parameters: $\alpha_a = 0.23622$, $\alpha_c = 0.212598$, $\alpha_{av} = 0.488189$ and $\alpha_{cv} = 0.976378$, $\omega = 1$ and maximum turning angle $\gamma = 10$ decimal degrees. We present three simulation snapshots, with the time units indicated near them.



SOURCE: Produced by the author. Appears in Freitas et al. (2018).

The third example (Figure 4.8) consists of obtaining formations in which the agents keep their relative positions fixed. The simulation is similar to the second example, with the VA's random walk. Here the difference is related to the agents' control parameter. As soon as one agent enters the FR and its speed converges to s_a , its control parameters are set to $\alpha_a = \alpha_c = \alpha_{cv} = 0$, α_s is maintained as is and finally $\alpha_{av} = 1$. It results in particles aligning only with the VA when inside the FR and the only reaction to other nearby agents is collision avoidance. Consequently, $F^i(t) = F_{av}$ when no collision is about to happen and $F^i(t) = F_s$ otherwise. This alignment-only state with the VA inside the FR guarantees the relative distances among agents fixed. An alternative would be to keep $\alpha_a \neq 0$ to tackle noise and any sort of external influence.

Figure 4.8 - Simulation results with the VA performing a random walk inside a bounded region as in Figure 4.7, but the agents maintain their relative positions fixed, after a transient (notice that relative positions do not change from $t=1375$ to $t=3675$). Parameters: $\alpha_a = 0.23622$, $\alpha_c = 0.212598$, $\alpha_{av} = 0.488189$ and $\alpha_{cv} = 0.976378$, $\omega = 1$ and maximum turning angle $\gamma = 10$ decimal degrees. We present three simulation snapshots, with the time units indicated near them.



SOURCE: Produced by the author. Appears in Freitas et al. (2018).

When the VA moves in a straight line as in the optimization setup, the individuals do not change their position very often inside the FR, except in the imminence of collisions. However, in situations where the VA changes its heading angle continuously, like the scenarios we presented in this Section, the agents constantly interact. If one wants the agents to establish a static formation, one idea would be to fol-

low the strategy of the third example, for fixed formations. Dynamic formations are desired in applications such as surveillance or exploration wherein one desires the agents' positions inside the group not to be predictable or static. On the other hand, in formations of satellite constellations, they must keep the relative positions fixed.

4.3 Conclusions

This Chapter presented the simulations and numerical results of the model for autonomous vehicle formation following a mobile reference. The focal point was to solve the inverse problem of finding proper parameters that drive the agents to the desired formations. Three objective functions are used to quantify the formations and their minimum correspond to the group configurations we want. We first solved the problem for each function and lastly present the results for the multiobjective version, considering all three functions in parallel. The last section was concerned with the simulation of three real-world problems: in the first, the group must develop a circular trajectory in a formation with varying relative positions among agents; the second consists on random motions inside a rectangular area, and; finally, the third example is as the second but with fixed relative positions, such that the formation keep a tight configuration.

5 PARTICLES WITH PHASE-COUPLED OSCILLATOR DYNAMICS: SIMULATIONS AND NUMERICAL RESULTS

Here we present simulations and numerical results for the PCOD model introduced in Section 3.3. Firstly, the control parameters' space is investigated in order to figure out which regions lead the particles to symmetric circular formations in a timely manner. Following is presented the effects of adding and removing agents to/from already stable formations. Another important scenario is the interchangeability of system configurations, going from one symmetric formation to another, which is addressed as well. We propose the so-called ‘‘Switching System’’ that consists of periodically switching the system potential, resulting in formations with non-overlapping particles and chaotic circular-like trajectories. Finally, the effects of fixed time delay in the communication between agents are investigated followed by simulations with a collision avoidance mechanism.

5.1 Effect of control parameters on cluster emergence

The symmetric arrangements discussed in Section 3.3 depend both on initial conditions and control parameters K_m , for $m = 1, \dots, M$ related to the number of clusters. The number of symmetric clusters strongly depends on initial conditions and, in particular, it can be different from M when K_m is not properly chosen. In other words, the system converges to a certain local minimum of the potential, instead of the global minimum with M clusters (Figure 3.6).

We address here the problem of finding sets of control parameters K_m for which the particles achieve symmetric M clusters for most initial conditions. We present in Section 5.3 that some symmetric formations are local minimum of others. This means that the original model does not work for some specific initial conditions.

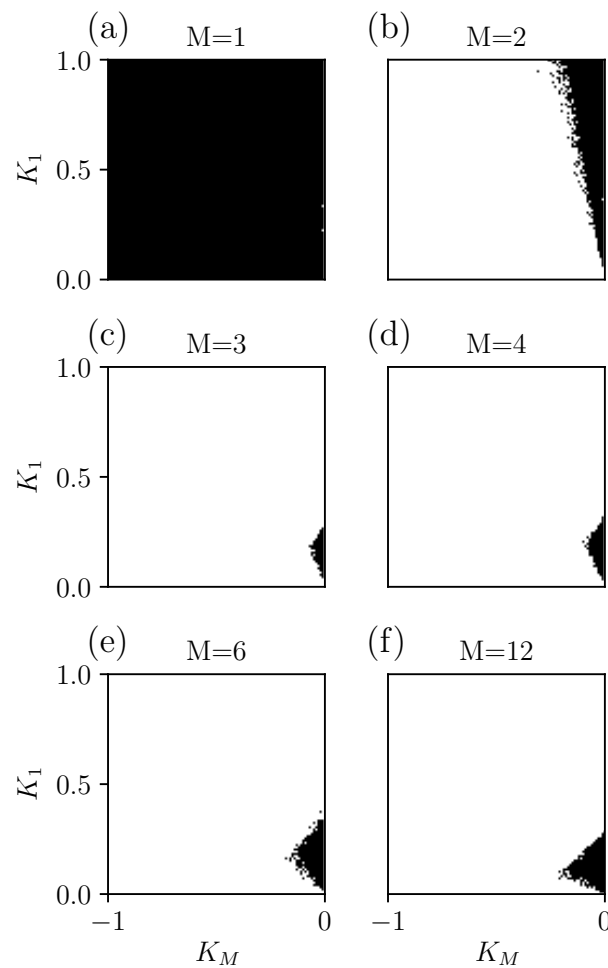
For simplicity, we assume the first positive $M - 1$ weights to be identical $K_1 = \dots = K_{M-1}$. We grouped them due to their common role that is to suppress the unwanted possible symmetric formations that could emerge.

We performed a numerical study of the model (3.14) with control (3.28) for different values of the parameters K_1 and K_M . The simulations are assessed with the m -th moments of the order parameter $p_{m\theta}$ of Equation (3.24).

The black regions of Figure 5.1 indicate which parameter values result in emerging symmetric formations with a relatively short transient time. More specifically, they depict simulations whose order parameters fulfill $m|p_{m\theta}| < \epsilon$ for $m = \{1, \dots, M - 1\}$

and $M|p_{M\theta}| > 1 - \epsilon$ with $\epsilon = 10^{-3}$. The moments $p_{m\theta}$ for each pair of parameter values K_1, K_M are computed by averaging over the results of three simulations each starting with different random initial conditions. The same integration time $t_f = 15000$ is employed at each simulation.

Figure 5.1 - Parameter space $K_M \times K_1$. The black regions correspond to the parameter values, for which symmetric M -cluster formations emerge after the transient $t_f = 15000$. More specifically, for these parameters, the conditions $m|p_{m\theta}| < 10^{-3}$ for $m < M$ and $M|p_{M\theta}| > 1 - 10^{-3}$ are fulfilled. Other parameters: $N = 12$, $\omega_0 = 0.05$.



SOURCE: Produced by the author. Appears in Freitas et al. (2019, Submitted).

When $M < N/2$ is not a divisor of N , clusters of slightly different sizes may emerge. We computed the respective order parameters for such cases and figured out that

there are no regions obeying $|p_\theta| < 10^{-3}$ and $M|p_{M\theta}| > 1 - 10^{-3}$ when $M < N/2$ and $N \bmod M \notin \mathbb{N}$ for $N = 12$ particles.

As a future work, one could find optimal K_m through heuristics (BÄCK; SCHWEFEL, 1993; DE SOUSA et al., 2003), considering the gains for the whole set $m = \{1, \dots, M\}$, instead of only K_1 and K_M . Besides, it might focus on a more specific setup that depends on the mission. Our results have a wider usage, not being target specific. With the heuristic, one could account for a specific number of agents, clusters, initial conditions, desired convergence time, actuators' constraints, etc.

5.2 Adding and removing particles

Real engineering systems must consider the replacement of broken equipment and a certain level of scalability. New agents may join formations and the system should be able to recover from possible failures of equipment. With this motivation, we conducted tests consisting of adding and removing particles to/from already stabilized symmetric circular formations.

We carried out simulations with a set of parameters K_M and K_1 from the stable regions of Figure 5.1 and $N = 12$. Besides, the particles can be added or removed in various ways and we study here some possibilities.

We begin with the case of new particles being added to the system. To the starting stable M clusters, N_{add} new particles are introduced, in accordance with one of the following strategies:

- A0) *All at random* (random phases and coordinates);
- A1) *All uniformly distributed between clusters*: they are placed exactly in the spots between neighboring clusters;
- A2) *All uniformly distributed inside clusters*;
- A3) *Add one by one randomly to already stable formations*: only one particle with random phase and coordinates is added to a system of $N := 12 + N_{\text{add}} - 1$ particles in M stable clusters. When $N_{\text{add}} = 0$, no particle is added, and $N := 12$;
- A4) *All in a cluster with random phases*: the new N_{add} particles are placed exactly inside one cluster, with random phases;

- A5) *All in one spot between two clusters with random phases*: one randomly chooses two clusters and adds all new particles exactly in the spot between them;
- A6) *All at a cluster with the same phase*: similar to A4, but with the same phases as the particles inside the cluster.

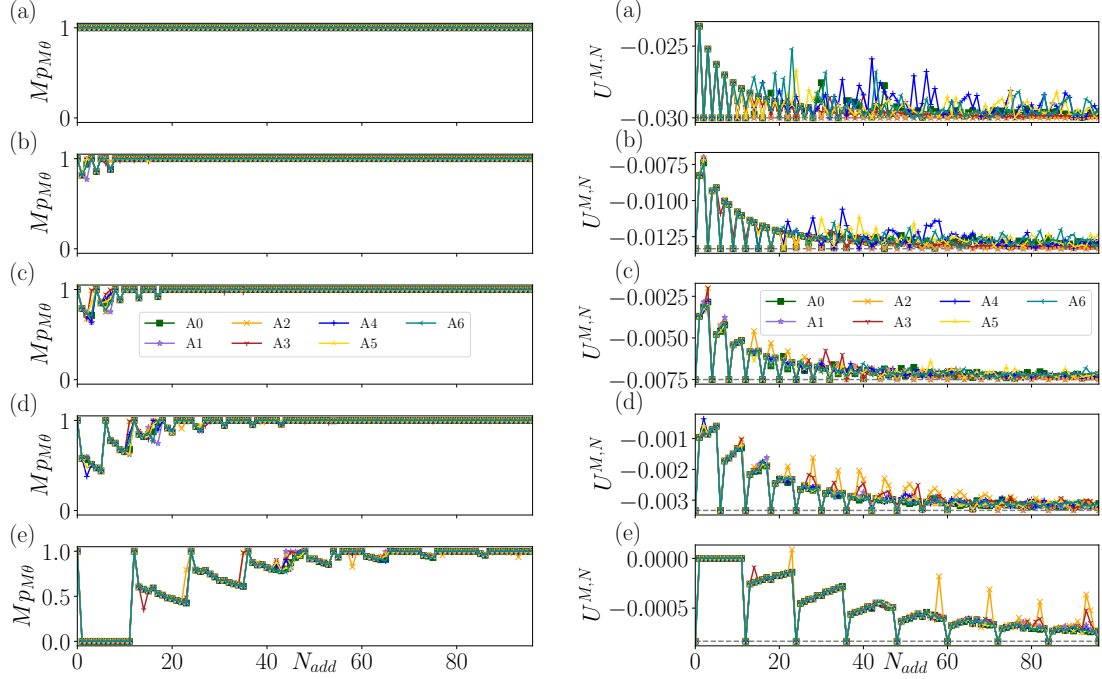
The persistence or destruction of the clusters are monitored by the normalized M -th moment of the order parameter $M|p_{M\theta}| \in [0, 1]$ and the corresponding $U^{M,N}$ potential of Equation (3.25). Simultaneous fulfillment of I) $M|p_{M\theta}| = 1$ and II) $U^{M,N} = (K_m N)/(2M^2)$ indicates that the system has reached a symmetric state with M clusters. When only I is fulfilled, all particles join clusters, but there is no balance.

Figure 5.2 shows the simulation results for $N = 12$, the cluster sizes $M = 2, 3, 4, 6, 12$, and different number of added particles N_{add} . Both the order parameter $M|p_{M\theta}|$ and the corresponding potential $U^{M,N}$ of each point of the graphs are computed by averaging over the results of five simulations with different random initial conditions. We have observed that for all strategies $M|p_{M\theta}|$ decreases with the increasing of the “mismatch” $n = N_{\text{add}} \bmod M \neq 0$ and suddenly jumps to close to 1 when $n = 0$. In other words, the order parameter decreases as the extra particles are added until the number of new members reaches a multiple of M .

The following three situations are distinguished: I) When $N_{\text{add}}/M \in \mathbb{N}$, the particles tend to uniformly distribute among the clusters and $M|p_{M\theta}| \rightarrow 1$ with increasing time; II) When $N \gg M$, $M|p_{M\theta}| \rightarrow 1$ up to a small ε -error even in the case when M is not multiple of N_{add} due to a relatively small perturbation by the added particles; III) Neither situation I or II takes place, i.e., both $N_{\text{add}}/M \notin \mathbb{N}$ and N is not too high in comparison to M . Thus $M|p_{M\theta}| < 1 - \varepsilon$ holds even after a long transient time.

Notice that there are places in which $M|p_{M\theta}| = 1$ and the potential does not reach its minimum. They correspond to a system of unbalanced M clusters. Besides, $M|p_{M\theta}|$ measures whether the clusters are uniformly distributed in the unit circle. The other $M - 1$ moments of the order parameter assess whether the clusters have the same number of elements. Consequently, the more potentials are present in the control the more the optimization focuses on having clusters of the same size and less on establishing uniformly distributed clusters of phases inside the formation. In Figure 5.2, the M -th order parameter oscillates more with increasing M .

Figure 5.2 - Normalized order parameter $Mp_{M\theta}$ (left) and potential $U^{M,N}$ (right) for different number N_{add} of added elements to already formed clusters. The dashed gray line on the right plot corresponds to the potential minimum $U^{M,N} = (K_m N)/(2M^2)$. The system starts with $N = 12$ particles with the following number of clusters: (a) $M = 2$, (b) $M = 3$, (c) $M = 4$, (d) $M = 6$, and (e) $M = 12$. The chosen integration time is $t = 15000$.



SOURCE: Produced by the author. Appears in Freitas et al. (2019, Submitted).

In general, if all particles are added in the same spatial position and phase, they enter the formation already as a new cluster, which triggers some cluster(s) to break in an attempt to reach some potential (local) minimum. For this specific case, the potentials U_m struggle more to converge to optimal values, compared to the setups with broader distributions of particles. The adding strategy number A6 fits this scenario. We also added many particles in one specific spot (chosen at random, or, for example, at the center of mass of the already established formation) with the same phases and the results are worse than the observed for strategy A6.

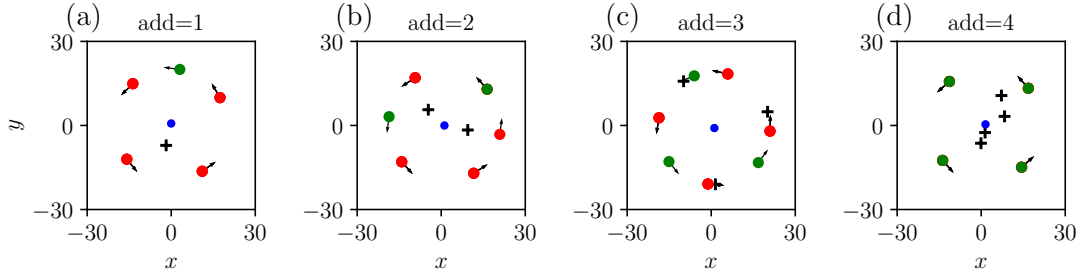
Strategies A0, A1, A2 and A3 produce the best results in terms of the order parameters and potentials close to optimal.

Strategies A4 and A5 correspond to new particles being placed in one single spot. In contrast to strategy A6, they have random phases and even so they also tend

to join the closest clusters. As particles are randomly placed in strategy A0, they are more likely to reach all clusters equally and then converge to a near optimum configuration.

Figure 5.3 presents final states of simulations for $N = 12$ particles divided into $M = 4$ clusters and N_{add} green colored added particles with initial conditions marked with crosses (strategy A0). For small N_{add} , there are n particles positioned between clusters and this explains why $M|p_{M\theta}|$ decreases for increasing n . When $N \gg M$ these isolated particles join the clusters, since $n \ll N$ and the contribution of those remaining particles is not high enough to strongly interfere in the potential minimization. This transition is noticeable in Figure 5.2 (c) for $M = 4$ when $N_{\text{add}} \geq 17$, for example.

Figure 5.3 - Positions of new added particles (green) and clusters (red) after transient $t_f = 15000$. Crosses denote randomly chosen initial positions of the added particles. Initial configuration: $N = 12$ particles, $M = 4$ clusters, $\omega_0 = 0.05$, $K_m = 0.18$ for $m < M$ and $K_M = -0.02$.



SOURCE: Produced by the author. Appears in Freitas et al. (2019, Submitted).

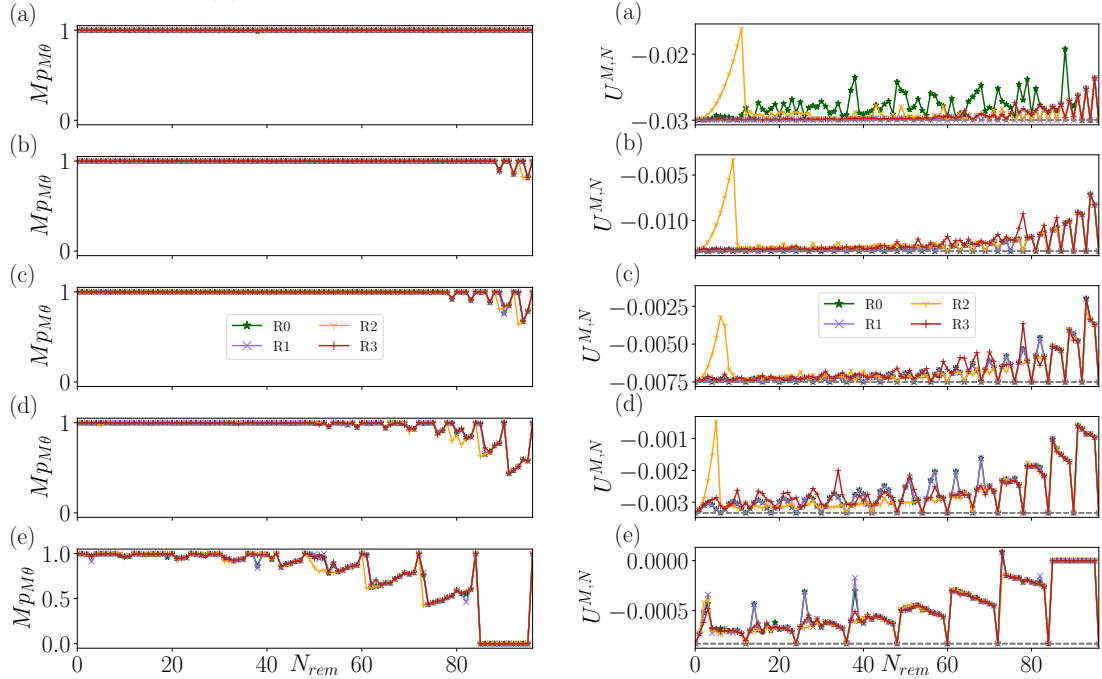
The second part of this section deals with the problem of removing particles from already stable cluster formations. The system starts with $N = 108$ particles and they are removed according to one of the following strategies:

- R0) *Randomly remove N_{rem} particles;*
- R1) *Remove in a balanced manner:* maintain the same number of participants in each cluster, or as close as possible to it.
- R2) *Remove one cluster at a time:* start removing from one cluster and proceed to the next only when the latter vanishes.
- R3) *Randomly remove one particle at a time from stable formations:* es-

establish the stable formation with $N := 108 - N_{\text{rem}} + 1$ particles and M clusters, and randomly pick one particle to be removed. When $N_{\text{rem}} = 0$, no particle is removed, and $N := 108$.

When removing N_{rem} particles from a system one finds similarities as well as differences to the case of adding. Let us define $q = N_{\text{rem}} \bmod M$. The left side of Figure 5.4 shows that $M|p_{M\theta}|$ grows for increasing q , i.e., $q = 1$ corresponds to local minimum, whilst $n = M - 1$ is the local minimum for the adding particles problem.

Figure 5.4 - Normalized order parameter $M|p_{M\theta}|$ (left) and potential $U^{M,N}$ (right) for different number N_{rem} of removed elements from already formed clusters. The dashed gray line on the right plot corresponds to the potential minimum $U^{M,N} = (K_m N)/(2M^2)$. The system starts with $N = 108$ particles with the following number of clusters: (a) $M = 2$, (b) $M = 3$, (c) $M = 4$, (d) $M = 6$, and (e) $M = 12$. The chosen integration time is $t = 15000$.



SOURCE: Produced by the author. Appears in Freitas et al. (2019, Submitted).

Strategy R3 presents the best result because it starts with $108 - N_{\text{rem}} + 1$ particles perfectly distributed in M clusters and at each iteration only one particle is removed. Thus one expects that the order parameter and the potentials keep close to optimum values.

Strategy R2 always produce unbalanced clusters for small N_{rem} as one can see in Figure 5.4, with high $U^{M,N}$. When N_{rem} is sufficiently large, it approaches the results of the other strategies (observe the potentials). Regarding the number of observed clusters, all strategies seem to behave the same, as the order parameters suggest.

Strategies R0 and R1 generate similar results, with an exception for $M = 2$, where strategy R1 is better.

Interestingly, both Figure 5.2 and Figure 5.4 show very similar results for the order parameter for the same configuration (total number of oscillators N and the targeted cluster size M) independently on the way how this configuration is achieved, i.e. either adding or removing the particles.

However, there are still some differences between the points in which the total number of particles is the same after the adding/removal operation is performed. We see for instance, the case $M = 6$ of Figure 5.2(d) and 5.4(d), with $N_{\text{add}} = 11$ and $N_{\text{rem}} = 85$ (corresponding to the same total number of oscillators $N = 23$), where $6|p_{6\theta}| = 0.68$ and $6|p_{6\theta}| = 0.99$, respectively. This means that a system of a given size, after the introduction of new elements, is more likely to perform worse than another system of the same size, after losing elements. In other words, in some rare cases, one can argue that the system is more able to recover from failures than to stabilize after receiving more particles.

5.3 Changing between formations

This section deals with the problem of changing the formation from one number of clusters M_f to another M_t . The sub-indexes f and t stand for “from” and “to”, respectively. We observe that the transition works perfectly in the following two situations:

- I) $M_f < M_t$;
- II) $M_f > M_t$ when $(M_f/M_t) \in \mathbb{N}$.

In other scenarios, the M_f cluster formation appears to be a local minimum of the potential $U^{M_t,N}$.

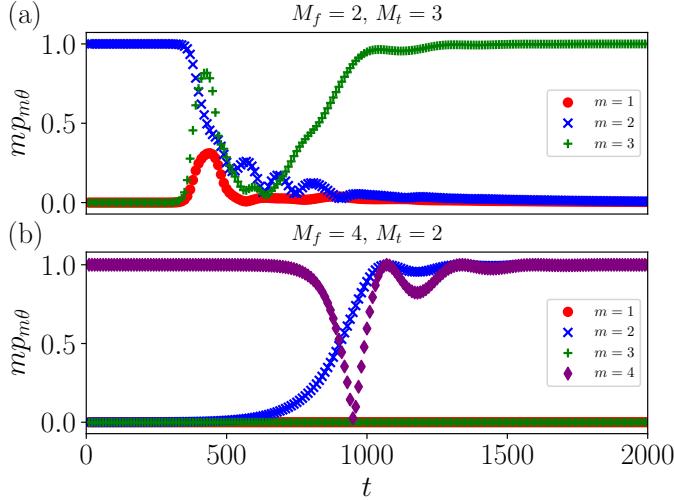
The explanation behind case I is that the gradient (3.27) of the potential $U^{U_t,N}$ is evaluated for $m \in [1, M_t]$ and, since the new number of clusters is higher than before, the corresponding potential $K_f U_f$ is included and the cluster formation related to it is suppressed.

In the second case $M_f > M_t$, the summation (3.27) of the new potential $U^{M_t,N}$

does not cover M_f . Therefore, the cluster state with M_f clusters is not explicitly considered in the optimization procedure. However, when $M_f = nM_t$ with some $n \in \mathbb{N}$, then $M_f|p_{M_f\theta}| = M_t|p_{M_t\theta}| = 1$, hence, all potentials related to multiples of M are minimized as well.

Figure 5.5 illustrates the two possibilities for (a) $M_f = 2$, $M_t = 3$ and (b) $M_f = 4$, $M_t = 2$. The small-scale oscillations (wiggling pattern) of the order parameters come from the transient processes since the phases do not occupy their positions in the new M_t clusters immediately. Instead, they move towards the desired places in an oscillatory motion. Although the order parameters display these local fluctuations, they have a clear long term direction. A similar pattern is observed in pulse-coupled neuronal ensembles (LÜCKEN et al., 2013) right after they are submitted to the so-called “coordinated reset stimulation”.

Figure 5.5 - Time series of the order parameters $m|p_{m\theta}|$ for system (3.14) with the control (3.28). The system starts with M_f symmetric clusters and its potential is switched from $U^{M_f,12}$ to $U^{M_t,12}$ at time $t = 0$. The order parameters indicate successful switching to the desired number of clusters M_t .



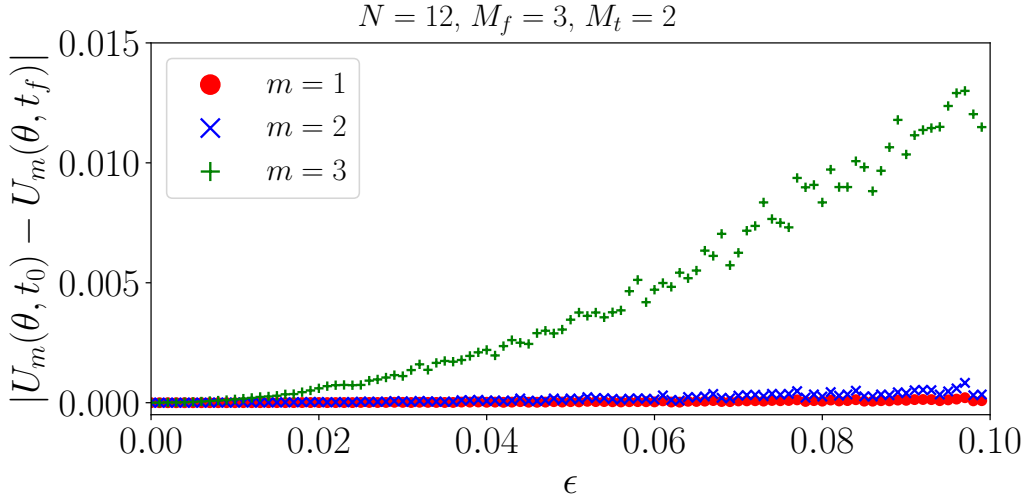
SOURCE: Produced by the author. Appears in Freitas et al. (2019, Submitted).

The problems arise when $M_f > M_t$ and M_f and M_t are not multiples. This means that the M_f -th potential, that is already at optimum, is not considered in the minimization process and it becomes impossible to break the existing cluster symmetry. In other words, the cluster formation with symmetric M_f clusters remains a local minimum of the new potential $U^{M_t,12}$. As a result, adding a small additive Gaussian noise in control (3.28) cannot solve effectively the problem, since it merely results

in fluctuations around a local minimum.

We support the claim that small perturbations in symmetric clusters produce no effect with the simulations of Figure 5.6. The system starts already with $M = 3$ clusters and the potentials $U_m(\boldsymbol{\theta})$ of Equation (3.25) are evaluated at time t_0 . After that the system is integrated with control (3.28), but with the new configuration $M = 2$. We know that this transition does not happen, for reasons we already discussed (Figure 5.7a). Random perturbations of intensity ϵ are introduced to this initial configuration at $t = 0$ in order to find out which ϵ breaks the initial cluster symmetry. We realized that the system is only able to reach the $M = 2$ cluster configuration for big ϵ . This means that the related potentials find local minimum at the cluster formations and the perturbation should be high enough for the system to leave them.

Figure 5.6 - Changing between formations with $M_f = 3$ and $M_t = 2$, for $N = 12$. Particles start at a symmetric circular formation with $M = 3$ and we added a small perturbation of amplitude ϵ and start the control (3.28) integration. We evaluated the potentials (3.25) at $t = 0$ and $t = 15000$ and observed that transitions start to occur when perturbations are high enough to make particles move from local minima.



SOURCE: Produced by the author.

Further tests have shown that if this perturbation persists during all the time, the 3-clusters configuration is broken and the new arises by the cost of having the particles always wiggling due to the noise. Maybe one could turn the noise source on at the

beginning of the transition and shut it down after some transient.

Instead, we tackle this problem with a noiseless strategy that comprises the introduction a correction term into the potential, such that the new potential reads

$$U_{M_f}^{M_t, N} := U^{M_t, N} + \frac{N}{2} \delta(M_f, M_t) K_f |p_{M_f \theta}|^2, \quad (5.1)$$

where

$$\delta(M_f, M_t) = \begin{cases} 1, & M_f > M_t \text{ and } M_f/M_t \notin \mathbb{N} \\ 0, & \text{otherwise} \end{cases}. \quad (5.2)$$

Here $K_m > 0$ for $m = \{1, 2, \dots, M_t - 1\}$, $K_f > 0$ and $K_m < 0$ for $m = M_t$. The new term aims to break the M_f cluster symmetry. The new gradient then reads

$$-\frac{\partial U_{M_f}^{M_t, N}}{\partial \theta_k} = \frac{1}{N} \sum_{m=1}^{M_t} \sum_{j=1}^N \frac{K_m}{m} \sin(m(\theta_k - \theta_j)) + \delta \frac{1}{N} \sum_{j=1}^N \frac{K_f}{M_f} \sin(M_f(\theta_k - \theta_j)). \quad (5.3)$$

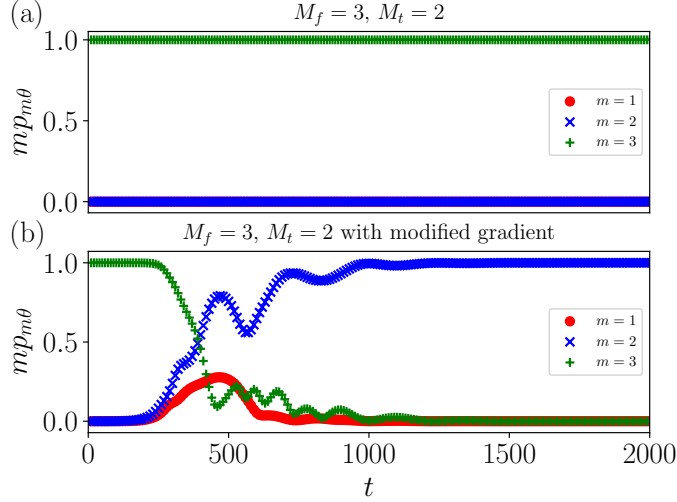
After replacing the former phase potential gradient in control (3.28) by this new version, we obtain

$$u_k(\mathbf{r}, \boldsymbol{\theta}) = \omega_0 (1 + K_0 \langle e^{i\theta_k}, P_k \mathbf{c} \rangle) - \frac{\partial U_{M_f}^{M_t, N}}{\partial \theta_k}. \quad (5.4)$$

Figure 5.7 shows that (a) the old control (3.28) fails and (b) the new control (5.4) enables switching from $M_f = 3$ cluster formation to $M_t = 2$.

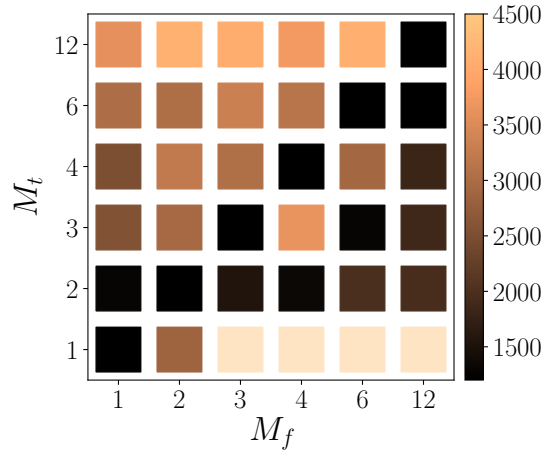
The model (3.14) with control (5.4) produces the transition times from M_f to M_t as shown in Figure 5.8. Here we provide some intuitive explanations for the observed transition times. The transition is usually more time consuming for $M_f < M_t$ than the opposite and the explanation can follow the arguments that are mentioned above: for $M_f > M_t$, although the system is not located at a local minimum, it still possesses initially a small gradient leading to a relatively slow repulsion from the initial configuration with M_f clusters. Contrarily, it tends to be fast when $M_f > M_t$ because the existing clusters simply merge. It can be also time-consuming if M_f and M_t are not multiples because it demands cluster breaking. Moreover, the transitions from $M_f > 2$ to $M_t = 1$ are the most expensive, because it is a huge effort to raise $M - 1$ potential values from minimum to maximum.

Figure 5.7 - Illustration of a successful control by the modified potential (5.4). Time series of the order parameters $m|p_{m\theta}|$ for different m using model (3.14), under conventional control (a) (3.28) and modified (b) (5.4), which is applied at time $t = 0$. The system stays initially in the symmetric M_f cluster state. Panel (b) shows successful switching between M_f to M_t symmetric cluster formation.



SOURCE: Produced by the author. Appears in Freitas et al. (2019, Submitted).

Figure 5.8 - Transition times for a switching from M_f to M_t symmetric cluster formations in system (3.14) with control (5.4). The changing time is calculated whenever the order parameters achieve $M|p_{M\theta}| > 0.999$ and $|p_\theta| < 0.001$. The almost white squares are of order 10000. Every bin is the average of 10 simulations.



SOURCE: Produced by the author. Appears in Freitas et al. (2019, Submitted).

We neglected the changes between numbers of clusters whose division N/M is not an integer because the resulting formations are not symmetric. The system with $N = 12$ particles and $M = 5$ clusters fits the situation studied in section 5.1 for M not divisor of N . The clusters are somehow formed, meanwhile the number of particles is not high enough to fulfill the conditions we imposed for the Figure 5.8, of $M|p_{M\theta}| > 0.999$ and $m|p_{m\theta}| < 0.001$ for $m = \{1, \dots, M - 1\}$.

One of the simple conclusions of this section is: splitting is worse than merging, except when one targets one single cluster.

5.4 The Switching System

This section introduces an approach for the generation of chaotic trajectories and clusters with non-overlapping elements. The system, which we call ‘‘Switching System’’ (SS) consists of model (3.14) under control (5.4) for M_t periodically switching between M_A and M_B with a certain period T . It means that each $T/2$ time units the system focuses on the minimization of one of the two potentials $U_{M_B}^{M_A, N}$ and $U_{M_A}^{M_B, N}$, correspondingly. Formally the new potential can be written as

$$U_{SS} = \Pi(t)U_{M_A}^{M_B, N} + (1 - \Pi(t))U_{M_B}^{M_A, N}, \quad (5.5)$$

where $\Pi(t)$ is the T -periodic piece-wise constant function with the value 1 for all $(t \bmod T) \in [0, T/2)$ and 0 otherwise.

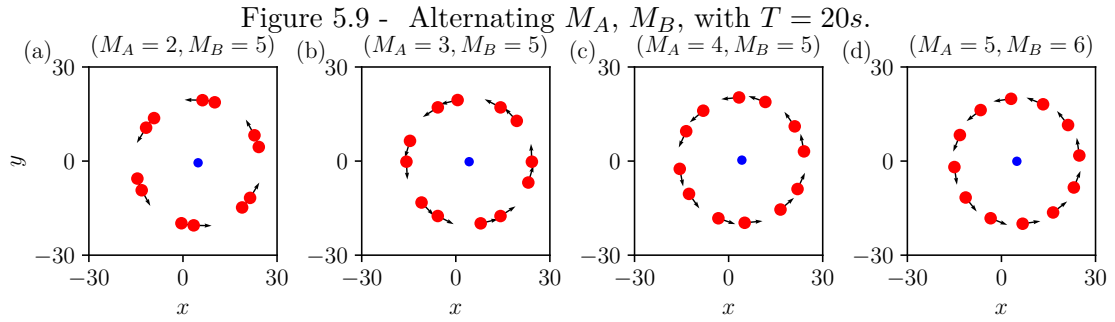
Simulations show that a formation converges to $M = \max \{M_A, M_B\}$ when M_A and M_B are multiples and the alternating period T is less than a critical value T_1 . The explanation comes from the fact that when one minimizes the potential (5.1) using, for example, $M = M_A < M_B$, the potentials for every other M multiple and higher than M_A are minimized as well. On the other hand, during the simulation, when the potential for M_B is active, the M_A 's is being suppressed. After a long enough transient, the potential related to M_B is at its minimum value giving rise to M_B clusters.

Moreover, there is an interval of periods, between T_1 and T_2 , within which the two potentials compete and do not reach their minimal values. This interval can be seen in Figure 5.10 at the first line with $(M_A, M_B) = (6, 12)$ for $(T_1, T_2) \approx (135, 220)$. This picture will be discussed later. For T slightly higher than T_2 , the system stabilizes with $M = \max \{M_A, M_B\}$ clusters in such a way that it becomes hard to break its symmetry. The scenario changes for $T \gg T_2$, when the transition occurs from one

formation to the other as presented in Figure 5.8.

5.4.1 Non-overlapping particles

Interestingly, when either M_A or M_B equals $N/2 - 1$, $\max\{M_A, M_B\} < N/2$ and $T < T_1$, the result is an ensemble of $N/2$ clusters with 2 particles each that do not overlap and keep their fixed relative distance. Figure 5.9 presents one example with $N = 12$ particles, for which $N/2 - 1 = 5$. The picture shows that as M_A increases, so increases the relative distance between participants of the same cluster.



SOURCE: Produced by the author. Appears in Freitas et al. (2019, Submitted).

Keeping stable fixed relative distances is important in real applications. Notice that here we do not employ a collision avoidance mechanism itself, such as in Section 3.3.4.

All possible results for different numbers of particles and periods $T < T_1$ are summarized in Table 5.1.

Table 5.1 - The Switching System outcomes for period $T < T_1$.

State	Necessary condition
Splay state	$\frac{N}{2} < \max\{M_A, M_B\} \leq N$
$\max\{M_A, M_B\}$ clusters	$N/M_A \in \mathbb{N}, N/M_B \in \mathbb{N}$ and $1 \leq \max\{M_A, M_B\} \leq \frac{N}{2}$
Non-overlapping particles	$N/2 \in \mathbb{N}$ (even), either M_A or M_B equals $\frac{N}{2} - 1$, $\max\{M_A, M_B\} = \frac{N}{2} - 1$ and M_A and M_B not multiples

5.4.2 Chaotic trajectories

We are now interested in the interval $T_1 < T < T_2$ for which the particles do not converge to a steady formation. It is convenient to consider discrete dynamics from the system (3.14) with potential (5.5) at the time Tn , $n \in \mathbb{N}$ with the set of $3N$ state variables x_i, y_i, θ_i . We use then the numerically computed mapping

$$y_{n+1} = f(y_n) \quad (5.6)$$

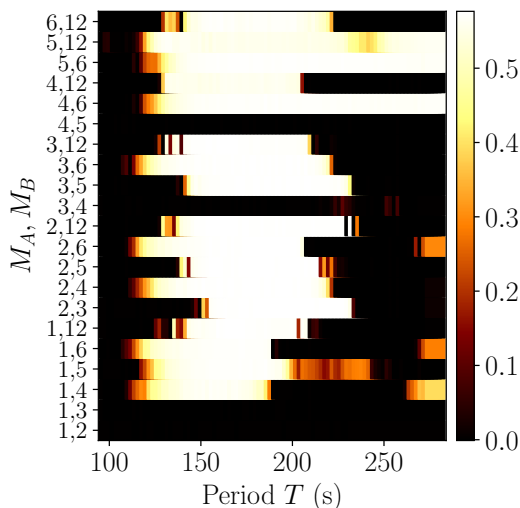
to calculate the largest Lyapunov exponents (LLE) (PARKER; CHUA, 1989) for different pairs (M_A, M_B) and periods T , so to infer whether the system is chaotic or not.

The LLE calculation is as follows:

- a) Form the $3N$ -dimensional state vector y that includes the values of all system variables.
- b) Iterate y in order to discard transients. We have iterated our system so that the original model (3.14) have been integrated for at least $t_f = 10000$ time units.
- c) Perturb the state $y^* = y + c$ with a small perturbation vector c of size $\|c\| = \epsilon$.
- d) Initialize $L_s = 0$. Repeat n times:
 - Iterate both y and y^* for k times.
 - Compute the difference between the two vectors $c_k := y_k - y_k^*$.
 - Calculate the norm $d := \|c_k\|$
 - Reinitialize $y := y_k$, $c := c_k/d$ and the perturbed state y^* to have the distance ϵ from y , but preserving the perturbation direction $y^* := y + \epsilon c$.
 - Compute the natural logarithm of the relative separation $L_f := \ln \frac{d}{\epsilon}$
 - Accumulate $L_s := L_s + L_f$
- e) The LLE is given by $\lambda = \frac{L_s}{kn}$

In contrast to autonomous differential equations, the generic mappings do not feature zero Lyapunov exponents. However, the mapping induced by the system (3.14) possesses an additional continuous symmetry in which what matters are not the angles, but the differences between them. Hence, the gradient term (3.27) is invariant with respect to the simultaneous shift of all variables θ_k by the same arbitrary constant angle φ . A result of this continuous symmetry is the zero Lyapunov exponent, characterizing the neutral perturbations of φ . Simulations confirm that this zero Lyapunov exponent (with numerical accuracy of $\approx 10^{-3}$) remains for periods $T < T_1$. In this range of parameter values, the other Lyapunov exponents appear to be negative, indicating the ordered dynamics. At $T_1 < T < T_2$ the LLE presents positive numbers, which indicates the presence of chaos, as illustrated by the bright colors of Figure 5.10.

Figure 5.10 - Largest Lyapunov Exponents for different M_A , M_B and T .



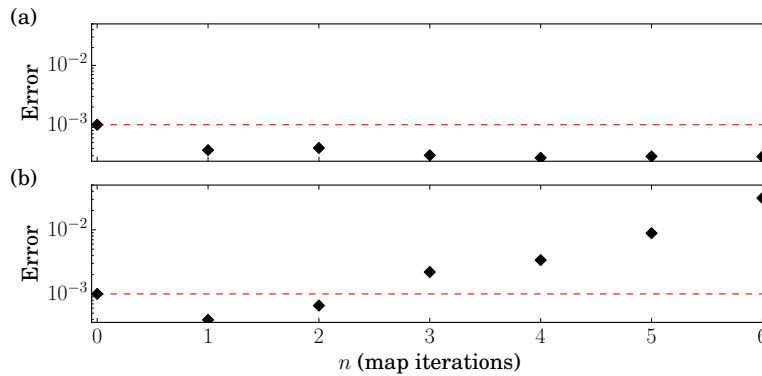
SOURCE: Produced by the author. Appears in Freitas et al. (2019, Submitted).

Figure 5.11 exhibits time series of the SS, (a) for zero LLE and (b) for positive λ . In (a) we instantiate the map and a copy with a perturbation of size ϵ . We integrate them both and see that their trajectories converge after some transient. On the other hand, in (b) an increasing deviation emerges between the system and its perturbed copy, that start to be noticeable after $n \approx 1/\lambda$ iterations as expected from the LLE theory.

Figure 5.12 shows time series of $\theta(nT)$ for the switched system with $N = 12$ parti-

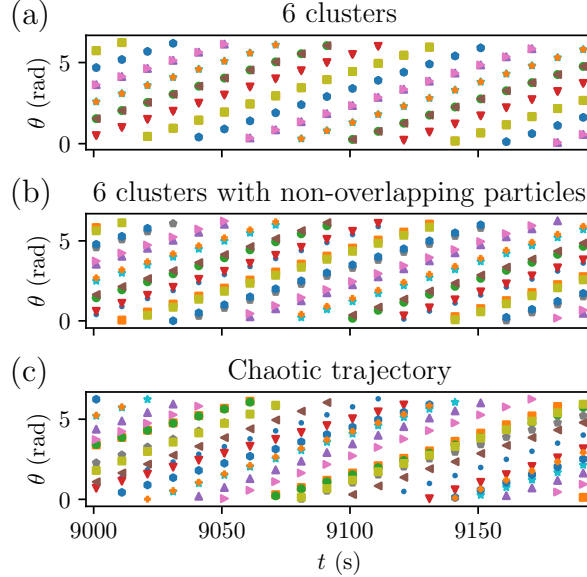
cles, $\omega_0 = 0.05$ and different M_A , M_B and T . The top sub-figure corresponds to a 6-clusters formation, i.e. each cluster contains two overlapping particles. The middle picture displays 6-clusters with non-overlapping particles, that is noticeable by the slight shift between neighboring phases, followed by a chaotic trajectory in the bottom figure.

Figure 5.11 - Error between the map (5.6) and a copy with a perturbation $\epsilon = 10^{-3}$ (horizontal dashed line) as time evolves: (a) Stable solution $M_A = 3$, $M_B = 6$, $T = 100$, $\lambda \approx 0$: trajectories do not diverge with the small perturbation; (b) Chaotic solutions $M_A = 3$, $M_B = 6$, $T = 160$: trajectories diverge with small perturbations from time $n = 1/\lambda$ on. Recall from Figure 5.10 that (b) has $\lambda = 0.57$, therefore trajectories should diverge at $n \approx 2$ map iterations, as observed.



SOURCE: Produced by the author.

Figure 5.12 - Time series of θ for the switched system with $N = 12$ particles, $\omega_0 = 0.05$ and control parameters from Section 5.1. From top to bottom: (a) $M_A = 2$, $M_B = 6$, $T = 40$; (b) $M_A = 2$, $M_B = 5$, $T = 40$ and; (c) $M_A = 2$, $M_B = 6$, $T = 175$.



SOURCE: Produced by the author. Appears in Freitas et al. (2019, Submitted).

5.5 Delayed communication

So far we have discussed results for instantaneous communication among agents. In this section, we address the problem of time delay in information propagation: particles receive data from the others with a certain time lag.

Time delay between dispatch and reception may show up due to the distance between agents. This problem is present in many systems like laser arrays, neuroscience, population dynamics, traffic systems (DIEKMANN et al., 1995; WU, 2001; ERNEUX, 2009; SMITH, 2010; ERNEUX et al., 2017; YANCHUK; GIACOMELLI, 2017). Alike, it is present in systems whose internal processing time may lag the information transmission and/or reception.

One interesting example that relates to our problem is the LISA Project (BAKER, J. et al., 2019), that consists of three spacecrafts in a triangular formation with the aim to seek for gravitational waves from space. As they are about one million miles apart, the communication is not real-time and the design must account for it.

Satellite constellations (NAG; SUMMERER, 2013; BANDYOPADHYAY et al., 2016) are also a trend nowadays, in various applications like the Cyclone Global Navigation Satellite System (CYGNSS) (NATIONAL AERONAUTICS AND SPACE ADMINISTRATION - NASA, 2017) whose mission is to measure the wind speed inside cyclones. As the constellations with small satellites are becoming popular and numerous, formation fly strategies are necessary.

Usually, the control of such systems is centralized and does not account for time delay, with each component simply following the orders of a central station. On the contrary, here we deal with autonomous agents that must adapt their states according to neighboring agents. Thus, the emergence of desired formations relies on the (sometimes delayed) incoming information.

We introduce an adaptation of control (3.28) for symmetric circular formations to handle a fixed time delay, as follows

$$u_k = \omega_0(1 + K_0 \langle e^{i\theta_k(t)}, P_k \mathbf{c}_k \rangle) + \frac{1}{N} \sum_{m=1}^M \sum_{j \neq k}^N \frac{K_m}{m} \sin(m(\theta_k(t) - \theta_j(t - \tau))) \quad (5.7)$$

with $\mathbf{c}_k = (c_1(t - \tau), c_2(t - \tau), \dots, c_k(t), \dots, c_N(t - \tau))$, to account for delay both in phase and in the center c_k coordinates.

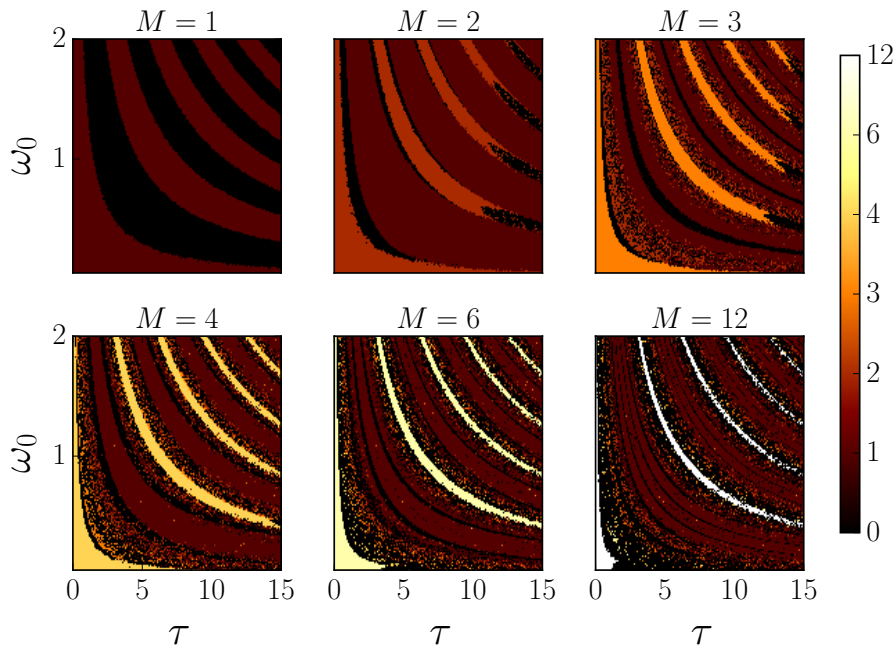
Fixed time delay is useful either when the distances between pairs of agents are similar most of the time, or the distance is not big enough for a lagged communication but they have all similar processing limitations. Consider as an example a satellite constellation in which the satellites' positions come from ground stations, or satellites in a Splay State, receiving neighbors' states at the same long distances among themselves. Both examples fulfill the conditions for fixed time delay.

Recall that the only information agents exchange are position and phase. A good strategy is to send the centers' coordinates c_k instead of position, in order to decrease the processing load, so that each particle receives \mathbf{c}_k and θ .

This setup differs from before due to the presence of delay, leading us from a system of Ordinary Differential Equations to another of Delay Differential Equations, as introduced in Section 2.3. The numerical integration is as the description of Section 2.5.

Simulations evidence that there is a dependence between ω_0 and τ , since ω_0 defines how fast a particle travels around the center, i.e., its period. Figure 5.13 shows this dependence for $N = 12$ particles and different M for varying delay τ . Colors represent the number of obtained clusters, that are characterized via the order parameters of Equation (3.24). We say that the system converged to M clusters when $m|p_{m\theta}| < \epsilon$ for $m < M$ and $M|p_{M\theta}| > 1 - \epsilon$, considering $\epsilon = 10^{-1}$, and call such solutions stable.

Figure 5.13 - Delay τ over natural frequency ω_0 . Colors represent the resulting number of clusters, in which “zero” means disorder. We used the phase order parameters to characterize the clusters, with $m|p_{m\theta}| < 10^{-1}$ for $m < M$ and $M|p_{M\theta}| > 1 - 10^{-1}$.



SOURCE: Produced by the author.

Notice that the system with small ω_0 is barely affected by delay. The effects start to appear with increasing delay and after some period the stable solutions reappear. For a simple explanation, observe Figure 5.13 for $M = 1$ and observe what happens for $\omega_0 = 1$. In the beginning, for $\tau \approx 0$ (dark red), the system converges to one cluster, as expected. By increasing τ a little further, we reach a region of disorder (low order parameters and zero distinguishable clusters). Increasing a bit more, there is again a stable region with one cluster and so on.

Interestingly, the subfigure for $M = 2$ presents stable regions with one and two clusters and again the black regions of disorder. In all other subfigures, we observe that there exists reappearance of stable solutions for all number of clusters $m \leq M$. The shape of the stability regions can be explained by the general reappearance properties of delay differential equations described in [Yanchuk and Perlikowski \(2009\)](#) and indicate that delay can be used as an effective control parameter as well.

These results are important to map the system control parameters. Consider for example a system with a fixed frequency and with a certain amount of delay so that it reaches an undesired region of the (ω_0, τ) parameter space. One solution to overcome this problem would be to add an artificial communication delay in order to enter the next stable region.

When $M = N$, the splay state, it is possible to reach any possible stable cluster configuration that is a divisor of N by just tuning the delay τ .

As future work, we will numerically find the correct boundaries between regions of [Figure 5.13](#). Besides, we will study a more general framework for this problem: a state-dependent delay. Nearby particles should be perceived faster than the farther ones, which poses a more complex problem.

5.6 Collision avoidance

Here we solve the inverse problem of finding proper parameters for the collision avoidance mechanism of [Section 3.3.4 \(FREITAS; MACAU, 2018\)](#). We employ the M-GEO algorithm targeting solutions that decrease the number of collisions and the order parameter [\(3.23\)](#).

The controls [\(3.36\)](#) and [\(3.37\)](#) possess parameters K and K_r . The former relates to the circular formations and the latter to the collisions control. One has to deal with the trade-off between them since $K \gg K_r$ might result in circular formations at the expense of several collisions. On the other hand, $K_r \gg K$ introduces excessive repulsion and the system never converges to the desired formation.

We model this multiobjective problem with the M-GEO algorithm with solutions of 14 bits, 7 for each design variable $K, K_r \in [0, 1]$, which corresponds to a precision $p = 0.01$ (recall [Equation \(2.26\)](#)).

The two objective functions to be minimized are:

- $|p_\theta|$: Equation (3.23). When $|p_\theta| \rightarrow 0$, we say the agents are in a balanced state. Recall that symmetric formations are a specific case of balanced formations.
- f_{ncoll} : the number of imminent collisions per second. When two particles i and j are within a certain distance $\|r_i - r_j\| < d$, the agents are in an imminent collision situation. A score is accumulated, by adding 1 unit per second.

The problem is designed as follows:

$$\begin{aligned} & \min \{|p_\theta|, f_{ncoll}\} \\ & \text{subjected to design variables: } K, K_r \in [0, 1], \end{aligned} \tag{5.8}$$

the simultaneous minimization of both $|p_\theta| \in [0, 1]$ and $f_{ncoll} \in [0, t_f]$, for t_f is the maximum simulation time of the model (3.14).

The M-GEO configurations are the following:

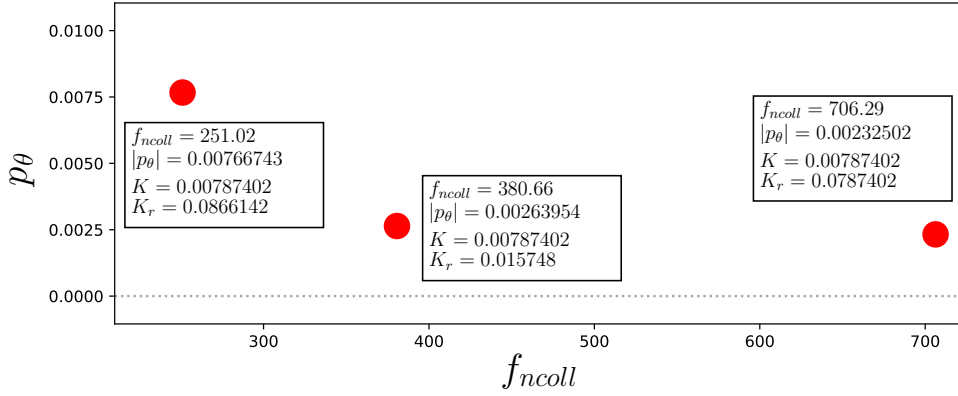
- $\tau = \{0.5, 1.0, 1.5, 2.0, 2.5\}$.
- Number of bits per design variable: 7, corresponding to a precision of 0.01;
- Number of runs for each τ : 50;
- NFE= 100000. It means that the algorithm evaluates the objective functions 2000 times for each τ .

The initial conditions and parameters for the model of phase-coupled oscillators are:

- $N = 6$ agents randomly positioned inside a rectangle of dimensions $l \times l$, for $l = \sqrt{N * \pi * 20}$;
- Control of Equation (3.36), for all-to-all coupling.
- $\omega_0 = 0.05$;
- $d = 5$, the collision radius;
- $K, K_r \in [0, 1]$.
- $t_f = 1000s$ is the total time of each simulation.

The obtained Pareto frontier is depicted in Figure 5.14. If we run the M-GEO with a more accurate precision p and a higher number of evaluations of the objective function NFE, other optimal values may appear. It means that the values found so far are possibly suboptimal solutions.

Figure 5.14 - Pareto frontier of the multiobjective optimization problem (minimization), with objective functions $|p_\theta|$ and f_{ncoll} , and design variables K and K_r .



SOURCE: Produced by the author. Appears in Freitas and Macau (2018).

Following we present simulations using the obtained parameters in three setups:

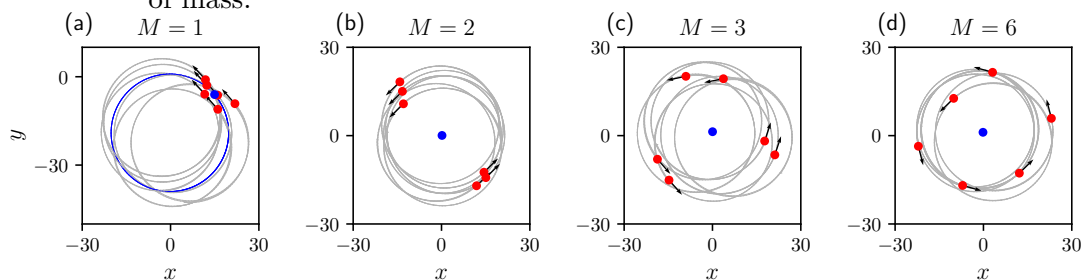
- a) All-to-all: each particle interact with every other;
- b) Ring topology: every particle has exactly two neighbors, such that the communication channels form a ring. This topology is a good option when the agents have limited processing capabilities and can only handle a few data. This assures less information exchange;
- c) Dynamic network: the network changes continuously. Only close neighbors within a certain sensory region are connected.

As in Chapter 4, we also choose here the solution that is closest to the utopian. This gives the design variables $K = 0.00787402$ and $K_r = 0.0866142$. Besides, this solution poses the least number of collisions and the difference between all $|p_\theta|$ is almost negligible.

Figure 5.15 presents the simulations for the all-to-all topology, with $N = 6$,

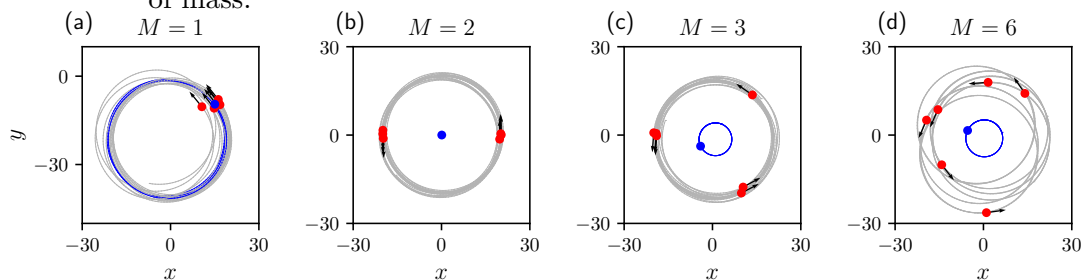
$\omega_0 = 0.05$, $d = 5$ and optimal parameters K and K_r . Formations seem to happen accordingly, in contrast with Figure 5.16 that exhibits results for not optimal parameters. The balancing between collision avoidance and the clusters does not hold in this last setup.

Figure 5.15 - All-to-all: symmetric circular formation with control (3.36). Configuration: $N = 6$, $K = 0.00787402$, $K_r = 0.0866142$, $\omega_0 = 0.05$, $\rho = 20$ and $d = 5$. The red circles correspond to the agents, and the blue circle is their center of mass.



SOURCE: Produced by the author. Adapted from Freitas and Macau (2018).

Figure 5.16 - All-to-all (not optimal): symmetric circular formation with control (3.36). Configuration: $N = 6$, $K = 0.1$, $K_r = 0.1$, $\omega_0 = 0.05$, $\rho = 20$ and $d = 5$. The red circles correspond to the agents, and the blue circle is their center of mass.



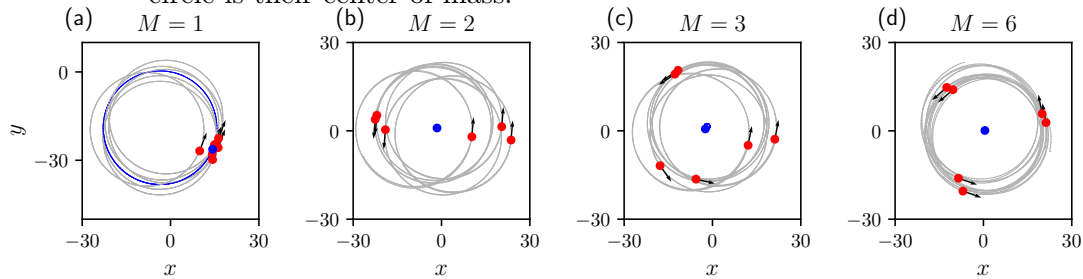
SOURCE: Produced by the author. Adapted from Freitas and Macau (2018).

The considered repulsion region has radius $d = 5$. In particular, we consider the agents are particles, without a real size. However, in real applications, the bigger the agents are the higher the radius d and/or the gain K_r must be, as they have to

start to avoid the neighbors before they reach a critical distance. The parameters d and K_r state the initial distance considered for the usage of *rep* and also the maneuver intensity.

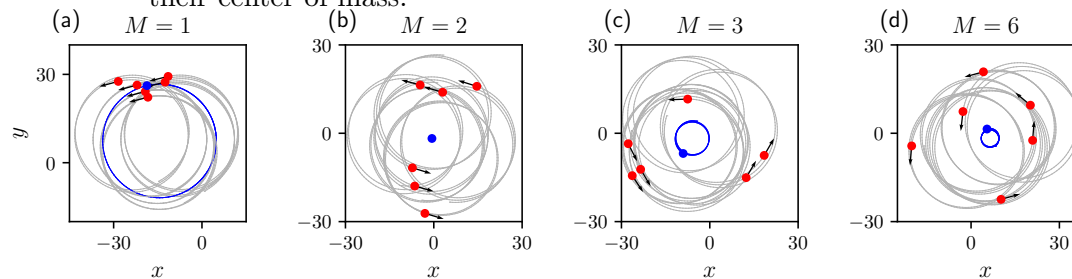
Figure 5.17 displays simulation results for a ring coupling topology, using control (3.37) and Figure 5.18 shows results for simulations with not optimal control parameters, for comparison purposes. The control (3.37), for network-based coupling, is an approximation of the control (3.36), for the all-to-all case. It means that the results are not completely equivalent.

Figure 5.17 - Ring-like network topology: symmetric circular formation with control (3.37). Configuration: $N = 6$, $K = 0.00787402$, $K_r = 0.0866142$, $\omega_0 = 0.05$, $\rho = 20$ and $d = 5$. The red circles correspond to the agents, and the blue circle is their center of mass.



SOURCE: Produced by the author. Adapted from Freitas and Macau (2018).

Figure 5.18 - Ring-like network topology (not optimal): symmetric circular formation with control (3.37). Configuration: $N = 6$, $K = 0.1$, $K_r = 0.1$, $\omega_0 = 0.05$, $\rho = 20$ and $d = 5$. The red circles correspond to the agents, and the blue circle is their center of mass.



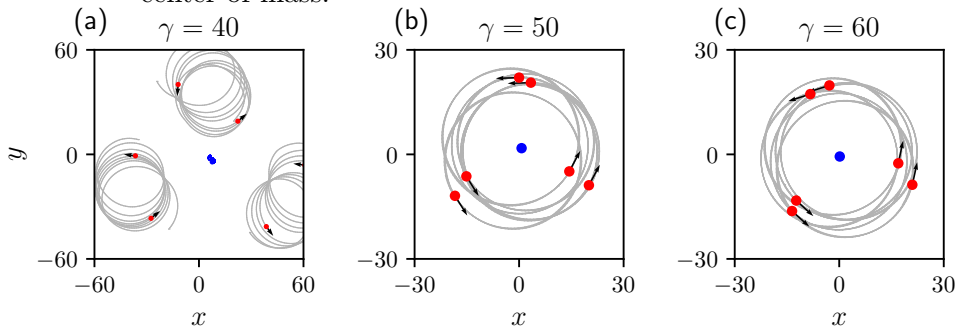
SOURCE: Produced by the author. Adapted from Freitas and Macau (2018).

The last simulation results are for dynamic networks in which the agent has a sensory region with radius γ . An agent j at a distance less or equal γ from agent i is said to be neighbor of i . A restriction we impose, for obvious reason, is that γ must be larger than d .

Dynamic networks do not guarantee the circulant property unless the radius γ has infinite size. If the agents' initial coordinates are close enough so that the maximum distance between two agents is $\gamma = 2\rho + \delta$, we can make sure all the agents will see each other, for certain $\delta > 0$. In this case, the final network is complete and the model should work accordingly.

Figure 5.19 presents simulation results for symmetric circular formations of $M = 3$ clusters, for different γ values. When $\gamma < 2\rho + \delta$, for $\delta > 0$, the circular formations rarely occur, due to the resulting networks are not circulant (Figure 5.19a). Figure 5.20 illustrates results of simulations with not optimal control parameters K and K_r .

Figure 5.19 - Dynamic networks: symmetric circular formation with control (3.37). Configuration: $N = 6$, $K = 0.00787402$, $K_r = 0.0866142$, $\omega_0 = 0.05$, $\rho = 20$ and $d = 5$. The red circles correspond to the agents, and the blue circle is their center of mass.

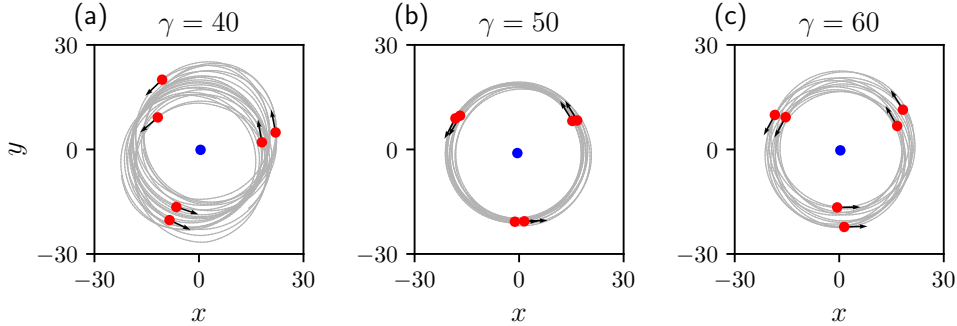


SOURCE: Produced by the author. Adapted from Freitas and Macau (2018).

The results of Figure 5.20 suggests that another optimization procedure should be performed. Notice that the formation emergence is better for not optimal configuration when $\gamma = 40$ than when using the found parameters.

Clearly, the results are better for the all-to-all setup, since the optimization was performed using this configuration. In order to overcome the not as good results for the other topologies, one should run the optimization for each scenario.

Figure 5.20 - Dynamic networks (not optimal): symmetric circular formation with control (3.37). Configuration: $N = 6$, $K = 0.1$, $K_r = 0.1$, $\omega_0 = 0.05$, $\rho = 20$ and $d = 5$. The red circles correspond to the agents, and the blue circle is their center of mass.



SOURCE: Produced by the author. Adapted from Freitas and Macau (2018).

5.7 Conclusions

This Chapter presented the results of the second part of the thesis, regarding symmetric circular formations with the model of particles with coupled-oscillators dynamics. We first explored the control parameter space with the aim to find regions where desired formations emerge in a timely manner. Next, we discussed the consequences of adding and removing particles to/from stable formations. There is a phase transition when the number of new particles to be added of the amount to be removed exceeds critical values. Following we introduce a new term into the potentials to overcome the problem of switching from one formation to the other. Without this term, some formations are a local minimum of others and the transition may never happen. Afterward, we introduced the Switching System, in which we periodically switch between potentials and reach two interesting behaviors, not observed in the real model: clusters of non-overlapping particles and chaotic circular-like trajectories. Such behaviors depend both on the chosen potentials and the switching period. Additionally, we discussed the influence of time delay within the communication among particles. We figured out that it is also a control parameter, capable of switching the system to different behaviors. Besides, some solutions reappear with increasing delay. Finally, we present some results with a collision avoidance strategy.

6 MOBILE ROBOT SIMULATIONS

This chapter presents simulations of autonomous mobile robots using the model (3.14) with control (3.28). The aim is to reduce the so-called reality gap, by showing that the model can be implemented in real-world applications.

We use the ARGoS¹ (Autonomous Robots Go Swarming) simulation environment (PINCIROLI et al., 2012) to emulate the Augmented Reality for Kilobots (ARK) system (REINA et al., 2017) for swarms of Kilobots (RUBENSTEIN et al., 2014).

The ARGoS simulator is a mobile robot simulator, able to reproduce large-scale swarms of robots of any kind. Their open-source code enables the development of new functionalities like sensors, actuators, robot components, visualizations, physics engines, and other communication means.

The Kilobots are tiny robots that weight 0.016 kg, has a circular shape of 33 mm of diameter, the height of 34 mm, are able to turn with an angular velocity of 45 degrees/s and move at approximately 1 cm/s. The robot has very simple hardware that allows it to communicate with neighbors up to 7 cm away by reflecting infrared (IR) light off the ground surface. It moves thanks to its two vibration motors that act as a differential drive system. It does not have wheels, but three fixed thin legs that do not move.

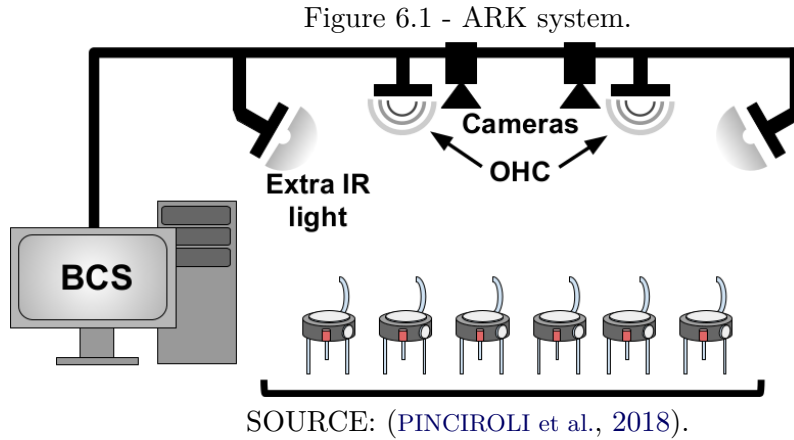
ARGoS is proven to be able to resemble the real Kilobots behavior (PINCIROLI et al., 2018) and the simulation source code is compatible with the Kilobots API (LAB, 2013), which can be deployed on real-world setups.

We use ARGoS to simulate the ARK system because the PCOD model demands more sensory capabilities than the Kilobots available resources. The ARK is composed of a computer station, cameras and overhead controllers (OHC), that track the Kilobots and send them messages (Figure 6.1). This makes possible to emulate other sensors including an all-to-all (and other network topologies) communication channel.

Kilobots controllers are implemented in ARGoS, so that we do not need to care about hardware details. The ARK is implemented in the form of a loop-function and one can adjust the tracking and message exchanging rates, among other parameters. Loop-functions are a set of hook functions executed during the main simulation

¹<https://www.argos-sim.info/>

loop.



Messages are sent from the ARK to the robots, which in turn receive them through the API compatible code, called “behavior” within the ARGoS modular organization. As soon as a Kilobots receive a message, it triggers a series of actions we design.

We chose to have a simulation environment as close as possible to a realistic setup, by using the parameters from Pinciroli et al. (2018).

Before diving into the Kilobots behaviors, we first introduce here a standard tool in control theory, the Proportional, Integral and Derivative (PID) regulator, invented in the first half of the 20th century (FRANKLIN et al., 1997).

This control aims to reduce the error $e(t)$ between the current robot state $s_c(t)$ and a reference $s_r(t)$. The robot must track the (varying) reference by adjusting its actuators. Consider that $s_r(t)$ comes from a model, say the PCOD, for example.

Given that $e(t) = s_c(t) - s_r(t)$ is the error in time instant t , the three following terms are the proportional

$$u(t) = Ke(t), \tag{6.1}$$

the integral control

$$u(t) = \frac{K}{T_I} \int_0^t e(\eta) d\eta, \quad (6.2)$$

and finally, the derivative control

$$u(t) = KT_D \dot{e}(t), \quad (6.3)$$

where K is the proportional gain, T_I the integral time and T_D the derivative time.

The proportional part is a first approximation of error removal. However, it does not fully eliminate the error due to a remaining small steady-state error. Besides, depending on the chosen gain K , it may result in a large transient overshoot.

By adding the integral of the error, it is possible to overcome this steady-state error, yet deteriorating the dynamic response. This last problem is handled with the derivative of the error, the last part of the PID regulator.

The approximations of these control terms to a discrete algebraic equation are the proportional

$$u(k) = Ke(k), \quad (6.4)$$

integral

$$u(k) = u(k-1) + \frac{K}{T_I} Te(k), \quad (6.5)$$

and derivative

$$u(k) = \frac{KT_D}{T} [e(k) - e(k-1)], \quad (6.6)$$

controls. The differential equation that relates $u(t)$ and $e(t)$ is

$$\dot{u} = k(\dot{e} + \frac{1}{T_I} e + T_D \ddot{e}). \quad (6.7)$$

The use of Euler’s method (twice for \ddot{e}) results in:

$$u(k) = u(k-1) + K \left[\left(1 + \frac{T}{T_I} + \frac{T_D}{T}\right) e(k) - \left(1 + 2\frac{T_D}{T}\right) e(k-1) + \frac{T_D}{T} e(k-2) \right]. \quad (6.8)$$

Now, consider that we are designing the PID for the robots to track the phases that come from the models. The robots actuators use the tracking system to reach the desired orientations. Each robot has θ_k as a reference and continuously adapts its vibration motors to decrease the difference between its real orientation and the model. This difference is the error $e(t) = \theta_k(t) - \Theta(t)$, for $\Theta(t)$ is the robot’s real orientation.

This error calculations $\hat{e}(kT)$ happens at discrete time, with sample time T . Besides, the system output $y = \Theta(t)$ and its dynamics are continuous. A system having both discrete and continuous signals is called *sampled-data* system. Thus, one has to determine the effect of the sample rate and select a rate that is sufficiently fast to meet all specifications (FRANKLIN et al., 1997).

The ARK system sends this error according to a latency of T seconds and as soon as the robot receives it, the tracking system is computed through Equation (6.8).

Our setup accounts for Kilobots with maximum angular velocity of $v_m = \pi/4$ rad/s, that are able to execute three commands: *Go straight*, *Turn left* and *Turn right*. Therefore, a discrete control system. The PID regulator works as follows, in Algorithm 1.

Algorithm 1 Kilobot control

- 1: Compute $u(k)$ with Equation (6.8)
 - 2: $\alpha = u(k)/v_m$
 - 3: **if** $\alpha > 1$ **then** $\alpha := 1$
 - 4: **else if** $\alpha < -1$ **then** $\alpha := -1$
 - 5: **if** $|\alpha| < 10^{-6}$ **then**
 - 6: *Go straight*
 - 7: **else if** $\alpha > 0$ **then**
 - 8: *Turn left* for α seconds
 - 9: *Go straight* for $1 - \alpha$ seconds.
 - 10: **else**
 - 11: *Turn right* for α seconds
 - 12: *Go straight* for $1 - \alpha$ seconds.
-

The algorithm computes the control signal and normalizes according to the maximum angular velocity. After that, the control response is bounded and the robot must turn to the chosen direction when needed and then go straight when the control is small enough. Here we empirically chose 10^{-6} as a threshold for the *Go straight* command.

The robot receives new errors $e(k)$ from the ARK system each 1 second. During this 1 second, it updates the error about 10 times as follows $e(k) := e(k) - u(k)$, so that the robots can continue the tracking during the interval between messages.

6.1 PCOD model

This Section is devoted to the deployment of the PCOD model of Section 3.3 into the Kilobots simulator. We introduced the speed variable since we are no longer dealing with unitary speed, and do not care about collisions.

Whenever a model is implemented in a real device, one needs to adapt it to because of hardware characteristics and limitations. Here, we care about the following physical constraint: linear and angular velocities need to be properly limited, so to avoid actuators overload.

Equation (3.14), for the PCOD model becomes:

$$\dot{r}_k = v e^{i\theta_k}, \quad (6.9a)$$

$$\dot{\theta}_k = u_k(\mathbf{r}, \boldsymbol{\theta}), \quad k = 1, \dots, N, \quad (6.9b)$$

with v being the Kilobot nominal speed. When looking to the specific situation where $\dot{\theta} = \omega_0$:

$$r_k(t) = r_k(0) + v \frac{i}{\omega_0} - v \frac{i}{\omega_0} e^{i\omega_0 t} \quad (6.10)$$

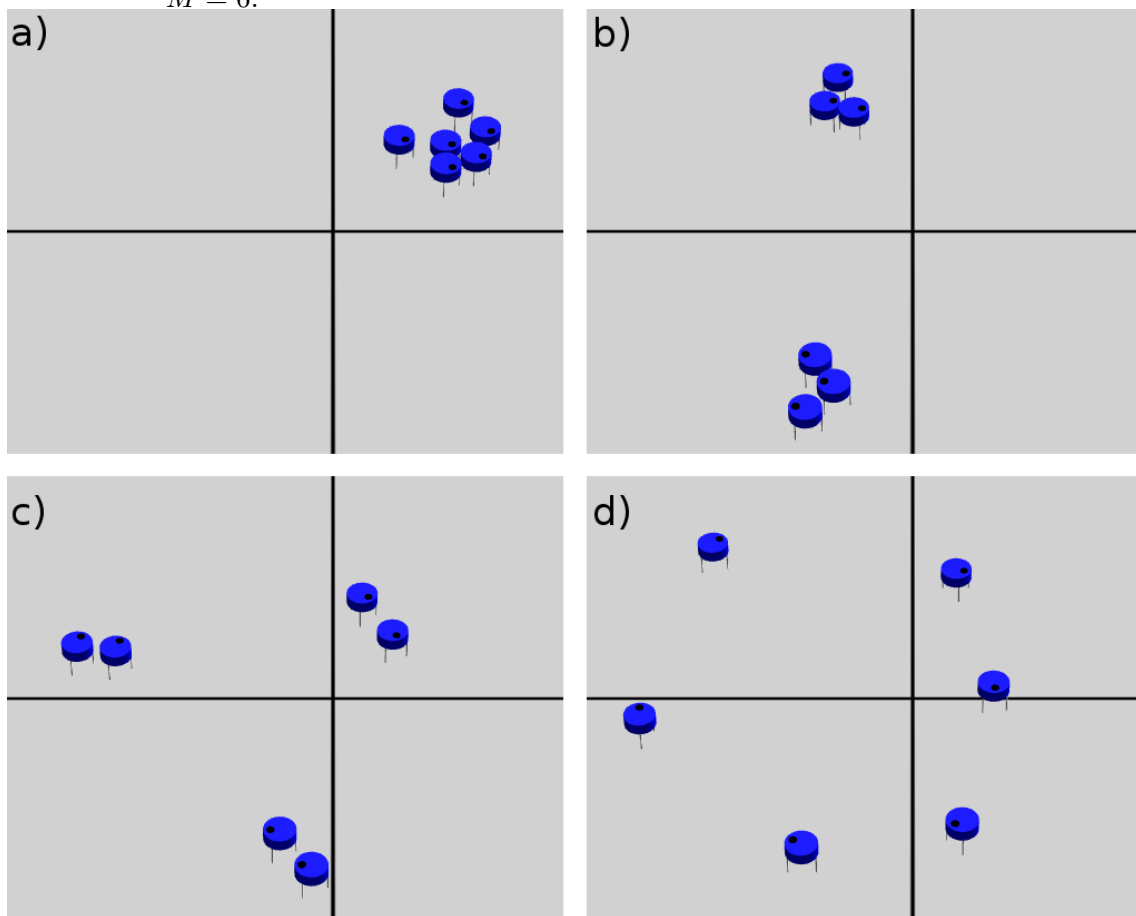
and thus the center of rotation is given by

$$c_k(t) = r_k(t) + v \frac{i}{\omega_0} e^{i\theta_k(t)} \quad (6.11)$$

that stands for the velocity vector rotated 90 degrees (or minus 90, depending on the ω_0 sign), normalized according to the circular trajectory radius $\rho_v = \frac{v}{|\omega_0|}$ and multiplied by the robot nominal speed.

Simulations of model (6.9) with control (3.28) and algorithm 1 are shown in Figure 6.2.

Figure 6.2 - Simulation of model (6.9) under the control for symmetric circular formations of Equation (3.28). Parameters: $N = 6$, $K_0 = 10$, $\omega_0 = 0.05$, $K_m = 0.18$ for $m < M$ and $K_M = -0.02$, $v = 0.01$. a) $M = 1$, b) $M = 2$, c) $M = 3$, d) $M = 6$.



SOURCE: Produced by the author.

6.1.1 Effect of Noise

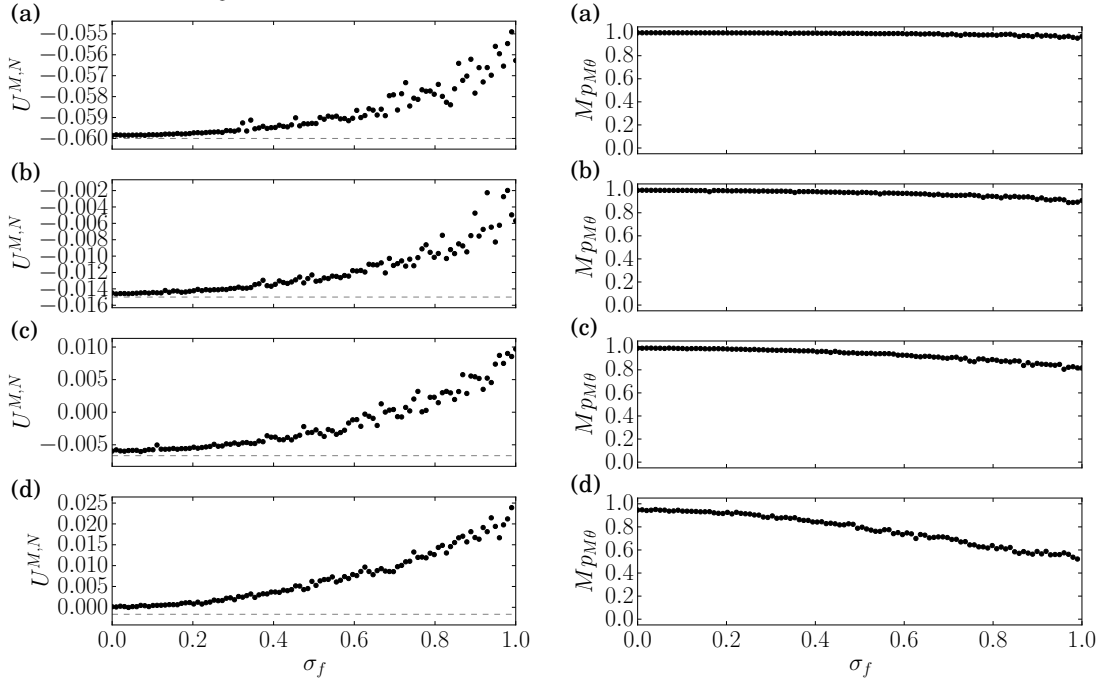
Noise is introduced on the differential drive system so that the left and right speeds account for calibration and environmental issues. Let the real velocity be

$\hat{v}_i = f_i(v_i + b_i)$, with v_i the nominal speed, b_i is a fixed bias added to each robot at the beginning of the simulation (calibration issues) and f_i is a per-step actuation noise (environmental problems), with $i \in \{l, r\}$ the left and right wheels identifier. Both f_i and b_i have Gaussian distributions.

After comparing results of a sample of 120 real and 600 simulated Kilobots, [Pincioli et al. \(2018\)](#) found that $\mu_b = -0,75 \text{ mm/s}$ and $\sigma_b = 1.96 \text{ mm/s}$ are the mean and standard deviations for b_i that better mimic the real world motions, when $f_i = 1$ (without white noise).

We vary the standard deviation σ_f of f_i and calculate the corresponding potentials and M -th order parameters of the formations, after a simulation of length $t = 5000$. The results of [Figure 6.3](#) are the average of 100 trials. It shows that the potentials grow and the respective order parameters decrease for increasing noise, as expected.

Figure 6.3 - Varying σ_f . Configuration: $N = 6$, $K_0 = 10$, $\omega_0 = 0.025$, $K_m = 0.18$ for $m < M$ and $K_M = -0.02$, $v = 0.01$. (a) $M = 1$, (b) $M = 2$, (c) $M = 3$, (d) $M = 6$.



SOURCE: Produced by the author.

The formations are well defined for small noise and start to distort when noise is high enough. Still, the system may be considered robust to noise up to some extent.

6.2 Conclusions

This Chapter proposed an implementation of the model of particles with coupled-oscillator dynamics into the ARGoS robot simulator. We introduced some adaptations in the model and discusses the effects of noise on the differential drive system and speed, the latter to account for calibration and environmental issues. The model seemed to behave well until a certain noise strength.

7 CONCLUSIONS AND FUTURE WORK

Collective motion is an ubiquitous phenomenon observed in schools of fish, flocks of birds, bacteria, colonies of ants and other various groups of living beings. The mechanisms behind these behaviors may be triggered due to several reasons, namely the imminent attack of a predator, mating rituals, foraging, etc. Unquestionably, each agent is autonomous to make decisions based on its perception of the surrounding environment, including the neighbors' states.

The decision-making process is driven by interaction rules that may also be employed in engineering systems in order to reach similar patterns. The aim is not to mimic the living beings, but to extract proper rules that lead the band to desired behaviors.

The motivation of this thesis is grounded in the technological advances in satellite constellations, groups of unmanned aerial vehicles and mobile robots. In the near future, such systems are going to be present everywhere and the individual control of each element will be unfeasible. Hence, they must have a high level of autonomy to stand their position within coveted formations.

The thesis presented two main approaches: a phenomenological reactive model of agents that follow a mobile reference in a tight formation, making use of bio-inspired interaction rules, and a model of particles with coupled-oscillator dynamics. In the first case, we dealt with the problem of quasi-parallel formations, heading to directions dictated by the so-called virtual agent, that represents a trajectory. The second model investigated formations in circular trajectories with particles grouping in clusters of the same size and uniformly distributed along the trajectory.

Regarding the first model, our results conclude that bio-inspired rules are effective, especially when combined with heuristics to determine the coefficients that weight their contributions. The evolutionary algorithm we employ is the Generalized Extremal Optimization (GEO) for mono-objective problems, and its counterpart for multiobjective problems, the M-GEO.

Three test case simulations are presented with the reactive model to express real-world problems: i) A formation that moves in circles; ii) a formation that randomly moves inside a rectangular area and; iii) the random motion inside a rectangular area but keeping fixed relative positions between agents.

The first simulation represents the setup of a data collection mission in which the formation must periodically visit some places. This has great importance in data

collection, surveillance, imaging, etc. The second and third simulation picture the scenario of formations moving inside a desired region, with the difference that the third maintains the relative positions between agents fixed. The first and second cases value unpredictability since the formation continuously change although it has a predefined dispersion, contrarily to the third simulation.

Some applications require circular trajectories. Take as an example the CYGNSS system, a satellite network that orbits Earth with the aim to compute the wind velocity inside cyclones. The satellites uniformly distribute around this trajectory and keep their position within the formation. However, the satellites of the CYGNSS are not autonomous and must be individually controlled, oppositely to future missions that will inevitably consider autonomous agents.

With this motivation, we studied the model of particles with coupled-oscillator dynamics for symmetric circular formations, whose controls are derived from potential functions. We observed through Monte Carlo simulations that there are specific regions in the control parameter space within which the stable formations emerge. The remaining areas might also result in circular trajectories, but they either depend on initial conditions or take too long to converge.

Furthermore, we investigated the system response to new particles being added. When there is only one cluster, it does not matter how many new elements are introduced, the system always converges to one cluster. With a proper choice of control parameters, this is also verified for two clusters. Things start to change with configurations of three or more clusters, since some new particles may never join them. This happens when the number of new particles is below a certain threshold and results in some simply sitting between stable clusters.

We realized that this happens because configurations with an unbalanced number of particles, in relation to the number of clusters, never reach the minimum of the potentials. When those particles sit between clusters, the potential has the minimum possible values for that specific configuration. After a critical number of new elements are added, the potential approaches the minimum when all particles join clusters.

This behavior is similar regardless of the way this operation is done: for particles included at random, or inside already stable clusters, or between clusters, all with the same initial conditions, etc. For instance, if they are uniformly included inside clusters, or at random, the potentials are usually closer to optimal. The explanation for the former is obvious. In the latter case, we observe that particles tend to be

attracted by clusters, which is easier when they have spread around and not grouped. On the other hand, if one adds lots of new agents at one single place, they are already a cluster, which leads to the costly operations of breaking and rearranging clusters.

The opposite case of particles being removed from stable clusters is investigated as well. Clusters start to break only when the number of removed elements is above a certain threshold. The total number of elements in the system when this threshold is reached is (almost) the same as in the addition case when the number of new agents reaches the aforementioned critical. In other words, two systems with the same number of agents, the first starting with many particles, having some removed, and the second starting with a few particles, having some added, behave the same. There are some rare cases in which the system that has particles removed is able to maintain the clusters more than the other.

Both situations resemble real-life systems that break and must be replaced or missions that scale up due to increasing funding or changes in requirements.

Furthermore, we proposed a strategy for changing cluster configurations. We realized that the potentials of some formations are a local minimum of others. This means that in order to exchange from one configuration to another, one must perturb the system. Our strategy was to include a new term into the potential to suppress the previous formation. We observe that some transitions happen faster, especially when the new number of clusters is higher than the previous because it is more expensive to break existing clusters than to merge.

Besides, we introduce the so-called Switching system that consists of periodically changing the model potentials. We set two parameters M_A and M_B , two number of clusters, respectively, and switch between their respective potentials with a certain period T . Under certain conditions the formation converges to $M = \max\{M_A, M_B\}$ clusters. Surprisingly, another possibility is the convergence of clusters of two participants each that do not overlap. They reach stable positions within the trajectory and keep nonzero relative positions inside each cluster fixed. Moreover, chaotic circular-like trajectories may emerge as well for certain combinations of M_A , M_B and T .

An important problem we also address is delayed information exchange between agents. In some applications, such as in satellite constellations, the communication happens from distant positions. We observed that delay plays the role of a control parameter. Depending on its intensity, different cluster configurations emerge, even

when all other parameters are fixed. Besides, it has a direct dependence on system frequency, having less impact for small frequencies. Basically, the system is more tolerant to delay when in low frequencies than in high. As delay increases, the system presents different cluster configurations and eventually reaches again the same solutions as in instantaneous communication. Yet such solutions reappear for delays that are multiples of the system period.

We propose a collision avoidance mechanism, motivated by real systems of moving agents. It is an anti-alignment between agents' heading angles that depends on a constant coupling strength. We employed the M-GEO algorithm to find proper model parameters that both decrease the number of collisions and guarantee the desired formations.

Lastly, we implemented the model on the ARGoS robot simulator, using the Kilobot platform and emulating a tracking system. Such platform has very limited architecture and poses an engineering challenge when it comes to long-range communication and internal processing. We assessed our implementation with the addition of noise into the robot controls. After all, the robots were able to reach the coveted symmetric circular formations in a timely manner for an acceptable range of perturbations.

As future work, we intend to deepen the investigation of the Switching system. So far we only observed formations of non-overlapping clusters with two particles each. We wonder whether is possible to achieve this behavior with different numbers of agents per group. Besides, it is still not clear the reason behind the emergence of such phenomena.

Another important point is that we have only considered fixed time delay and messages from farther vehicles should take more time to arrive than from close ones. Hence, the next step would be the implementation of a state-dependent time delay.

The only constraint for the choice of the PCOD model control parameters was that they should belong to the stable regions we found. For simplicity, we grouped some parameters, but a more proper strategy would be to run an optimization routine with them as design variables for every setup.

Other possibilities for the circular formations are second-order models that allow for radii prescriptions due to their frequency synchronization nature.

Last but not least, we intend to release a more decentralized implementation with the ARGoS simulator, leaving the processing part for the robots instead of the central

computer. Additionally, other robot platforms should be tested.

REFERENCES

ACEBRÓN, J. A.; BONILLA, L. L.; VICENTE, C. J. P.; RITORT, F.; SPIGLER, R. The kuramoto model: a simple paradigm for synchronization phenomena.

Reviews of Modern Physics, v. 77, p. 137–185, Apr 2005. 2

ALBI, G.; PARESCHI, L.; ZANELLA, M. Boltzmann-type control of opinion consensus through leaders. **Philosophical Transactions of the Royal Society of London A: Mathematical, Physical and Engineering Sciences**, v. 372, n. 2028, 2014. ISSN 1364-503X. 26

ALGAR, S. D.; STEMLER, T.; SMALL, M. From flocs to flocks. In: _____. **A mathematical modeling approach from nonlinear dynamics to complex systems**. Cham: Springer International Publishing, 2019. p. 157–175. ISBN 978-3-319-78512-7. 1

BÄCK, T.; SCHWEFEL, H.-P. An overview of evolutionary algorithms for parameter optimization. **Evolutionary Computation**, v. 1, n. 1, p. 1–23, 1993. ISSN 1063-6560. 59

BAKER, J. et al. **The laser interferometer space antenna: unveiling the millihertz gravitational wave sky**. 2019. Available from: <https://lisa.nasa.gov/documentsAstro2020.html>. Access in: 10 Sept. 2019. 5, 74

BALAZS, B.; VÁSÁRHELYI, G. Coordinated dense aerial traffic with self-driving drones. In: IEEE INTERNATIONAL CONFERENCE ON ROBOTICS AND AUTOMATION (ICRA). **Proceedings...** Brisbane, Australia: IEEE, 2018. 1

BALLERINI, M.; CABIBBO, N.; CANDELIER, R.; CAVAGNA, A.; CISBANI, E.; GIARDINA, I.; LECOMTE, V.; ORLANDI, A.; PARISI, G.; PROCACCINI, A.; VIALE, M.; ZDRAVKOVIC, V. Interaction ruling animal collective behavior depends on topological rather than metric distance: evidence from a field study. **Proceedings of the National Academy of Sciences**, v. 105, n. 4, p. 1232–1237, 2008. 1

BANDYOPADHYAY, S.; FOUST, R.; SUBRAMANIAN, G. P.; CHUNG, S.-J.; HADAEGH, F. Y. Review of formation flying and constellation missions using nanosatellites. **Journal of Spacecraft and Rockets**, v. 53, n. 3, p. 567–578, 2016. ISSN 0022-4650. 75

- BECCO, C.; VANDEWALLE, N.; DELCOURT, J.; PONCIN, P. Experimental evidences of a structural and dynamical transition in fish school. **Physica A: Statistical Mechanics and its Applications**, v. 367, p. 487–493, 2006. ISSN 0378-4371. 1
- CHUNG, S. J.; BANDYOPADHYAY, S.; FOUST, R.; SUBRAMANIAN, G. P.; HADAEGH, F. Y. Review of formation flying and constellation missions using nanosatellites. **Journal of Spacecraft and Rockets**, v. 53, n. 3, 2016. ISSN 00224650. 5
- COUZIN, I. D.; KRAUSE, J.; JAMES, R.; RUXTON, G. D.; FRANKS, N. R. Collective memory and spatial sorting in animal groups. **Journal of Theoretical Biology**, v. 218, n. 1, p. 1–11, 2002. ISSN 0022-5193. 1, 4, 24, 29, 46
- CUCKER, F.; SMALE, S. Emergent behavior in flocks. **IEEE Transactions on Automatic Control**, p. 852–862, 2007. 1
- CUCO, A. P. C.; DE SOUSA, F. L.; VLASSOV, V. V.; SILVA NETO, A. J. Multi-objective design optimization of a new space radiator. **Optimization and Engineering**, v. 12, n. 3, p. 393–406, 9 2011. 18, 19, 20
- CZIRÓK, A.; BEN-JACOB, E.; COHEN, I.; VICSEK, T. Formation of complex bacterial colonies via self-generated vortices. **Physical Review E**, v. 54, n. 2, p. 1791–1801, 8 1996. 1
- DE SOUSA, F. L.; RAMOS, F. M.; PAGLIONE, P.; GIRARDI, R. M. New Stochastic Algorithm for Design Optimization. **AIAA Journal**, v. 41, n. 9, p. 1808–1818, 2003. ISSN 1533-385X. 18, 19, 46, 59
- DIEKMANN, O.; GILS, S. A. van; LUNEL, S. M. V.; WALTHER, H. O. **Delay equations: functional-, complex-, and nonlinear analysis**. [S.l.]: Springer, 1995. 74
- DIERKS, T.; BRENNER, B.; JAGANNATHAN, S. Neural network-based optimal control of mobile robot formations with reduced information exchange. **IEEE Transactions on Control Systems Technology**, v. 21, n. 4, p. 1407–1415, 2013. ISSN 1063-6536. 2
- DUARTE, M.; COSTA, V.; GOMES, J.; RODRIGUES, T.; SILVA, F.; OLIVEIRA, S. M.; CHRISTENSEN, A. L. Evolution of collective behaviors for a real swarm of aquatic surface robots. **PLOS ONE**, v. 11, n. 3, p. 1–25, 2016. 2, 6
- ERNEUX, T. **Applied delay differential equations**. [S.l.]: Springer, 2009. 204 p. (Surveys and Tutorials in the Applied Mathematical Sciences, v. 3). 14, 74

ERNEUX, T.; JAVALOYES, J.; WOLFRUM, M.; YANCHUK, S. Introduction to focus issue: time-delay dynamics. **Chaos: An Interdisciplinary Journal of Nonlinear Science**, v. 27, n. 11, p. 114201, 11 2017. ISSN 1054-1500. Available from: <<http://aip.scitation.org/doi/10.1063/1.5011354>>. 14, 74

FOGEL, D. B. Foundations of evolutionary computation. In: **SCHUM, K.; SISTI, A. F. (Ed.). Modeling and Simulation for Military Applications**. [S.l.]: SPIE, 2006. v. 6228. 17

FRANKLIN, G. F.; WORKMAN, M. L.; POWELL, D. **Digital control of dynamic systems**. 3. ed. Boston, MA, USA: Addison-Wesley Longman, 1997. ISBN 0201820544. 86, 88

FREITAS, C.; MACAU, E.; PIKOVSKY, A. Partial synchronization in networks of non-linearly coupled oscillators: the deserter hubs model. **Chaos: An Interdisciplinary Journal of Nonlinear Science**, v. 25, n. 4, p. 043119, 2015. 2

FREITAS, C.; MACAU, E.; VIANA, R. L. Synchronization versus neighborhood similarity in complex networks of nonidentical oscillators. **Physical Review E**, v. 92, p. 032901, Sep 2015. 2, 7

FREITAS, V. L. S. **Estratégias de controle bioinspiradas e baseadas em sincronização para veículos artificiais**. 153 p. Dissertação (Mestrado em Computação Aplicada) — Instituto Nacional de Pesquisas Espaciais (INPE), São José dos Campos, 2016. 23, 25

FREITAS, V. L. S.; LACERDA, J. C.; MACAU, E. E. N. Complex networks approach for dynamical characterization of nonlinear systems. **International Journal of Bifurcation and Chaos**, v. 29, n. 13, p. 1950188, 2019. 6

FREITAS, V. L. S.; MACAU, E. E. Collision avoidance mechanism for symmetric circular formations of unitary mass autonomous vehicles at constant speed. **Mathematical Problems in Engineering**, v. 2018, p. 11, 2018. 2, 6, 77, 79, 80, 81, 82, 83

FREITAS, V. L. S.; MACAU, E. E. N. Control strategy for symmetric circular formations of mobile agents with collision avoidance. In: 8TH INTERNATIONAL CONFERENCE ON PHYSICS AND CONTROL (PHYSCON). **Proceedings...** Florence, Italy: IPACS, 2017. Available from: <<http://lib.physcon.ru/doc?id=b6acb68acb8a>>. 6

_____. Reactive agent-based model for convergence of autonomous vehicles to parallel formations heading to predefined directions of motion. In: 9TH INTERNATIONAL CONFERENCE ON AGENTS AND ARTIFICIAL INTELLIGENCE - VOLUME 1: ICAART. **Proceedings...** [S.l.]: ScitePress, 2017. p. 166–173. ISBN 978-989-758-219-6. [1](#), [2](#), [23](#), [25](#)

FREITAS, V. L. S.; QUILES, M. G.; MACAU, E. E. N. Controle baseado em redes neurais artificiais para agentes móveis em formação. In: **Proceeding Series of the Brazilian Society of Applied and Computational Mathematics**, v. **6**, n. **1**. [S.l.: s.n.], 2017b. [2](#), [6](#)

FREITAS, V. L. S.; REIS, B. M. F.; TOMMASELLI, A. M. G. Automatic shadow detection in aerial and terrestrial images. **Boletim de Ciências Geodésicas**, v. 23, n. 4, 2017. ISSN 1413-4853. [6](#)

FREITAS, V. L. S.; SOUSA, F. L. D.; MACAU, E. E. N. Reactive model for autonomous vehicles formation following a mobile reference. **Applied Mathematical Modelling**, v. 61, p. 167–180, 2018. ISSN 0307-904X. [1](#), [2](#), [4](#), [6](#), [23](#), [29](#), [47](#), [48](#), [49](#), [50](#), [52](#), [53](#), [54](#)

FREITAS, V. L. S.; YANCHUK, S.; ZAKS, M.; MACAU, E. E. N. On the control of symmetric circular formations of mobile agents and the generation of chaotic trajectories. **Communications in Nonlinear Science and Numerical Simulation**, 2019, Submitted. [2](#), [5](#), [6](#), [58](#), [61](#), [62](#), [63](#), [65](#), [68](#), [70](#), [72](#), [74](#)

GOTMARE, A.; BHATTACHARJEE, S. S.; PATIDAR, R.; GEORGE, N. V. Swarm and evolutionary computing algorithms for system identification and filter design: a comprehensive review. **Swarm and Evolutionary Computation**, v. 32, p. 68–84, 2017. ISSN 2210-6502. [17](#)

GRZYBOWSKI, J. M. V.; MACAU, E. E. N.; YONEYAMA, T. On the formulation and solution of the isochronal synchronization stability problem in delay-coupled complex networks. **Chaos**, v. 22, p. 033152, 2012. [14](#)

HABIBI, G.; KINGSTON, Z.; XIE, W.; JELLINS, M.; MCLURKIN, J. Distributed centroid estimation and motion controllers for collective transport by multi-robot systems. In: IEEE INTERNATIONAL CONFERENCE ON ROBOTICS AND AUTOMATION (ICRA). **Proceedings...** [S.l.]: IEEE, 2015. p. 1282–1288. ISSN 1050-4729. [2](#)

HALE, J. K.; LUNEL, S. M. V. **Introduction to functional differential equations**. Springer-Verlag, 1993. 447 p. ISSN 00765392. ISBN 978-1-4612-8741-4.

Available from: <<http://link.springer.com/10.1007/978-1-4612-4342-7>>.

14

HERBERT-READ, J. E.; PERNA, A.; MANN, R. P.; SCHAERF, T. M.; SUMPTER, D. J. T.; WARD, A. J. W. Inferring the rules of interaction of shoaling fish. **Proceedings of the National Academy of Sciences**, v. 108, n. 46, p. 18726–18731, 2011. 1, 24

HIRSCH, M.; SMALE, S.; DEVANEY, R. **Differential equations, dynamical systems, and an introduction to chaos**. [S.l.]: Elsevier, 2004. ISBN 9780123497031. 7, 8

JAIN, A.; GHOSE, D. Collective circular motion in synchronized and balanced formations with second-order rotational dynamics. **Communications in Nonlinear Science and Numerical Simulation**, v. 54, p. 156–173, 2018. ISSN 10075704. 2, 7, 40

JIRUSKA, P.; CURTIS, M. de; JEFFERYYS, J. G. R.; SCHEVON, C. A.; SCHIFF, S. J.; SCHINDLER, K. Synchronization and desynchronization in epilepsy: controversies and hypotheses. **The Journal of Physiology**, v. 591, n. 4, p. 787–797, 2013. Available from: <<https://physoc.onlinelibrary.wiley.com/doi/abs/10.1113/jphysiol.2012.239590>>. 9

JUSTH, E. W.; KRISHNAPRASAD, P. S. Equilibria and steering laws for planar formations. **Systems and Control Letters**, v. 52, n. 1, p. 25–38, 2004. ISSN 0167-6911. 32

KATZ, Y.; TUNSTROM, K.; IOANNOU, C. C.; HUEPE, C.; COUZIN, I. D. Inferring the structure and dynamics of interactions in schooling fish. **Proceedings of the National Academy of Sciences**, v. 108, n. 46, p. 18720–18725, 2011. 1, 29

KITANO, H.; ASADA, M.; KUNIYOSHI, Y.; NODA, I.; OSAWA, E. Robocup: the robot world cup initiative. In: **Proceedings...** New York: ACM, 1997. p. 340–347. ISBN 0-89791-877-0. 5

KURAMOTO, Y. **Chemical oscillations, waves, and turbulence**. New York: Springer-Verlag, 1984. 2, 9, 12, 35

LAB, H. U. S. **Kilobotics**. 2013. Available from: <<https://www.kilobotics.com/>>. Access in: May 2019. 85

LEONARD, N. E.; PALEY, D. A.; LEKIEN, F.; SEPULCHRE, R.; FRATANTONI, D. M.; DAVIS, R. E. Collective motion, sensor networks, and ocean sampling. **Proceedings of the IEEE**, v. 95, n. 1, p. 48–74, 1 2007. ISSN 0018-9219. 2, 6, 40

LI, Z.; GE, S. S.; LIU, S. Contact-force distribution optimization and control for quadruped robots using both gradient and adaptive neural networks. **IEEE Transactions on Neural Networks and Learning Systems**, v. 25, n. 8, p. 1460–1473, 2014. ISSN 2162-237X. 2

LÜCKEN, L.; YANCHUK, S.; POPOVYCH, O. V.; TASS, P. A. Desynchronization boost by non-uniform coordinated reset stimulation in ensembles of pulse-coupled neurons. **Frontiers in Computational Neuroscience**, v. 7, 2013. ISSN 1662-5188. 65

MAKRIS, N. C.; RATILAL, P.; JAGANNATHAN, S.; GONG, Z.; ANDREWS, M.; BERTSATOS, I.; GODØ, O. R.; NERO, R. W.; JECH, J. M. Critical population density triggers rapid formation of vast oceanic fish shoals. **Science**, v. 323, n. 5922, p. 1734–1737, 2009. 1

MALLADA, E.; TANG, A. Synchronization of weakly coupled oscillators: coupling, delay and topology. **Journal of Physics A: Mathematical and Theoretical**, v. 46, n. 50, p. 505101, 2013. 11, 12, 14

NAG, S.; SUMMERER, L. Behaviour based, autonomous and distributed scatter manoeuvres for satellite swarms. **Acta Astronautica**, 2013. ISSN 00945765. 75

NATIONAL AERONAUTICS AND SPACE ADMINISTRATION - NASA. **Cyclone Global Navigation Satellite System (CYGNSS)**. 2017. Available from: <<https://www.nasa.gov/cygnss>>. Access in: Sept. 2017. 5, 75

NOETEL, J.; FREITAS, V. L. S.; MACAU, E. E. N.; SCHIMANSKY-GEIER, L. Optimal noise in a stochastic model for local search. **Physical Review E**, v. 98, p. 022128, Aug 2018. Available from: <<https://link.aps.org/doi/10.1103/PhysRevE.98.022128>>. 6

_____. Search and return model for stochastic path integrators. **Chaos: An Interdisciplinary Journal of Nonlinear Science**, v. 28, n. 10, p. 106302, 2018. Available from: <<https://doi.org/10.1063/1.5040108>>. 6

O'KEEFFE, K. P.; HONG, H.; STROGATZ, S. H. Oscillators that sync and swarm. **Nature Communications**, v. 8, n. 1, p. 1504, 2017. ISSN 2041-1723. Available from: <<https://doi.org/10.1038/s41467-017-01190-3>>. 7

PALEY, D. A. **Cooperative control of collective motion for ocean sampling with autonomous vehicles**. Dissertation (PhD in Mechanical and Aerospace Engineering) — Princeton University, Princeton, 2007. 4, 32

PARKER, T. S.; CHUA, L. O. **Practical numerical algorithms for chaotic systems**. [S.l.]: Springer-Verlag New York, 1989. ISBN 0-387-96688-9. 71

PETER, F.; GONG, C. C.; PIKOVSKY, A. Microscopic correlations in the finite-size kuramoto model of coupled oscillators. **Physical Review E**, v. 100, p. 032210, Sep 2019. Available from: <<https://link.aps.org/doi/10.1103/PhysRevE.100.032210>>. 2, 7

PETER, F.; PIKOVSKY, A. Transition to collective oscillations in finite kuramoto ensembles. **Physical Review E**, v. 97, p. 032310, Mar 2018. Available from: <<https://link.aps.org/doi/10.1103/PhysRevE.97.032310>>. 7

PIKOVSKY, A.; ROSENBLUM, M.; KURTHS, J. **Synchronization: a universal concept in nonlinear sciences**. Cambridge: Pres Syndicate of the University of Cambridge, 2001. 11

PINCIROLI, C.; TALAMALI, M. S.; REINA, A.; MARSHALL, J. A. R.; TRIANNI, V. Simulating kilobots within argos: models and experimental validation. In: **DORIGO, M.; BIRATTARI, M.; BLUM, C.; CHRISTENSEN, A.; REINA, A.; TRIANNI, V. (Ed.). Swarm intelligence**. [S.l.]: Berlin: Springer, 2018. 5, 85, 86, 91

PINCIROLI, C.; TRIANNI, V.; O'GRADY, R.; PINI, G.; BRUTSCHY, A.; BRAMBILLA, M.; MATHEWS, N.; FERRANTE, E.; Di Caro, G.; DUCATELLE, F.; BIRATTARI, M.; GAMBARDELLA, L. M.; DORIGO, M. ARGoS: A modular, parallel, multi-engine simulator for multi-robot systems. **Swarm Intelligence**, v. 6, n. 4, p. 271–295, 2012. ISSN 15476510. 5, 85

POTTS, W. K. The chorus-line hypothesis of manoeuvre coordination in avian flocks. **Nature**, v. 309, n. 5966, p. 344–345, 1984. 1

PROTACHEVICZ, P. R.; BORGES, F. S.; LAMEU, E. L.; JI, P.; IAROSZ, K. C.; KIHARA, A. H.; CALDAS, I. L.; SZEZECH, J. D.; BAPTISTA, M. S.; MACAU, E. E. N.; ANTONOPOULOS, C. G.; BATISTA, A. M.; KURTHS, J. Bistable

- firing pattern in a neural network model. **Frontiers in Computational Neuroscience**, v. 13, p. 19, 2019. ISSN 1662-5188. Available from: <<https://www.frontiersin.org/article/10.3389/fncom.2019.00019>>. 9
- REINA, A.; COPE, A. J.; NIKOLAIDIS, E.; MARSHALL, J. A. R.; SABO, C. Ark: Augmented reality for kilobots. **IEEE Robotics and Automation Letters**, v. 2, n. 3, p. 1755–1761, 2017. ISSN 2377-3766. 5, 85
- REYNOLDS, C. W. Flocks, herds and schools: a distributed behavioral model. **SIGGRAPH Computer Graphics**, v. 21, n. 4, p. 25–34, 8 1987. ISSN 0097-8930. 1, 23, 24
- ROBOCUP FEDERATION. **RoboCup Federation official website**. 2016. Available from: <<http://www.robocup.org/>>. Access in: Aug. 2017. 5
- RUBENSTEIN, M.; AHLER, C.; HOFF, N.; CABRERA, A. Kilobot: a low cost robot with scalable operations designed for collective behaviors. **Robotics and Autonomous Systems**, v. 62, n. 7, p. 966–975, jul 2014. ISSN 0921-8890. Available from: <<https://www.sciencedirect.com/science/article/pii/S0921889013001474>>. 5, 85
- RUSSEL, S. J.; NORVIG, P. **Artificial Intelligence**. 3. ed. [S.l.]: Pearson Education, 2010. (Prentice Hall Series in Artificial Intelligence). 25
- SCHETTER, T.; CAMPBELL, M.; SURKA, D. Multiple agent-based autonomy for satellite constellations. **Artificial Intelligence**, v. 145, n. 1/2, p. 147–180, 2003. ISSN 0004-3702. 5
- SEPULCHRE, R.; PALEY, D. A.; LEONARD, N. E. Stabilization of planar collective motion: all-to-all communication. **IEEE Transactions on Automatic Control**, v. 52, n. 5, p. 811–824, 2007. ISSN 0018-9286. 2, 4, 5, 32, 33, 34, 35
- _____. Stabilization of planar collective motion with limited communication. **IEEE Transactions on Automatic Control**, v. 53, n. 3, p. 706–719, 4 2008. ISSN 0018-9286. 2, 39, 40
- SHEN, J. J. Cucker-smale flocking under hierarchical leadership. **SIAM Journal on Applied Mathematics**, v. 68, n. 3, p. 694–719, 2007. 26
- SMITH, H. L. **An introduction to delay differential equations with applications to the life sciences**. New York, NY: Springer Science+ Business Media, 2010. (Texts in Applied Mathematics, v. 57). ISBN 978-1-4419-7645-1.

Available from: <<http://link.springer.com/10.1007/978-1-4419-7646-8>>. 74

STANLEY, K. O.; MIIKKULAINEN, R. Evolving neural networks through augmenting topologies. **Evolutionary Computation**, v. 10, n. 2, p. 99–127, jun 2002. ISSN 1063-6560. 2

STRADNER, J.; THENIUS, R.; ZAHADAT, P.; HAMANN, H.; CRAILSHEIM, K.; SCHMICKL, T. Algorithmic requirements for swarm intelligence in differently coupled collective systems. **Chaos, Solitons and Fractals**, v. 50, p. 100–114, 2013. ISSN 09600779. 3

STROGATZ, S.; STEWART, I. Coupled oscillators and biological synchronization. **Scientific American**, v. 269, n. 6, p. 102–9, 1993. 9, 11

STROGATZ, S. H. **Nonlinear dynamics and chaos**: with applications to physics, biology, chemistry and engineering. [S.l.]: Westview Press, 1994. 7, 8, 9, 14, 15

_____. From kuramoto to crawford: exploring the onset of synchronization in populations of coupled oscillators. **Physica D**, v. 143, n. 1-4, p. 1–20, sep. 2000. ISSN 0167-2789. 11, 12, 44

STROGATZ, S. H.; ABRAMS, D. M.; MCROBIE, A.; ECKHARDT, B.; OTT, E. Crowd synchrony on the Millennium Bridge. **Nature**, v. 438, n. 7064, p. 43–44, 2005. ISSN 1476-4687. Available from: <<https://doi.org/10.1038/438043a>>. 9

SUMPTER, D. J. T. The principles of collective animal behaviour. **Philosophical Transactions of the Royal Society of London B: Biological Sciences**, v. 361, n. 1465, p. 5–22, 2006. ISSN 0962-8436. 1

VÁSÁRHELYI, G.; VIRÁGH, C.; SOMORJAI, G.; NEPUSZ, T.; EIBEN, A. E.; VICSEK, T. Optimized flocking of autonomous drones in confined environments. **Science Robotics**, v. 3, n. 20, 2018. ISSN 24709476. 1

VICSEK, T.; CZIRÓK, A.; BEN-JACOB, E.; COHEN, I.; SHOCHET, O. Novel type of phase transition in a system of self-driven particles. **Physical Review Letters**, v. 75, n. 6, p. 1226–1229, 8 1995. 1

VICSEK, T.; ZAFEIRIS, A. Collective motion. **Physics Reports**, v. 517, n. 3?4, p. 71 – 140, 2012. ISSN 0370-1573. Collective motion. 1

VLASOV, V.; MACAU, E. E. N.; PIKOVSKY, A. Synchronization of oscillators in a Kuramoto-type model with generic coupling. **Chaos: An Interdisciplinary Journal of Nonlinear Science**, v. 24, n. 2, p. 23120, 2014. 2

VLASOV, V.; PIKOVSKY, A.; MACAU, E. E. N. Star-type oscillatory networks with generic Kuramoto-type coupling: a model for “Japanese drums synchrony”. **Chaos: An Interdisciplinary Journal of Nonlinear Science**, v. 25, n. 12, p. 123120, 2015. 2

WINFREE, A. T. Biological rhythms and the behavior of populations of coupled oscillators. **Journal of Theoretical Biology**, v. 16, n. 1, p. 15–42, 1967. ISSN 0022-5193. 9

WU, J. **Introduction to neural dynamics and signal transmission delay**. [S.l.]: Walter de Gruyter, 2001. 1–192 p. ISBN 9783110305159. 74

YANCHUK, S.; GIACOMELLI, G. Spatio-temporal phenomena in complex systems with time delays. **Journal of Physics A: Mathematical and Theoretical**, v. 50, n. 10, p. 103001, 3 2017. ISSN 1751-8113. Available from: <<http://stacks.iop.org/1751-8121/50/i=10/a=103001?key=crossref.f760c062e912b820ac69c9174ac61305>>. 14, 74

YANCHUK, S.; PERLIKOWSKI, P. Delay and periodicity. **Physical Review E**, v. 79, n. 4, p. 46221, 2009. Available from: <<https://link.aps.org/doi/10.1103/PhysRevE.79.046221>>. 77

YAO, F.; LI, J.; CHEN, Y.; CHU, X.; ZHAO, B. Task allocation strategies for cooperative task planning of multi-autonomous satellite constellation. **Advances in Space Research**, v. 63, n. 2, p. 1073–1084, 2019. ISSN 0273-1177. 5

YEUNG, M. K. S.; STROGATZ, S. H. Time delay in the kuramoto model of coupled oscillators. **Physical Review Letters**, v. 82, n. 3, p. 648–651, 1999. 14

ZIEGEL, E.; PRESS, W.; FLANNERY, B.; TEUKOLSKY, S.; VETTERLING, W. **Numerical recipes: the art of scientific computing**. 3.ed. Cambridge: Cambridge University Press, 2007. ISBN 9780521880688. 15, 17

PUBLICAÇÕES TÉCNICO-CIENTÍFICAS EDITADAS PELO INPE

Teses e Dissertações (TDI)

Teses e Dissertações apresentadas nos Cursos de Pós-Graduação do INPE.

Manuais Técnicos (MAN)

São publicações de caráter técnico que incluem normas, procedimentos, instruções e orientações.

Notas Técnico-Científicas (NTC)

Incluem resultados preliminares de pesquisa, descrição de equipamentos, descrição e ou documentação de programas de computador, descrição de sistemas e experimentos, apresentação de testes, dados, atlas, e documentação de projetos de engenharia.

Relatórios de Pesquisa (RPQ)

Reportam resultados ou progressos de pesquisas tanto de natureza técnica quanto científica, cujo nível seja compatível com o de uma publicação em periódico nacional ou internacional.

Propostas e Relatórios de Projetos (PRP)

São propostas de projetos técnico-científicos e relatórios de acompanhamento de projetos, atividades e convênios.

Publicações Didáticas (PUD)

Incluem apostilas, notas de aula e manuais didáticos.

Publicações Seriadas

São os seriados técnico-científicos: boletins, periódicos, anuários e anais de eventos (simpósios e congressos). Constam destas publicações o Internacional Standard Serial Number (ISSN), que é um código único e definitivo para identificação de títulos de seriados.

Programas de Computador (PDC)

São a seqüência de instruções ou códigos, expressos em uma linguagem de programação compilada ou interpretada, a ser executada por um computador para alcançar um determinado objetivo. Aceitam-se tanto programas fonte quanto os executáveis.

Pré-publicações (PRE)

Todos os artigos publicados em periódicos, anais e como capítulos de livros.